TECHNISCHE UNIVERSITÄT MÜNCHEN

TUM School of Engineering and Design

Framework for generating representative volume elements of random ligament networks

Iman Davoodi Kermani

Vollständiger Abdruck der von der TUM School of Engineering and Design der Technischen Universität München zur Erlangung eines

Doktors der Ingenieurwissenschaften (Dr.-Ing.)

genehmigten Dissertation.

Vorsitz:	Priv.-Doz. Dr.-Ing. habil. Christian Krempaszky
Prüfer*innen der Dissertation:	
	1. Prof. Dr.-Ing. Christian J. Cyron
	2. Prof. Dr.-Ing. Wolfgang A. Wall

Die Dissertation wurde am 20.06.2023 bei der Technischen Universität München eingereicht und durch die TUM School of Engineering and Design am 08.12.2023 angenommen.

Abstract

Materials with fibrous microstructures play a significant role in biology and engineering due to their diverse properties and applications. Therefore, the generation, characterization, and modeling of these materials have received increasing attention in recent decades. Despite numerous studies analyzing the mechanical behavior of fibrous materials, some fundamental questions about their properties remain unanswered. For example, it is still unresolved in significant parts which microstructural descriptors of a fiber network determine the macromechanical properties of the network or to what extent the mechanical properties depend on individual microstructural descriptors of the network. To answer these key questions, it is required to develop a numerical tool which can generate a large variety of fibrous microstructures with predefined descriptors.

In this dissertation, a two-stage numerical approach is proposed to generate representative volume elements (RVEs) of random fiber networks with the desired predefined descriptors at both the network and fiber/ligament levels. The generated RVEs are homogeneous, fully connected, and periodic. That is, in addition to the uniform distribution of fibers throughout the RVE, there is at least one connection path between each pair of points in the fiber phase through that phase. The proposed approach is computationally highly efficient and well parallelizable. The numerical code is developed in Matlab, and the finite element method is applied to study the mechanical properties of the generated RVEs.

In the first stage of the approach developed for this dissertation, a numerical optimization algorithm, called the simulated annealing method, is used to generate a network structure. Various network level descriptors are studied, and it is found that the mechanical properties of fiber microstructures in the linear regime are determined almost exclusively by four key descriptors. These are the number ligaments per volume, the mean junction valency, the mean distance between the adjacent junctions and the mean direction cosine between ligaments adjacent to the same node. Considering different values of these four descriptors, more than 2500 RVEs are generated, and based on the numerical results of mechanical studies, the relationship between these descriptors and macromechanical properties is investigated.

In the second stage of the approach developed for this dissertation, the desired ligament shape is assigned to the ligaments within the RVEs generated in the first stage. The ligaments can have a curvature and variable thickness along their centerline. The curvature and thickness of the ligaments are described mathematically by Taylor and Fourier series, respectively, so that the approach can in principle model ligaments of any shape. Considering ligaments of different curvature and thickness, almost 5000 realizations of ligamentous RVEs are generated. The mechanical properties of these RVEs are calculated using the finite element method, and the relationship between the ligament level descriptors and the macroscopic mechanical properties is studied.

The proposed approach provides, for the first time, a general framework for generating random networks of ligaments, where the descriptors can be tailor-made predefined at both the network and ligament level. The approach can be easily modified for any other combination of descriptors different from the one considered in this work. Therefore, the proposed approach allows further studies on the mechanical behavior of ligamentous microstructures to determine their structure-property relationship.

Zusammenfassung

Materialien mit faserigen Mikrostrukturen spielen aufgrund ihrer vielfältigen Eigenschaften und Anwendungen eine wichtige Rolle in der Biologie und im Ingenieurwesen. Daher wurden der Erzeugung, Charakterisierung und Modellierung dieser Materialien in den letzten Jahrzehnten immer mehr Aufmerksamkeit geschenkt. Trotz zahlreicher Studien zur Analyse des mechanischen Verhaltens von Fasermaterialien bleiben einige grundlegende Fragen zu ihren Eigenschaften unbeantwortet. So ist es beispielsweise immer noch in erheblichen Teilen ungeklärt, welche mikrostrukturellen Deskriptoren eines Fasernetzwerks die makromechanischen Eigenschaften des Netzwerks bestimmen oder inwieweit die mechanischen Eigenschaften von einzelnen mikrostrukturellen Deskriptoren des Netzwerks abhängen. Zur Beantwortung dieser Schlüsselfragen ist es erforderlich, ein numerisches Werkzeug zu entwickeln, das eine große Vielfalt von faserigen Mikrostrukturen mit vordefinierten Deskriptoren erzeugen kann.

In dieser Dissertation wird ein zweistufiger numerischer Ansatz vorgeschlagen, mit dem repräsentative Volumenelemente (RVEs) von Zufallsfasernetzwerken mit den gewünschten vordefinierten Deskriptoren sowohl auf Netzwerk- als auch auf Faser- bzw. Ligamentebene erzeugt werden können. Die generierten RVEs sind homogen, vollständig verbunden und periodisch. Das heißt, zusätzlich zur gleichmäßigen Verteilung der Fasern im gesamten RVE gibt es zwischen jedem Punktpaar in der Faserphase mindestens einen Verbindungsweg durch diese Phase. Der vorgeschlagene Ansatz ist rechnerisch sehr effizient und gut parallelisierbar. Der numerische Code wurde in Matlab entwickelt, und die Finite-Elemente-Methode wurde angewandt, um die mechanischen Eigenschaften der erzeugten RVEs zu untersuchen.

In der ersten Stufe des für diese Dissertation entwickelten Verfahrens wird ein numerischer Optimierungsalgorithmus, die so genannte Simulated-Annealing-Methode, verwendet, um eine Netzwerkstruktur zu generieren. Es wurden verschiedene Deskriptoren auf Netzwerkebene untersucht, und es zeigte sich, dass die mechanischen Eigenschaften von Fasermikrostrukturen im linearen Regime fast ausschließlich durch vier Schlüsseldeskriptoren bestimmt werden. Dabei handelt es sich um die Anzahl der Fasern pro Volumen, die mittlere Knotenpunktsvalenz, den mittleren Abstand zwischen den benachbarten Knotenpunkten und den mittleren Richtungskosinus zwischen den an denselben Knotenpunkt angrenzenden Fasern. Unter Berücksichtigung verschiedener Werte dieser vier Deskriptoren wurden mehr als 2500 RVEs erzeugt, und auf der Grundlage der numerischen Ergebnisse mechanischer Studien wurde der Zusammenhang zwischen diesen Deskriptoren und den makromechanischen Eigenschaften untersucht.

In der zweiten Stufe des für diese Dissertation entwickelten Verfahrens wird den Ligamenten innerhalb der in der ersten Stufe erzeugten RVEs die gewünschte Ligamentform zugewiesen. Die Ligamente können eine Krümmung aufweisen sowie eine variable Dicke entlang ihrer Mittellinie. Die Krümmung und die Dicke der Ligamente werden mathematisch durch Taylor- bzw. Fourier-Reihen beschrieben, so dass der Ansatz grundsätzlich Ligamente beliebiger Form modellieren kann. Unter Berücksichtigung von Ligamenten verschiedener Krümmung und Dicke werden fast 5000 Realisierungen von Ligament-RVEs erzeugt. Die mechanischen Eigenschaften dieser RVEs wurden mit der Finite-Elemente-Methode berechnet und die Beziehung zwischen den Deskriptoren auf Ligamentebene und den makroskopischen mechanischen Eigenschaften untersucht.

Der vorgeschlagene Ansatz bietet zum ersten Mal einen allgemeinen Ansatz zur Erzeugung von zufälligen Netzwerken von Ligamenten, bei dem die Deskriptoren sowohl auf Netzwerk-

als auch auf Ligamentebene maßgeschneidert vordefiniert werden können. Der Ansatz kann leicht für jede andere Kombination von Deskriptoren modifiziert werden, die sich von der in dieser Arbeit betrachteten unterscheidet. Daher ermöglicht der vorgeschlagene Ansatz weitere Studien über das mechanische Verhalten von Ligament-Mikrostrukturen, um deren Struktur-Eigenschafts-Beziehung zu ermitteln.

Acknowledgement

This dissertation has been written between 2017 and 2023 as part of my work as research assistant at the Chair of Computational Mechanics at Technical University of Munich. Now, at the end of my PhD journey, I wish to show my appreciation to all the great people who helped and supported me along this path. I would also like to acknowledge the financially support by **German Academic Exchange Service (DAAD)**.

First and foremost, I would like to express my deepest gratitude to my supervisor, **Prof. Christian Cyron**. Without his consistent support and guidance, this thesis would have never been accomplished. His commitment to do everything in the best and perfect form will inspire me in my whole life. I would like to extend my sincere thanks to him for all his administrative support which for me as a foreign student was a critical issue. I am also grateful to **Prof. Wolfgang Wall**, the head of the chair, to **Ms. Renata Nagl**, the assistant of the chair, and to all the members of the admin team for their administrative support. I am extremely grateful to **Jonas Eichinger**, the colleague who helped me the most from the first days of my PhD up to its end with his valuable suggestions, feedback, and collaborations. Thanks should also go to all the colleagues in the chair with whom I spent a memorable and enjoyable time, especially to **Mostafa Faraji**, **Andrea La Spina**, **Sebastian Fuchs**, and **Sebastian Brandstäter**. I would be remiss in not mentioning the help of **Roland Aydin** in the first days of my work at the Institute.

This research has been carried out for three years at the Institute for Continuum and Materials Mechanics at Hamburg University of Technology. I had the pleasure of working with the institute members and would like to acknowledge their help. Special thanks to **Ms. Inka Schenk** and **Ms. Bettina Schrieber**, the former and the present assistants of the institute. Many thanks to **Maximilian Schmitter** and **Prof. Norbert Huber** for the productive scientific discussions and their collaborations in this study. Thanks should also go to **Kian Abdolazizi** who was always available for friendly discussions, especially about our common interest in gym. In Hamburg, I also collaborated with the Institute of Material Systems Modeling at Helmholz-Zentrum Hereon. I am really grateful to the colleagues there, especially to **Dr. Ingo Scheider** and **Ms. Setphanie Koch** for all their supports regarding the administrative issues.

Last but not least, I heartfully appreciate the support of my family during these years. Words cannot express my gratitude to my **PARENTS** who trusted and helped me in each step of my life, and I am always indebted to them. I would like to extend my sincere thanks to my brother **Amir**, who always motivated and encouraged me and helped me a lot to be able to focus on my work although he was far away. I could not have concluded this journey without my lovely wife, **Negin**, from whom I received the most encouragement, support, motivation, and love in the last three years. She was with me in ups and downs of this way and ensured me that I could overcome all obstacles to reach my destination.

I also place on record my sense of gratitude to everyone, who directly or indirectly, lent their hand in this journey.

Munich, June 2023 Iman Davoodi Kermani

Contents

1 Introduction

1.1 Motivation

Ligament microstructures can be widely found in both industrial and biological materials. In addition to the materials in which the fibrous microstructure is obvious, considering a series of simplifications, the microscopic structure of various materials can be modeled as a network of fibers or ligaments. Therefore, generating, characterization, and analysis of mechanical behavior of these networks attained an increasing attention in the last decades. Despite the quantity and diversity of research in this field, there are still many unanswered questions regarding the modeling of ligamentous microstructures. The first step to find the answer to these questions is developing a numerical tool which can generate various networks of ligaments with specific characteristics. In this dissertation, a general and computationally efficient approach is suggested, providing a framework for further studies. In the rest of this section, a number of previous studies most related to our work are briefly discussed and it is explained how the present work can improve the available models.

A prevalent example of fibrous network in biology is the network formed by collagen which shapes and reinforces tissues such as skin, tendons, and bone [1]. Due to the key role of these structures in bioengineering, numerous studies are performed to generate such networks [2, 3, 4] and in many of them, finite element method (FEM) has been used to simulate the mechanical behavior of the generated networks [5, 6]. Based on the numerical results, biomaterials with fibrous structures indicate strain-stiffening characteristic [7, 8, 9, 10] and it found that there is a relation between the network architecture and their mechanical properties [11, 4, 1, 12].

Nanoporous materials (NPMs) are another example of heterogeneous materials with ligamentous microstructure which have abundant applications in engineering. They are the product of a chemical or electrochemical dealloying process [13] and have a bicontinuous microstructure which can be modeled as a ligamentous network. Due to the fascinating and various properties resulted from their complex microstructure, NPMs are of great interest [14, 15, 16, 17, 18]. Various research has been accomplished to develop three-dimensional models of nanoporous materials [19, 20, 21, 22]. They have analyzed the mechanical behavior of NPMs [23, 24, 25] and investigated the relations between the microstructure and the macroscopic behavior of these materials [26, 27, 28]. However, although the ligamentous microstructure of NPMs is completely random, in most of the mentioned studies, nanoporous materials are modeled as a fully structured network [29] or as a structured lattices with some random changes [30, 31].

The complexity of ligamentous microstructures makes it too complicated to develop an analytical model of ligament networks. Therefore, numerical models are required to study the macroscopic mechanical behavior of ligamentous networks. To develop such a numerical model, we need to specify a so-called representative volume element (RVE). The representative volume elements should be as small as possible to reduce the computational costs. However, they must

be large enough to represent the geometrical and physical properties of the material. The representative volume element of a random ligamentous material plays a similar role as of the unit cell in a structured network. Accordingly, specifying an appropriate RVE would be a principal step in numerical modeling of ligamentous materials; hence many studies in this field focused on generating such a volume element [32, 33, 34, 35, 36, 37, 38]. Since it is not possible to define an RVE which represents the entire properties of the material, depending on the field of interest, one or a group of material characteristics may be considered in the numerical model.

In the literature, different descriptors of network level such as point-correlation function [39, 40, 41], cluster-correlation function [42], chord distribution function [43], lineal-path function [44], radial distribution function [45], and pore-size distribution function [46] were considered as network specifications for reconstruction of a heterogeneous microstructure. Moreover, the numerical simulations revealed that the macroscopic mechanical properties of ligamentous networks also depend on the geometrical descriptors of ligaments [47, 48, 27, 49, 50].

When the desired morphological descriptors are determined, different optimization methods such as simulated annealing (SA) [51], genetic algorithms (GA) [52], or fast Fourier transform (FFT) [53] can be used as a numerical tool to reconstruct a heterogeneous RVE [54, 55]. In fact, the reconstruction of a heterogeneous material is an optimization problem which looks for a final solution that has the minimum difference with the desired RVE based on the selected descriptors. Among the numerical methods mentioned before, the simulated annealing approach is the most popular method in reconstruction of different heterogeneous materials [45, 56, 57, 2, 58]. That is due to the ability of SA in finding the global optimum among various local optima and the efficiency of this approach from computational point of view. Therefore, SA is employed in this thesis to reconstruct the representative volume elements of ligamentous microstructures.

The mechanical behavior of generated ligamentous RVEs is investigated by either finite element method (FEM) [59, 60, 61, 62] or molecular dynamic (MD) [63, 64]. That makes it possible to study the relation between macroscopic mechanical properties and the microscopic descriptors in ligamentous materials [30, 65]. However, to perform a comprehensive study about the relation of macroscopic properties and network descriptors, it is required to have a tool for generating networks of ligaments with desired predefined microstructural descriptors. That means, this tool must be able to control every single descriptor considered in the generating procedure. Therefore, by controlling the variation of each microstructural descriptor when the others are kept constant, it would be possible to study the relation between that specific variable descriptor and the mechanical properties of the network. To the best of the author's knowledge, such a network generating tool is not available in the literature.

To summarize the brief review presented above, the available numerical models of ligamentous materials cannot answer the following fundamental questions regarding their macromechanical behavior:

- Which descriptors of network level and to what extent can determine the mechanical properties at the macroscale?
- What is the relationship between descriptors of ligamentous microstructure (both in network and ligament level) and the macroscopic material properties?

To answer these questions, in this dissertation, a computationally efficient network generating approach is proposed. The suggested approach generates homogeneous and isotropic RVEs in

which the ligament phase is continuous not only within a single RVE but also in the case of larger material volumes resulted from repetition of RVEs along with each other. This approach provides a framework in which the different descriptors can be added/removed to/from the reconstruction procedure. Therefore, due to the ability of the proposed approach in generating a large number of ligamentous microstructures with predefined desired descriptors, it would be possible to perform a comprehensive study about the dependency of macroscopic properties on microstructural descriptors.

The proposed approach generates ligamentous RVEs in two stages. At the first stage, considering the network level descriptors, the overall network structure is generated. At the second stage, the shape of components is assigned to the network generated at the first stage. A schematic workflow of this approach is indicated in Figure 1.1.

1.2 Overview

The remainder of this dissertation is organized as follows: in chapter 2, first, the definition of morphological descriptors considered in the proposed network generating approach is provided. These descriptors are classified into two categories of network level and component level descriptors. Afterwards, the simulated annealing method is briefly explained. Finally, the suggested two-stage approach is described in detail. In chapter 3, a summary and the authors' contributions of Paper A [66] and Paper B [67] are given. The full texts are reprinted in A.1 and A.2, respectively. Chapter 4 presents a brief conclusion of this thesis and an outline of the potential future research.

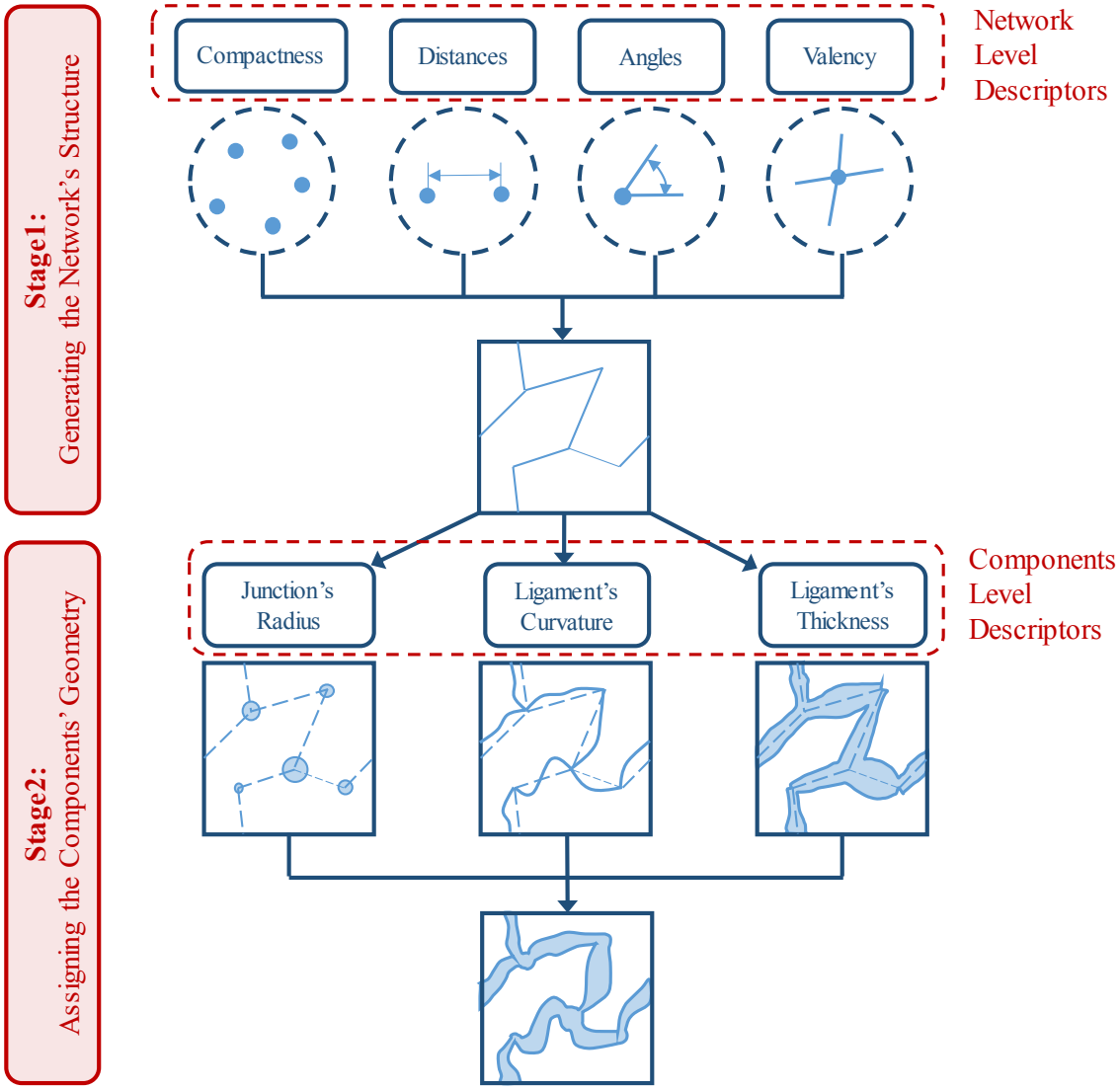

Figure 1.1: Workflow of the proposed two-stage ligamentous network generating approach. At the first stage, it generates the network structure based on predefined network level descriptors. At the second stage, it assigns the components' geometry to the product of stage one.

2 Methodology

An approach which can generate representative volume elements of ligamentous materials with complex microstructures is still in demand. In this thesis, a two-stage approach is proposed to generate ligamentous RVEs not only with predefined network morphology but also with desired ligament shapes. This approach produces the overall network structure at the first stage and assigns the shape to the individual ligaments at the second stage. In addition, the generated RVEs by this approach are homogeneous, isotropic, fully periodic and connected. This chapter is structured as follows: in section 2.1, the microstructural descriptors considered in the network generating approach are described. The simulated annealing method, the numerical optimization algorithm applied in the proposed approach, is introduced in section 2.2. Finally, in section 2.3, the two-stage network generating approach is explained step-by-step.

2.1 Descriptors

The characteristics of a microstructure can be determined by a number of so-called *descriptors*. The representative volume element of a ligamentous microstructure is composed by a number of *ligaments* or *fibers* connected to each other at specific points called *junctions* or *nodes* (see Figure 2.1). Therefore, each descriptor of a ligamentous microstructure measures a specific characteristic of its components (i.e., its junctions or its ligaments). Depending on the field of study, a set of descriptors may be used to characterize the material properties. The purpose of this dissertation is to generate RVEs representing the mechanical properties of ligamentous material. Therefore, among numerous assumable descriptors of such materials, the focus is on the microstructural descriptors having the strongest relationship with the mechanical properties. This section presents only the mathematical definitions of investigated descriptors. The proposed approach generates RVEs at two distinct stages, first generates the overall network and then forms the components geometry. Similar classification is applied to the descriptors, and they are categorized as network level and component level descriptors, respectively defined in 2.1.1 and 2.1.2.

2.1.1 Descriptors of network level

The first stage of the proposed approach generates the overall structure of the network regardless of the components' geometry. The descriptors considered for generating the overall structure of the network are classified as *network level descriptors*. These descriptors specify a characteristic of the network independent of its components' shape. In other words, they determine the arrangement of components within the RVE. In addition to the descriptors defined in the following, many other descriptors of network level can be defined, some of which are introduced in Paper A. The numerical studies performed in Paper A [66] indicated that the linear mechanical

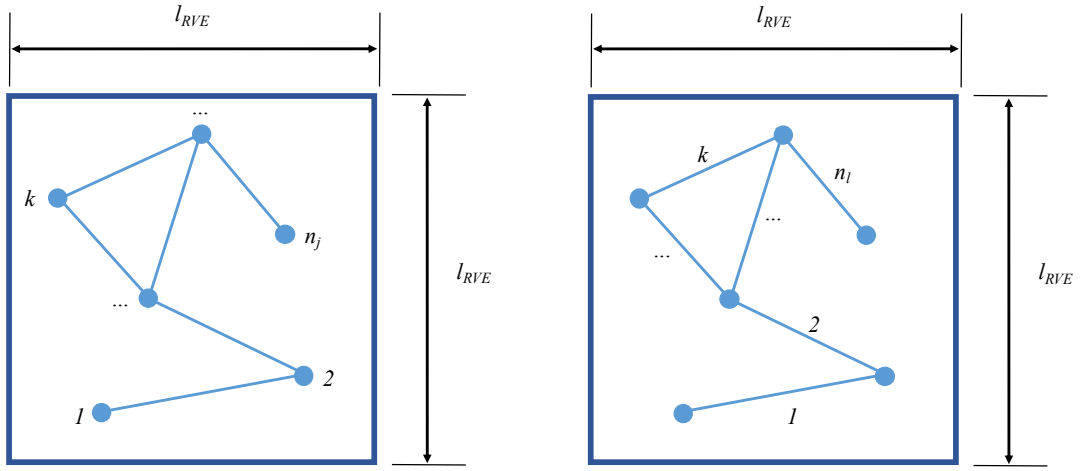

Figure 2.1: A simple 2D schematic of a ligamentous RVE with the size of l_{RVE} composed of (a) n_j junctions drawn as solid circles and (b) n_l ligaments drawn as straight connecting lines.

properties of fiber networks are mainly determined by only four descriptors of network level. In the following, the definitions of these four descriptors are presented. Since the ligaments in the generated RVEs must form a fully connected network, the connectedness is also considered as a network level descriptor and explained here.

- *Junction valency distribution* V

  In a ligamentous network, a pair of junctions which are directly connected to each other by a ligament are called *adjacent* junctions. The valency of k-th junction v^k is the number of its adjacent junctions or equivalently, the number of ligaments connected to this junction. Accordingly, the valencies are positive integers and the valency equals to one represents a dead-end ligament which depending on the respective real example may be practical assumption or not. Here, for the sake of generality the junction with valency of one is also allowed. The junction valency distribution V is the probability distribution of the junction valencies in the RVE.

- *Adjacent junctions' distance distribution* L

  The probability distribution of the euclidean distance between all pairs of adjacent junctions within the RVE is considered as a descriptor of the network level. For example, k-th junction in Figure 2.2-(a) is adjacent with q-, r- and s-th junctions through m-, p- and n-th ligaments, respectively and the corresponding distances are shown as l^m, l^p and l^n. In the networks with straight ligaments, the adjacent junctions' distance is equal to the length of the respective ligament.

- *Direction cosine distribution C*

  Connecting a junction to its adjacent junctions by imaginary lines forms angles between each pair of lines as indicated in Figure 2.2(b). In this Figure, the dashed lines represent the imaginary connecting lines and their corresponding angles are illustrated. The lines connecting the k-th junction with the valency of v^k to its adjacent junctions construct $v^k \times (v^k-1)/2$ angles. Computing the cosine of all the angles and repeating the computation for all the junctions within the RVE gives a set of cosines. The probability distribution of this set is called direction cosine distribution and considered as a descriptor of network level. Direction cosine distribution together with the adjacent junctions' distance distribution determine the relative position of junctions throughout the RVE.

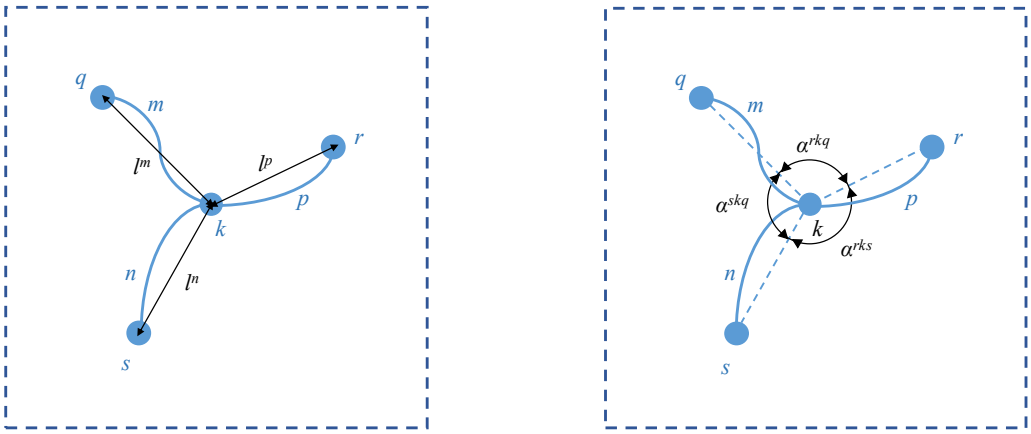

Figure 2.2: Visualization of definition of (a) adjacent junctions' distance and (b) direction cosine for a sample junction j^k in a 2D-view.

- *Compactness of the network*

  The number of network components per unit volume of the RVE indicates the compactness of the network. A ligamentous microstructure is composed of ligaments and junctions. Therefore, the compactness of a ligamentous network is determined by the number of ligaments per unit volume of RVE N_l, and the number of junctions per unit volume of RVE N_j. However, for the RVEs with specified valency distribution, the following relation exist between the number of ligaments n_l, and the number of junctions n_j

$$n_l = \frac{1}{2}\sum_{k=1}^{n_j} v^k, \tag{2.1}$$

where v^k is the valency of k-th junction. Therefore, determining either N_l or N_j, determines the compactness of the network.

- *Connectedness*

  This is a boolean descriptor which checks whether the ligament phase in a ligamentous microstructure is fully connected. Connectedness in a ligamentous network means that there is at least one connecting path through the ligament phase between each pair of points of this phase. It is the connectedness inside the RVE which is called *internal connectedness*. In addition, since the proposed approach is designed to generate periodic RVEs, the network must be also *externally connected*. That means, the ligament phase must also be connected within a larger volume of material produced by the repetition of RVE in directions aligned with its edges. Therefore, a *fully connected* network is both internally and externally connected.

2.1.2 Descriptors of component level

The *component level descriptors* are the descriptors which describe the geometry of network components i.e., the ligaments and the junctions. In the following, the mathematical definitions of the microstructural descriptors used to shape the components of the generated RVE are presented.

- *Junction's radius distribution* r_j

  The junctions within the network are modeled as spheres where the radius of k-th junction is shown by r_j^k. The probability distribution of junctions' radii is assumed as a component level descriptor.

- *Ligament's cross-section radius* r_l

  The cross-section of ligaments in the generated RVEs is assumed to be circular with variable radius along the ligament's centerline. For the k-th ligament, a local coordinate system, $x^k y^k z^k$ is defined in which the x^k-axis passes through the start and end junctions of the ligament. The radius of this ligament at an arbitrary point x^k is $r_l^k(x^k)$ which can be expressed as a sum of polynomials

$$r_l^k\left(x^k\right) = \sum_{i=0}^{i_{max}} d_i^k \left(x^k\right)^i, \qquad 0 \leq x^k \leq l^k, \tag{2.2}$$

  where l^k is the euclidean distance between the start and end junctions of k-th ligament. If the function $r_l^k(x^k)$ is determined, the coefficients d_i^k can be calculated by the Taylor series

$$d_i^k = \frac{r_l^{k(i)}(0)}{i!}, \tag{2.3}$$

  where $r_l^{k(i)}(0)$ is the i-th derivative of $r_l^k(x^k)$ at $x^k = 0$. Otherwise, the desired function of ligament's cross-section radius can be produced by setting the coefficients d_i^k (see Paper B).

- *Ligament's curvature* κ

  For simplicity, it is assumed that the centerline of the k-th curved ligament lies entirely in the $x^k y^k$-plane. As explained above, the local x^k-axis connects the junctions confining the k-th ligament. The centerline of this ligament can be expressed by a Fourier series as follows

$$y^k\left(x^k\right) = \frac{a_0^k}{2} + \sum_{n=1}^{f_{max}} \left[a_n^k \, cos\left(\frac{\pi n x^k}{l^k}\right) + b_n^k \, sin\left(\frac{\pi n x^k}{l^k}\right) \right], \tag{2.4}$$

  where

$$a_n^k = \frac{2}{l^k} \int_0^{l^k} y^k\left(x^k\right) cos\left(\frac{\pi n x^k}{l^k}\right) dx^k, \tag{2.5a}$$

$$b_n^k = \frac{2}{l^k} \int_0^{l^k} y^k\left(x^k\right) sin\left(\frac{\pi n x^k}{l^k}\right) dx^k. \tag{2.5b}$$

  The curvature of k-th ligament $\kappa^k\left(x^k\right)$ can be calculated by the following relation

$$\kappa^k\left(x^k\right) = \frac{\left| \frac{d^2 y^k}{\left(dx^k\right)^2} \right|}{\left[1 + \left(\frac{dy^k}{dx^k}\right)^2\right]^{\frac{3}{2}}}. \tag{2.6}$$

  To model the networks with known ligaments' curvature, the coefficients a_n^k and b_n^k are determined by Eqs. (2.5a) and (2.5b). Otherwise, the desired curvature can be produced by setting these coefficients.

The three component level descriptors explained in this section are illustrated for a sample ligament in Figure 2.3.

2.2 Simulated annealing method

The network generating approach proposed in this thesis employs a numerical optimization method named *Simulated annealing* (SA). The general concepts of SA are presented here. To find the desired microstructure, SA starts from an initial random structure and gradually optimizes it by applying small random changes to it. However, in the intermediate steps, SA may replace the current structure by a worse structure according to the descriptors considered for the target microstructure. In other words, such steps are not toward the optimum structure but rather away from it. However, these steps guarantee finding the global optimum instead of getting trapped in the local optima. The probability of replacing a structure with a worse structure decreases as the iteration goes forth. In fact, this method's name refers to the annealing technique in metallurgy, which includes an initial heating followed by a gradual and controlled cooling

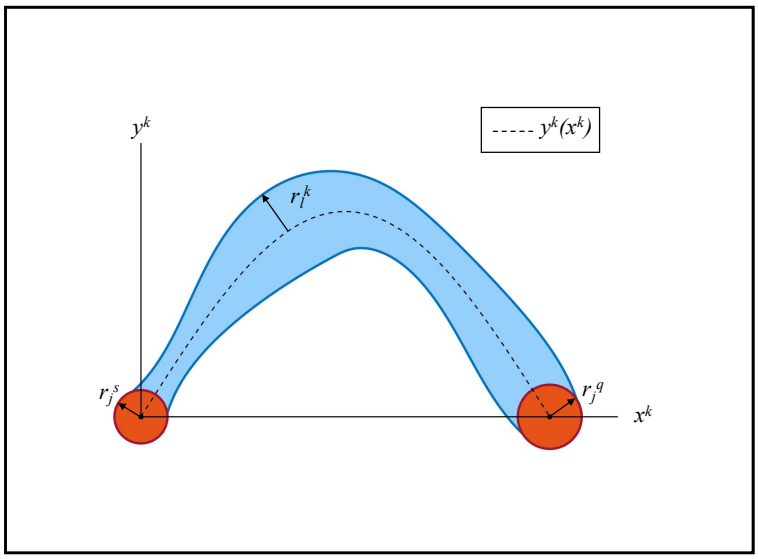

Figure 2.3: A 2D-view of k-th ligament connecting the s-th junction to the q-th junction.

procedure to change the material microstructures to improve its properties. Similarly, in the simulated annealing method, the probability of selecting a worse structure is deliberately set to be high in the beginning and decreases gradually in each iteration.

Based on the given overview, to apply the simulated annealing optimization method, the following items must be clearly defined:

- *Initial solution*

  To start the optimization procedure, it is necessary to have an initial random solution to the problem. In the network generating problem, the initial solution can be any arbitrary microstructure which fulfills the general constraints of the problem.

- *Perturbation mechanism*

  In each iteration, a new solution to the optimization problem is suggested which must be in the current solution's neighborhood. That means, the new solution is obtained by applying slight changes to the current solution. The perturbation mechanism determines these changes. For every optimization problem the appropriate perturbation mechanism must be designed. This mechanism must apply random changes which do not violate the overall constraints of the problem. Notice that the suggested solution at each iteration may be accepted or rejected.

- *Energy function*

  During the optimization procedure, the SA compares the considered descriptors of suggested solutions with those of the optimum solution. The mathematical parameter which

measures the difference between the descriptors of suggested and the optimum solution is called energy function (cost function or objective function). Therefore, the energy function of the optimum solution is zero.

- *Cooling schedule*

  As discussed previously, in each step of the SA, a new solution is suggested. The method accepts suggestions which reduce the energy function. However, it is probable that the SA accepts a new suggested solution which increases the energy function. This probability is controlled by a temperature-like variable and the cooling schedule determines how this variable decreases in each iteration.

- *Cut-off criterion*

  Depending on the desired accuracy or run-time, a cut-off criterion can be defined which determines when the SA must be terminated. Although the overall precision of solutions increases with increasing the number of iterations, it can be too time-consuming or computationally expensive. Therefore, the cut-off criterion determines the maximum allowed number of iterations or the minimum acceptable accuracy.

Here, it should be emphasized that the above-mentioned items should be defined for any individual optimization problem depending on the assumptions and constraints of the problem. They may vary from case to case and there is not any general mathematical definition of them. The overall schematic of SA is plotted as a flowchart in Figure 2.4.

2.3 RVE generating approach

In this section, the two stages of the proposed RVE generating approach are explained in detail. In subsection 2.3.1, it is explained how the simulated annealing method is used at the first stage of the approach to generate the overall structure of the network. The second stage of the approach is described in 2.3.2. At the second stage, the geometry of components is assigned to the network produced at the first stage.

2.3.1 Stage 1, generating the overall network structure

The first stage of the proposed RVE generating approach produces a network of fibers considering the network level descriptors without taking into account the geometry of components. As mentioned in 2.1.1, the network level descriptors considered in this work are the compactness of the network, junction valency distribution, adjacent junctions' distance distribution, and direction cosine distribution. In addition, the generated RVEs must be fully connected (see 2.1.1). At this stage, first, a fully connected random network of ligaments is generated. The number of ligaments (i.e., the compactness of the network) and the junction valency distribution of the generated RVE exactly match the predefined target values. This random RVE is considered as the initial solution for the simulated annealing method. Therefore, the perturbation mechanism of the SA is designed such that it does not change the number of ligaments, the valency of the junctions, or the connectedness of the RVE. That means, the target values of the compactness

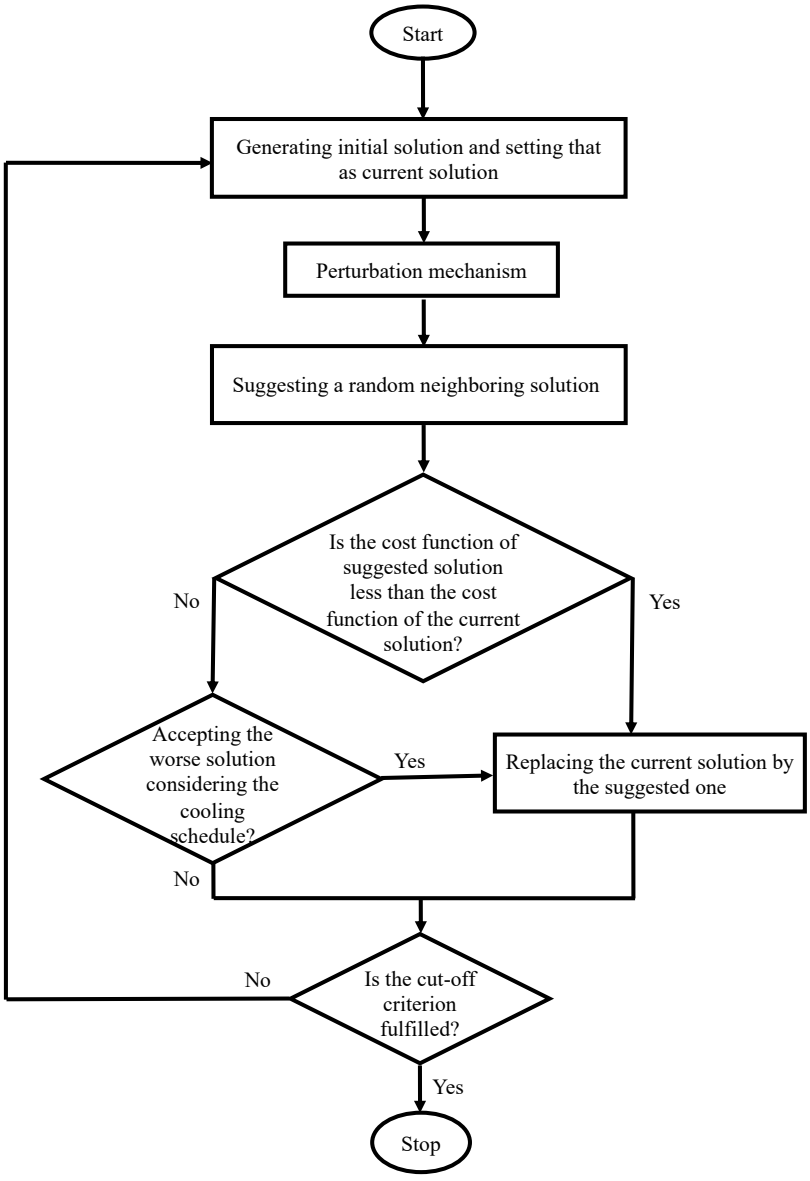

Figure 2.4: Flowchart of the simulated annealing method.

of the network, the junction valency distribution, and the connectedness are fulfilled in the initial solution and kept unchanged until the end of the optimization procedure. Accordingly, SA optimizes the two other descriptors, i.e., the adjacent junctions' distance distribution and the direction cosine distribution. The only constraint of this optimization problem is the maximum allowed distance between the adjacent junctions l_{max}. To reduce the finite size effect, a maximum distance equals to one-third of the RVE edge length is assumed between the adjacent junctions ($l_{max} \leq l_{RVE}$). In the following, first, the procedure of generating random initial network is explained. Afterwards, the other items of SA (see 2.2) are mathematically defined.

Initial solution

To generate a fully connected random network of ligaments with predefined compactness and junction valency distribution, different algorithms can be designed. The most computationally expensive part of such algorithms is the part checking the connectedness of the network. Moreover, considering the constraint $l_{max} \leq l_{RVE}/3$, looking for eligible pairs of junctions can be the most time-consuming part. It may be impossible to eliminate these calculations, however it is desired to reduce them as much as possible. Considering the mentioned costs, a fast and computationally efficient algorithm is proposed. The algorithm generates the network in three steps as follows:

1. *Generating desired number of junctions*

   First, a cubic RVE with the edge length of l_{RVE} is generated. The origin of the global coordinate system XYZ is in one of the corners of the RVE and the coordinate axes are parallel to the edges of this RVE. Having the target junction valency distribution V, and the target ligament density N_l, the number of junctions per unit volume N_j is determined by Eq. (2.1). Consequently, the number of junctions in this RVE is $n_j = N_j \times (l_{RVE})^3$. To reduce the computational costs of checking the maximum distance constraint, the RVE is divided into a set of $6^3 = 216$ equal-sized cubic subdomains. By this partitioning, the distance between any pair of junctions located in a similar subdomain is less than $l_{RVE}/3$. Now, the junctions are generated at random positions throughout the subdomains in such a way that all the subdomains contain an equal number of junctions. Note that it is not always possible to generate exactly an equal number of junctions in all subdomains. In these cases, some subdomains contain only one more junction than the other subdomains. A 2D schematic of this step is illustrated in Figure 2.5(a).

2. *Connecting the junctions with the minimum number of ligaments*

   The purpose of this step is to connect all the junctions generated in the previous step by the minimum number of ligaments. That means, at the end of this step the network is internally connected. Despite each connection is added between a random pair of junctions, for the sake of uniformity, the minimum number of connections required for an internally connected network are added here. For an RVE containing n_j junctions, $(n_j - 1)$ ligaments are needed to construct an internally connected network. To generate the connections (each connection corresponds to a ligament), first, a random pair of junctions both within the same subdomain is selected and a ligament is added between them. The procedure is repeated for the subdomain until it becomes internally connected. For a sample subdomain

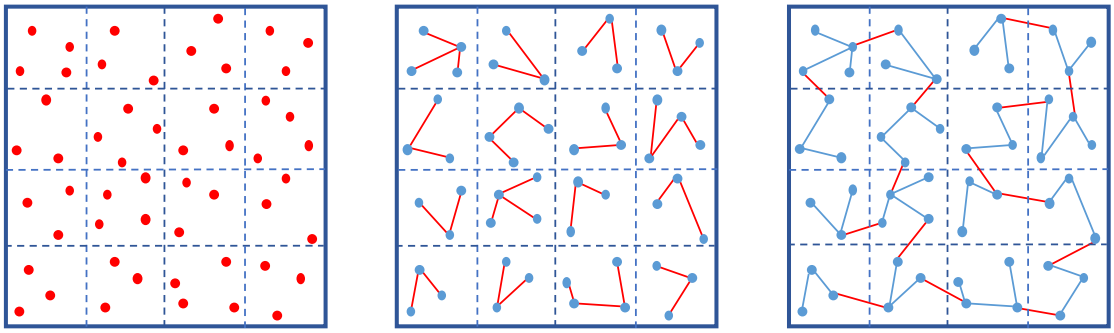

(a) (b) (c)

Figure 2.5: A 2D illustration of the algorithm for generating the initial network, (a) step 1, imaginary subdomains, and the generated junctions, (b) step 2, internally connecting the subdomains, and (c) step 2, connecting the subdomains to make the whole RVE internally connected. In each section, the newly added components are drawn in red.

containing 5 junctions, at least 4 ligaments are required to make it internally connected. In an analogous manner, connections are added to the other subdomains until all of them become internally connected (see Figure 2.5(b)). So far, no extra calculation for checking the maximum distance constraint is required. From now on, the connections are added in such a way that they connect a random junction in a subdomain to another random junction in a neighboring subdomain (the ligaments plotted in red in Figure 2.5(c)). Each newly added ligament must decrease the number of subdomains which do not have any connection with the other subdomains. The ligaments are added between the subdomains until all the subdomains have a connection to one of their neighboring subdomains. Now, the RVE is internally connected with the minimum number of ligaments. When a connection between the subdomains is added, the maximum distance constraint of $l_{RVE}/3$ must be checked. Also, when a pair of junctions is nominated for a new connection, it must be checked that the connection does not violate the target junction valency distribution. In case of violating the maximum distance constraint or the target valency distribution, the suggested connection is rejected and replaced by another suggestion.

3. *Adding ligaments to fulfill the target junction valency distribution*

   In the last step, $(n_l - n_j + 1)$ remaining ligaments are added one-by-one to the RVE generated at the previous steps. To this end, a pair of junctions is randomly selected. If the euclidean distance between the selected junctions is less than $l_{RVE}/3$ and adding a connection between them does not violate the predefined target valency distribution, the connection is added to the network. Otherwise, another pair of junctions is tried. The junctions can freely be chosen from all the junctions within the RVE without any limitation regarding their positions. In addition, to achieve the externally connectedness, it is also allowed to select a junction from the identical ghost RVEs placed around the RVE (the RVEs demonstrated in gray in Figure 2.6). Each 3D RVE has 26 neighboring ghost RVEs. To be externally connected, the RVE must be connected to its neighboring RVEs in each

coordinate direction by at least one ligament. Externally connectedness must be checked at the end of the step. If the generated RVE is not externally connected, the whole step must be repeated.

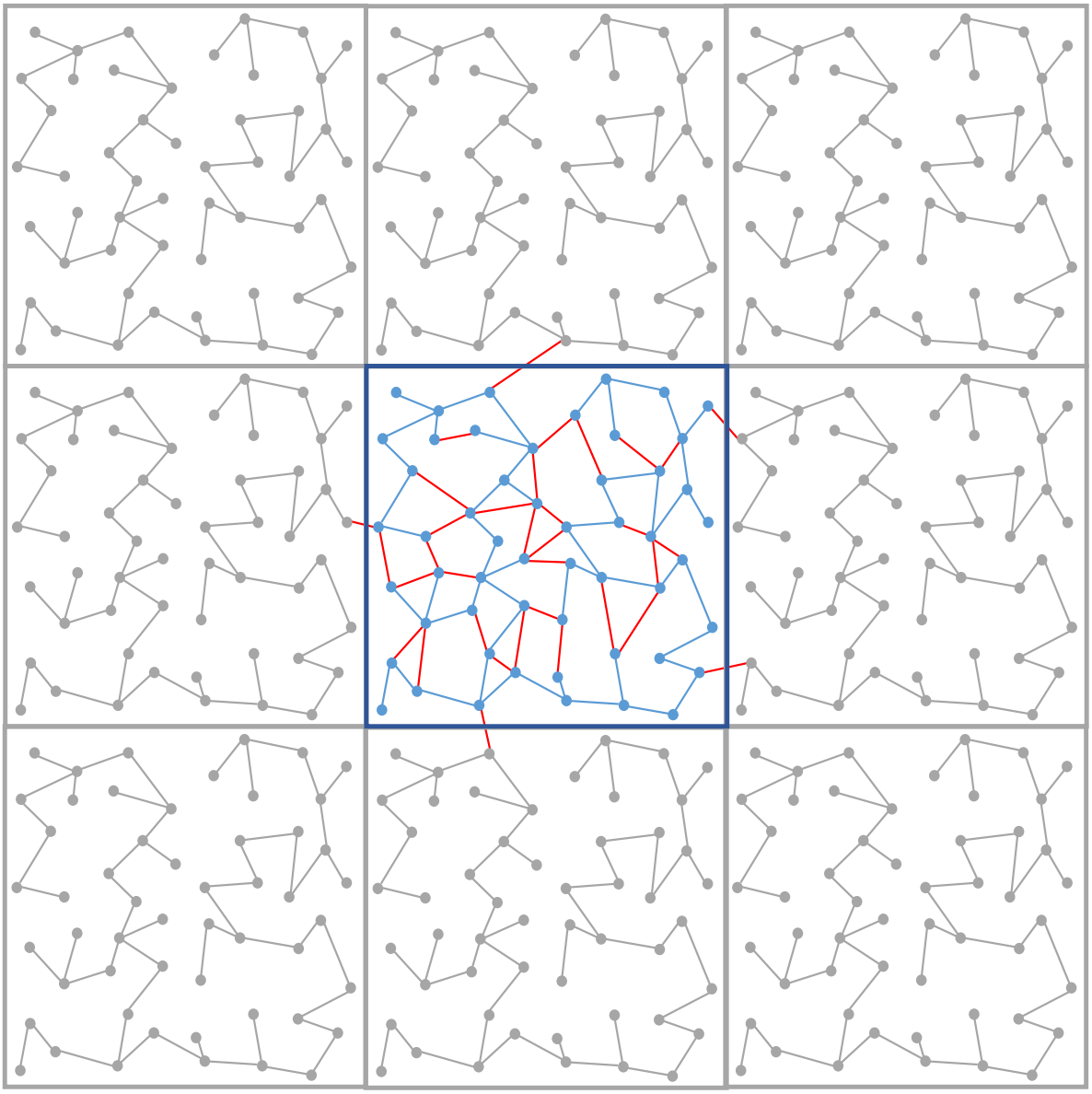

Figure 2.6: A sample 2D ligamentous network (the colorful RVE). The ligaments added to the RVE in steps 2 and 3, are plotted in red and blue, respectively. The neighboring ghost RVEs are drawn in gray.

The explained algorithm generates ligamentous RVEs with desired predefined compactness of the network and junction valency distribution. In addition, the generated RVEs are homogeneous and fully connected.

Perturbation mechanism

The perturbation mechanism determines how the changes are applied to the generated RVE. In this study, the perturbations must not change the compactness of the network, nor the junction valency distribution, nor the connectedness of the network. In addition, they must be random and compatible with the maximum distance constraint. Considering the mentioned constraints, two different perturbation mechanisms are suggested as follows:

Mechanism type 1, moving a random junction: in this mechanism, a junction within the RVE is randomly selected and moved along a random displacement vector (Figure 2.7(a)). That means, both the magnitude and the direction of the displacement vector are random. To apply a small perturbation, the maximum magnitude of the displacement vector is assumed to be $L_{RVE}/20$. This perturbation mechanism may violate the maximum distance constraint. Therefore, after the perturbation, the euclidean distances between the translated junction and all its adjacent junctions must be checked. In case of violating the constraint, the suggested solution is rejected and replaced by another suggestion.

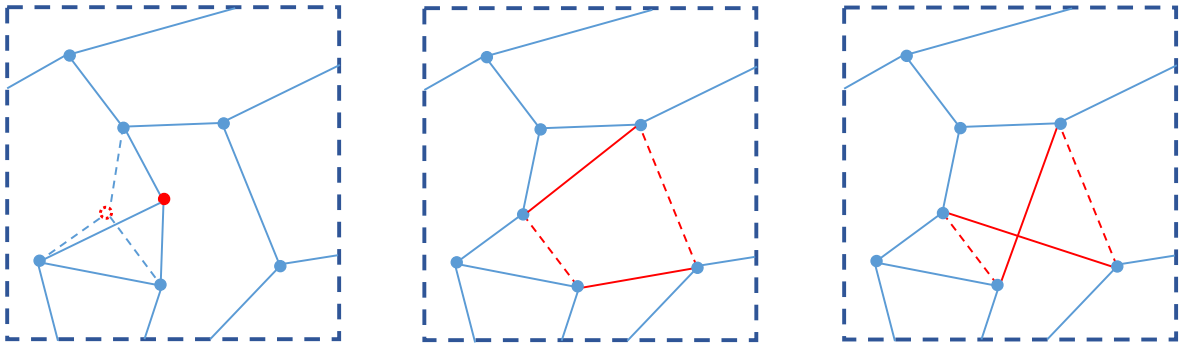

(a) (b) (c)

Figure 2.7: Perturbation mechanism (a) type 1, and (b, c) type 2. The perturbed components are plotted in red. Dashed and solid lines indicate the components before and after perturbation, respectively.

Mechanism type 2, shifting the connections between two pairs of adjacent junctions: in this mechanism, a pair of random ligaments is deleted and then a new pair is added. The added ligaments must connect the respective junctions of the deleted ligaments. Therefore, for each pair of deleted ligaments, there are two alternative pairs for adding. The two alternatives for a pair of deleted ligaments in a sample 2D network are depicted in Figure 2.7(b) and (c). This perturbation mechanism does not change the network's compactness, nor the junction valency distribution. However, the distances between the new adjacent junctions and the connectedness of the perturbed network must be checked. If the maximum distance constraint is violated or the new configuration is not fully connected, the suggested solution is rejected, and another solution must be suggested.

Energy function

To compare the suggested solution with the optimum solution or with the current solution, a measure is required. That is the energy function E which can generally be expressed as

$$E = \sum_{m=1}^{n_d} w_m \cdot E_m, \tag{2.7}$$

where n_d is the number of descriptors optimizing by SA. E_m is the energy function of the m-th descriptors and w_m is its corresponding weighting coefficient. In the current study, $n_d = 2$ since SA optimizes the two descriptors of adjacent junctions' distance distribution L and direction cosine distribution C. Therefore, the Eq. (2.7) can be written as

$$E = w_L \cdot E_L + w_C \cdot E_C. \tag{2.8}$$

E_L and E_C are measured via the Cramer-von Mises test [68] as

$$E_L = \frac{1}{12n_L} + \sum_{i=1}^{n_L} \left[\frac{2i-1}{2n_L} - c_L(x_{Li}) \right]^2, \tag{2.9}$$

and

$$E_C = \frac{1}{12n_C} + \sum_{i=1}^{n_C} \left[\frac{2i-1}{2n_C} - c_C(x_{Ci}) \right]^2. \tag{2.10}$$

In Eq. (2.9), c_L is the cumulative distribution function of adjacent junctions' distance and x_{Li} are its realizations. n_L is the number of realizations of L which equals the number of ligaments, $n_L = n_l$. Similarly, in Eq. (2.10), c_C is the cumulative distribution function of direction cosine and x_{Ci} are its realizations. n_C is the number of realizations of C. That is

$$n_C = \frac{1}{2} \sum_{i=1}^{n_j} v_i \times (v_i - 1). \tag{2.11}$$

Cooling schedule

If the perturbation results in a decrease in the energy function, the current network is replaced by the perturbed network. Because a network with lower energy function is more similar to the desired network. However, SA may replace the current network with a perturbed network with higher energy function. This probability is controlled by a cooling schedule and decreases during the optimization procedure. Among the various schedules proposed in the literature, the following function is employed in this dissertation

$$T_i = T_0 \cdot d_r^{(i-1)}, \tag{2.12}$$

where T_0 and T_i are the initial temperature and the temperature at the i-th iteration, respectively and, d_r is the decay rate. Here, the initial temperature T_0 is considered to be 1 and the decay rate d_r is set to 0.9. Note that the proper value of these parameters can be different for various problems. There are not any predetermined values for them, however suggestions can be found in the literature [69].

Considering the defined cooling schedule, the chance of accepting a perturbed network at i-th iteration p^i_{accept} is expressed as

$$p^i_{accept}(\Delta E) = \begin{cases} 1 & \Delta E \leq 0 \\ exp(-\Delta E/T_i), & \Delta E > 0 \end{cases}, \tag{2.13}$$

where $\Delta E = E_i - E_{i-1}$.

Cut-off criterion

In this study, the maximum number of iterations is $1,000,000$ ($i_{max} = 1,000,000$). The minimum acceptable precision is attained if the energy function of each descriptor be less than 0.01 (i.e., $E_L < 0.01$ and $E_C < 0.01$). Accordingly, each of these criteria fulfilled sooner terminates the SA.

Now, the simulated annealing method is completely determined and can be used to generate tailor-made ligamentous networks. An overall network structure of a sample RVE generated by the first step of the proposed approach is plotted in Figure 2.8(a).

In this dissertation, considering different target descriptors of network level, more than 2500 sample RVEs are generated, and their mechanical properties are calculated. The corresponding numerical results are presented in Paper A.

2.3.2 Stage 2, assigning the components' geometry

At the first stage, employing the simulated annealing method, ligamentous microstructures with desired predefined descriptors are generated. In that stage, the ligamentous RVEs are generated without considering the shape of junctions and ligaments. In other words, at the first stage of the proposed approach, the junctions and the ligaments are modeled as points and line segments, respectively. Although it is only a simplified model of ligamentous materials with complex microstructure, it provides a valuable understanding of these materials (see Paper A). At the second stage of the proposed approach, the component level descriptors are assigned to the ligamentous microstructure generated at the first stage. The component level descriptors considered in this thesis are: i) junction's radius distribution, ii) ligament's cross-section radius, and iii) ligament's curvature (definitions presented in 2.1.2). In the following, it is explained how they are assigned to the overall network structure.

Radius of junctions

The junctions are modeled as spheres and a probability distribution function is defined for the junctions' radius. The probability distribution function, named r_j, determines the likelihood of the junctions' radius in the interval of $[r_{min}, r_{max}]$. To assign radius to the junction based on the predefined distribution, first, a set of n_j discrete values in the range of $[r_{min}, r_{max}]$ is generated. The generated set must have the same probability distribution as r_j (for more details, refer to Paper B). Then, each element of the generated set is randomly assigned to a junction. The value of this element is the radius of the corresponding junction.

Radius of Ligaments

Using Eq. (2.2) and setting the d_i^k, ligaments with desired cross-section radius can be generated. It is assumed that the ligament's cross-section radius at its start and end points is equal to the radius of the respective junctions. For example, consider the k-th ligament, illustrated in Figure 2.3, which starts at the s-th junction and ends at the q-th junction. The cross-section radius of the k-th ligament at its start and end points is

$$r_l^k(x^k)|_{x^k=0} = r_j^s, \qquad r_l^k(x^k)|_{x^k=l^k} = r_j^q, \tag{2.14}$$

where r_j^s and r_j^q are the radius of the s-th and the q-th junctions, respectively.

In this study, setting i_{max} in Eq. (2.2) to 2, the ligaments' cross-section radius is modeled by quadratic polynomials as

$$r_l^k(x^k) = d_2^k(x^k)^2 + d_1^k x^k + d_0^k. \tag{2.15}$$

Setting the coefficient d_2^k to desired values, the coefficients d_1^k and d_0^k are determined by the relations presented in Eq. (2.14). Note that for a convex, concave, and conical ligament shape, the coefficient d_2^k is negative, positive, and zero, respectively.

Curvature of Ligaments

In this thesis, for simplicity, only the ligaments with sinusoidal curvature are studied. That means, in Eq. (2.4), $f_{max} = 1$ and $a_0^k = a_1^k = 0$. Accordingly, the equation (2.4) can be rewritten as

$$y^k(x^k) = b_1^k \, sin\left(\frac{\pi x^k}{l^k}\right). \tag{2.16}$$

Setting the free parameter b_1^k to different values, ligaments with various curvatures can be modeled. Note that the Eq. (2.16) is defined in the local coordinate system $x^k y^k z^k$ corresponding to the k-th ligament. The x^k-axis connects the two junctions confining the k-th ligament and the curved ligament is positioned entirely in the $x^k y^k$-plane. Mapping from the local to the global coordinate system can be performed by a translation followed by a series of rotations (details are presented in Paper B).

It should be mentioned that, at the second stage of the proposed approach, each ligament is shaped independently; hence in case of RVEs with high number of ligaments or complex ligaments' geometry, parallel computing can be performed.

A sample RVE with curved convex ligaments generated by the proposed two-stage approach is plotted in Figure 2.8.

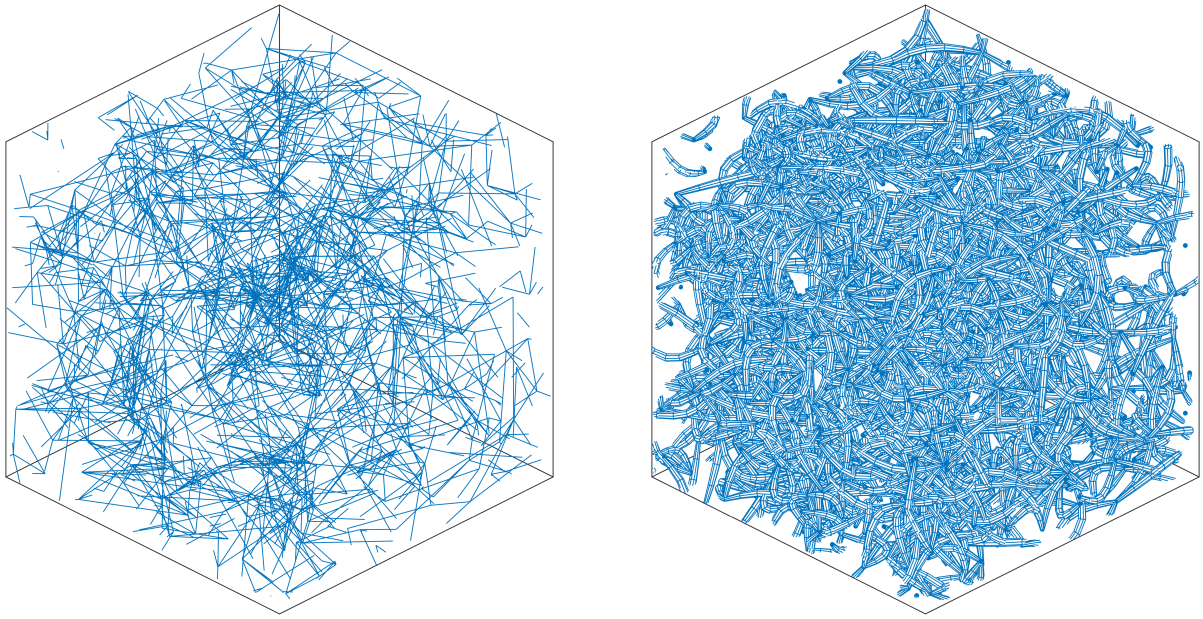

(a) (b)

Figure 2.8: A sample ligamentous RVE generated by the proposed approach in this dissertation at the end of its (a) first, and (b) second stages.

Combining different values of descriptors at both network and component levels, 4940 sample RVEs are generated. Their mechanical properties are calculated by the finite element method and the numerical results are investigated in Paper B.

3 Summary of publications

This paper-based dissertation is written based on the publications Paper A [66] and Paper B [67]:

- I. Davoodi Kermani, M. Schmitter, J. F. Eichinger, R. C. Aydin, C. J. Cyron. Computational study of the geometric properties governing the linear mechanical behavior of fiber networks. *Computational Materials Science*, 199:110711, 2021.
- I. Davoodi Kermani, L. Dyckhoff, R. C. Aydin, N. Huber, C. J. Cyron. Simulated annealing framework for generating representative volume elements of materials with complex ligamentous microstructures. *Computational Materials Science*, 228:112302,2023.

A summary and the authors' contributions of these publications are presented in this chapter and their full texts are reprinted in Appendix A.

3.1 Paper A

Computational study of the geometric properties governing the linear mechanical behavior of fiber networks

Iman Davoodi Kermani, Maximilian Schmitter, Jonas F. Eichinger, Roland C. Aydin, Christian J. Cyron

3.1.1 Summary

Fiber microstructures, due to their widespread applications in biological and engineering materials, gained an increasing attention in recent years. Therefore, many studies focused on generating, characterization, and analysis of fibrous materials. However, the mechanical behavior of these materials is still not completely determined. To enable this study, it is required to develop a model of fibrous networks. The complexity of random fiber microstructures made it almost impossible to develop a theoretical model of these structures. Therefore, the initial step to study the mechanical properties of a fiber network would be to develop a computationally efficient model of the network.

In this study, based on the simulated annealing optimization method, we proposed a network generating algorithm which can generate tailor-made representative volume elements (RVEs) of fiber microstructures. The generated fiber microstructures form a continuous fiber phase both within a single RVE and within the larger material volumes resulted by repetition of the RVE in one or more directions aligned with its edges. Furthermore, the generated RVEs by the suggested approach are homogeneous and isometric.

Using the suggested method and considering the number of fibers per volume, the nodes' valency distribution, the fibers' length distribution, and the direction cosine distribution as target descriptors, more than 2500 sample RVEs are generated. The macromechanical properties of all these RVEs are calculated by finite element method. This provided sufficient materials to perform a comprehensive study regarding the relation between the macroscopic mechanical properties and microstructural descriptors of the fiber networks. This investigation indicated that the macroscopic Young's modulus and Poisson's ratio of the network will be determined by determining the four mentioned descriptors.

Based on the numerical results of the finite element analysis, the Young's modulus increases with increasing the mean valency. However, the macroscopic stiffness of the network decreases with increasing the averaged fibers' length or increasing the mean value of the direction cosine distribution. The linear dependency of Young's modulus on the number of fibers per volume is explained by a simple theoretical analysis. The results indicated that the Poisson's ratio does not change significantly with variation of the studied descriptors.

3.1.2 Author contributions

Iman Davoodi Kermani designed the study and developed the Matlab code for generating the RVE of fiber network. The finite element code was developed by Maximilian Schmitter. Iman Davoodi Kermani carried out all the computations and plotted the results. The methodology and

analysis were done based on critical discussions between Iman Davoodi Kermani and Christian J. Cyron. The manuscript was initially prepared by Iman Davoodi Kermani and finalized after critical feedback and contribution provided by other authors.

3.2 Paper B

Simulated annealing framework for generating representative volume elements of materials with complex ligamentous microstructures

Iman Davoodi Kermani, Lena Dyckhoff, Roland C. Aydin, Norbert Huber,
Christian J. Cyron

3.2.1 Summary

Various materials, from nanoporous metals to biological tissues, are formed by ligamentous microstructure. In real examples, the ligaments within a ligamentous material have complex geometries. They are curved and have variable cross-section area. In addition, in many examples of ligamentous microstructures, the overall network is completely random although they may have some specific characteristics. Therefore, it is computationally expensive to develop a model which can produce representative volume elements (RVEs) of ligamentous materials considering all these complexities.

Despite multitudinous research in modeling of ligamentous microstructures, there is not yet a general and efficient approach to generate these microstructures with desired descriptors. In this paper, we proposed an efficient two-stage network generating approach which produces representative volume elements of ligamentous networks with predefined descriptors of both network and component levels.

The first stage of this approach generated an overall structure of the network considering the descriptors: i) number of ligaments per volume, ii) junctions' valency distribution, iii) adjacent junctions' distance distribution, and iv) direction cosine distribution. At this stage, similar to the approach presented in Paper A [66], the simulated annealing optimization method was applied to generate the overall network microstructure.

At the second stage, we assigned the descriptors of component level to the overall network structure produced at the first stage. The component level descriptors considered at this stage were: i) the junction's radius distribution, ii) ligaments cross-section radius, and iii) ligaments curvature. We used fundamental mathematical functions to describe the ligaments' thickness and curvature. This enabled the approach to produce ligamentous microstructures with a large variety of ligaments shapes.

To indicate the ability and efficiency of this approach in generating networks of ligaments, we generated more than 4900 sample RVEs with various microstructural descriptors. The mechanical behavior of generated RVEs were studied by the finite element method. The numerical results provided valuable information regarding the relation between macroscopic mechanical properties and microstructural descriptors. It was indicated that the famous Gibson-Ashby scaling law [70] which is commonly used to model the mechanical properties of porous materials, cannot consistently predict the properties. Therefore, a modified version of this scaling law was suggested.

3.2.2 Author contributions

Iman Davoodi Kermani designed the framework and developed the numerical code for generating the ligamentous representative volume elements. Lena Dyckhoff and Norbert Huber developed the finite element code and performed the mechanical calculations of the RVEs generated by Iman Davoodi Kermani. Christian J. Cyron contributed to the conceptualization and methodology. Iman Davoodi Kermani plotted the figures and discussed them with Christian. J. Cyron and Norbert Huber. Iman Davoodi Kermani drafted the manuscript and other authors reviewed it and provided valuable comments.

4 Conclusion and Outlook

4.1 Conclusion

Various materials from biological tissues to industrial materials have ligamentous microstructures. Due to the specific characteristics and diverse applications of ligamentous materials, many research has focused on the analysis of their mechanical behavior. Therefore, numerous studies have been carried out to develop theoretical or numerical models of ligament networks. However, it is not yet clearly determined which microstructural descriptors and to what extent determine the macromechanical properties of ligamentous materials. To find the answer to this question, it is necessary to be able to generate representative volume elements of these materials which are sufficiently large to represent the material properties though they are as small as possible for the sake of computational costs.

In this thesis, a two-stage computationally efficient approach was proposed which for the first time can generate representative volume element of ligamentous microstructures with predefined descriptors of both network and ligament level. This approach provides a very general framework which can be applied to different descriptors with different target values. Since the RVEs are generated randomly, they are homogeneous and isometric. Moreover, the ligaments within an RVE form a bicontinuous microstructure. In addition, the ligament phase is continuous in larger material volumes resulted from the repetition of RVE in one of the three directions aligned with its edges.

In the first stage of this approach, it was assumed that all the ligaments are straight and have a constant cross-section radius. A numerical optimization method called simulated annealing was used to generate fiber microstructures with desired predefined descriptors. Considering different values for the descriptors: i) number of fibers per volume, ii) junctions' valency distribution, iii) adjacent junctions' distance distribution, and iv) direction cosine distribution, more than 2500 sample RVEs of fiber networks were generated. The relation between these descriptors and macromechanical properties of the generated RVEs was studied by the numerical results of the finite element analysis. This study indicated that the four mentioned descriptors largely determine the linear mechanical properties, Young's modulus and Poisson's ratio. Interestingly, it showed that by determining these descriptors, some other morphological or graph-theory-based [71, 72, 73, 74] descriptors are determined.

The numerical results of this stage, presented in Paper A, revealed that there is a linear relation between the number of fibers per volume and the macroscopic Young's modulus explained by a simple theoretical analysis. Based on the numerical results at this stage, it was found that the Young's modulus of fibrous networks depends on the *mean value* of junctions' valency, adjacent junctions' distance, and direction cosine distributions but not on the corresponding *distributions*. In these networks, the stiffness increases in a quadratic manner with increasing the mean valency where it decreases linearly with increasing mean adjacent junctions' distance and mean direction

cosine. The numerical results also indicated that, i) the dependency of Young's modulus on the fiber density and junctions' valency is higher compared to the other two descriptors and, ii) the dependency of Young's modulus on the studied descriptors is much stronger than the dependency of Poisson's ratio.

In the second stage of this approach, the ligaments' geometry was added to the networks generated at the first stage. The junctions are modeled as spheres and the ligaments as curved cylinders with variable cross-section radius along their centerlines. Therefore, the component level descriptors considered in this model can be listed as: i) junctions' radius, ii) ligaments' cross-section radius and, iii) ligaments' curvature. Since the geometry of each ligament is defined individually and independent of the other ligaments, the microstructures with complex geometries can be modeled by performing parallel computations. Considering different values of network and component level descriptors, nearly 5000 realizations of ligamentous microstructures were generated, and finite element analysis was used to investigate the scaling relation between microstructural descriptors and stiffness of the generated RVEs (see Paper B).

The comparison of numerical results with the Gibson-Ashby scaling law [70], a scaling relation which is commonly used to model the mechanical properties of nonporous materials, revealed that this scaling law is not valid for the cases in which the solid fraction changes due to a change of the network architecture. For instance, in the networks with constant volume fraction, the Young's modulus decreases linearly with increasing the number of ligaments. This study became possible for the first time because the approach proposed in this dissertation can control the descriptors of generated RVEs; hence it enables generating a large number of microstructures which are different only in one descriptor. Therefore, this approach enables the study of the relation between macroscopic material properties and every single descriptor. Despite the fact that the Gibson-Ashby scaling law is not valid for all cases, some numerical results are in agreement with the available studies. For example, in the networks with fixed topology and for the case in which all the junctions have the same radius, the macroscopic stiffness increases with increasing the radius of ligaments with a power law whose component varies between 1 and 2 which is in agreement with [30]. The macroscopic stiffness showed a similar behavior to the change of ligaments' convexity. In contrast, the dependency of macroscopic stiffness on the ligaments' curvature can be modeled as a power law with a negative component which is in agreement with [31].

4.2 Outlook

In this section, some of the potential future research based on the approach proposed in this thesis are presented. In addition, it is explained how the suggested approach can be generalized and improved.

At both stages of this approach, only the linear mechanical properties of ligament networks are investigated. However, large deformation, plasticity, and failure of ligament networks strongly depend on their microstructure [54, 75, 76]. Therefore, a substantial future step in realization of mechanical behavior of ligamentous materials can be the mechanical analysis of such networks at large deformation.

The mechanical properties of nonporous metals are usually described by a scaling law originally suggested by Gibson-Ashby [70]. Similarly, in this thesis, the numerical results of the proposed approach are compared with the modified versions of this law presented in the literature (see Paper B). Since, for the first time it was possible to produce random ligamentous RVEs with predefined descriptors, a more detailed study about the relation of microstructural descriptors and macromechanical properties was performed. It was concluded that the Gibson-Ashby scaling law in its present format is not consistently valid. Therefore, a modified version of this scaling law was proposed. Although nearly 5000 realizations of ligamentous RVEs were generated and studied to determine the scaling behavior of mechanical properties, much more realizations are required to completely specify the modified version of Gibson-Ashby scaling law. Such a comprehensive investigation can be a potential future work.

In this dissertation, to reduce the complexity of numerical model, the interpenetrating of ligaments is not taken into consideration for modeling. Although this simplification may not have a significant effect on the networks with low volume fractions, the interpenetration of ligaments in the networks with high volume fractions is inevitable. Therefore, an extension to the proposed two-stage approach would be the model in which the interpretation of the ligaments is taken into the calculations.

Furthermore, the contact between the fibers within a network is highly likely, especially at large deformations. However, due to its complexity, this phenomenon is not considered in numerical modeling presented in this thesis. Investigation of ligamentous networks under various loading conditions with consideration of contact between the deformed ligaments can be a potential future study to complete the results of the current research.

Bibliography

[1] K. Jansen, A. Licup, A. Sharma, R. Rens, F. MacKintosh, and G. Koenderink. The role of network architecture in collagen mechanics. *Biophysical Journal*, 114:2665–2678, 2018.

[2] S. B. Lindström, D. A Vader, A. Kulachenko, and D. A. Weitz. Biopolymer network geometries: Characterization, regeneration, and elastic properties. *Physical Review E*, 82, 2010.

[3] T. Jin and I. Stanciulescu. Numerical simulation of fibrous biomaterials with randomly distributed fiber network structure. *Biomechanics and Modeling in Mechanobiology*, 15:817–830, 2015.

[4] H. Hatami-Marbini. Simulation of the mechanical behavior of random fiber networks with different microstructure. *The European Physical Journal E*, 41:817–830, 2018.

[5] C. Cyron, K. Müller, A. Bausch, and W. Wall. Micromechanical simulations of biopolymer networks with finite elements. *Journal of Computational Physics*, 244:236–251, 2013.

[6] S. B. Lindström, A. Kulachenko, L. M. Jawerth, and D. A. Vader. Finite-strain, finite-size mechanics of rigidly cross-linked biopolymer networks. *Soft Matter*, 9:7302–7313, 2013.

[7] P. R. Onck, T. Koeman, T. van Dillen, and E. van der Giessen. Alternative explanation of stiffening in cross-linked semiflexible networks. *Physical Review Letters*, 95, 2005.

[8] A. Kabla and L. Mahadevan. Nonlinear mechanics of soft fibrous networks. *Journal of The Royal Society Interface*, 4:99–106, 2006.

[9] G. Žagar, P. R. Onck, and E. van der Giessen. Elasticity of rigidly cross-linked networks of athermal filaments. *Macromolecules*, 44, 2011.

[10] M. Vahabi, A. Sharma, A. Licup, A. van Oosten, P. Galie, P. Janmey, and F. MacKintosh. Elasticity of fibrous networks under uniaxial prestress. *Soft Matter*, 12:5050–5060, 2016.

[11] E. M. Huisman, T. van Dillen, P. R. Onck, and E. van der Giessen. Three-dimensional cross-linked f-actin networks: Relation between network architecture and mechanical behavior. *Physical Review Letters*, 99, 2007.

[12] P. Taufalele, J. VanderBurgh, A. Muñoz, M. Zanotelli, and C. Reinhart-King. Fiber alignment drives changes in architectural and mechanical features in collagen matrices. *PLOS ONE*, 14:e0216537, 2019.

[13] Z. Zhang, Y. Wang, Z. Qi, W. Zhang, J. Qin, and J. Frenzel. Generalized fabrication of nanoporous metals (au, pd, pt, ag, and cu) through chemical dealloying. *The Journal of Physical Chemistry C*, 113:12629–12636, 2009.

[14] R. Xia, X. Feng, and G. Wang. Effective elastic properties of nanoporous materials with hierarchical structure. *Acta Materialia*, 59:6801–6808, 2011.

[15] R. Xia, R. Wu, Y. Liu, and X. Sun. The role of computer simulation in nanoporous metals—a review. *Materials*, 8:5060–5083, 2015.

[16] Y. Ji, Y. Xing, F. Zhou, X. Li, Y. Chen, and L. Shao. The mechanical characteristics of monolithic nanoporous copper and its composites. *Advanced Engineering Materials*, 20:1800574, 2018.

[17] Y. X. Gan, Y. Zhang, and J. B. Gan. Nanoporous metals processed by dealloying and their applications. *AIMS Materials Science*, 5:1141–1183, 2018.

[18] C. Richert and N. Huber. A review of experimentally informed micromechanical modeling of nanoporous metals: From structural descriptors to predictive structure–property relationships. *Materials*, 13:3307, 2020.

[19] H. Rösner, S. Parida, D. Kramer, C. Volkert, and J. Weissmüller. Reconstructing a nanoporous metal in three dimensions: An electron tomography study of dealloyed gold leaf. *Advanced Engineering Materials*, 9:535–541, 2007.

[20] Z. Qi and J. Weissmüller. Hierarchical nested-network nanostructure by dealloying. *ACS Nano*, 7:5948–5954, 2013.

[21] Z. Qi, U. Vainio, A. Kornowski, M. Ritter, H. Weller, H. Jin, and J. Weissmüller. Porous gold with a nested-network architecture and ultrafine structure. *Advanced Functional Materials*, 25:2530–2536, 2015.

[22] E. Larsson, D. Gürsoy, F. De Carlo, E. Lilleodden, M. Storm, F. Wilde, K. Hu, M. Müller, and I. Greving. Nanoporous gold: a hierarchical and multiscale 3d test pattern for characterizing x-ray nano-tomography systems. *Journal of Synchrotron Radiation*, 26:194–204, 2019.

[23] J. Weissmüller, R. Newman, H. Jin, A. Hodge, and J. Kysar. Nanoporous metals by alloy corrosion: Formation and mechanical properties. *MRS Bulletin*, 34:577–586, 2009.

[24] A. Odermatt, C. Richert, and N. Huber. Prediction of elastic-plastic deformation of nanoporous metals by fem beam modeling: A bottom-up approach from ligaments to real microstructures. *Materials Science and Engineering: A*, 791:139700, 2020.

[25] M. Nasr Esfahani and M. Jabbari. Molecular dynamics simulations of deformation mechanisms in the mechanical response of nanoporous gold. *Materials*, 13:2071, 2020.

[26] A. Mathur and J. Erlebacher. Size dependence of effective young's modulus of nanoporous gold. *Applied Physics Letters*, 90:061910, 2007.

[27] G. Pia and F. Delogu. Nanoporous au: Statistical analysis of morphological features and evaluation of their influence on the elastic deformation behavior by phenomenological modeling. *Acta Materialia*, 85:250–260, 2015.

[28] N. Huber. Connections between topology and macroscopic mechanical properties of three-dimensional open-pore materials. *Frontiers in Materials*, 5, 2018.

[29] G. Pia and F. Delogu. Mechanical properties of nanoporous au: From empirical evidence to phenomenological modeling. *Metals*, 5:1665–1694, 2015.

[30] N. Huber, R. N. Viswanath, N. Mameka, J. Markmann, and J. Weißmüller. Scaling laws of nanoporous metals under uniaxial compression. *Acta Materialia*, 67:252–265, 2014.

[31] B. Roschning and N. Huber. Scaling laws of nanoporous gold under uniaxial compression: Effects of structural disorder on the solid fraction, elastic poisson's ratio, young's modulus and yield strength. *Journal of the Mechanics and Physics of Solids*, 92:55–71, 2016.

[32] V. Kouznetsova, M. Geers, and W. Brekelmans. Multi-scale constitutive modelling of heterogeneous materials with a gradient-enhanced computational homogenization scheme. *International Journal for Numerical Methods in Engineering*, 54:1235–1260, 2002.

[33] T. Kanit, S. Forest, I. Galliet, V. Mounoury, and D. Jeulin. Determination of the size of the representative volume element for random composites: statistical and numerical approach. *International Journal of Solids and Structures*, 40:3647–3679, 2003.

[34] L. T. Harper, C. Qian, T. A. Turner, S. Li, and N. A. Warrior. Representative volume elements for discontinuous carbon fibre composites – part 1: Boundary conditions. *Composites Science and Technology*, 72:225–234, 2012.

[35] L. T. Harper, C. Qian, T. A. Turner, S. Li, and N. A. Warrior. Representative volume elements for discontinuous carbon fibre composites – part 2: Determining the critical size. *Composites Science and Technology*, 72:204–210, 2012.

[36] K. Hu, M. Ziehmer, K. Wang, and E. T. Lilleodden. Nanoporous gold: 3d structural analyses of representative volumes and their implications on scaling relations of mechanical behaviour. *Philosophical Magazine*, 96:3322–3335, 2016.

[37] C. Soyarslan, S. Bargmann, M. Pradas, and J. Weissmüller. 3d stochastic bicontinuous microstructures: Generation, topology and elasticity. *Acta Materialia*, 149:326–340, 2018.

[38] K. Schneider. *Computational micromechanics of matrix-inclusion composites*. Dr.-ing. thesis, Technischen Universität Hamburg (TUHH), 2019.

[39] Y. Jiao, F. Stillinger, and S. Torquato. Modeling heterogeneous materials via two-point correlation functions: Basic principles. *Physical Review E*, 76, 2007.

[40] Y. Jiao, F. Stillinger, and S. Torquato. Modeling heterogeneous materials via two-point correlation functions. ii. algorithmic details and applications. *Physical Review E*, 77, 2008.

[41] G. Papakosta, J. Nolan, N. Vordos, D. Gkika, M. Kainourgiakis, and A. Mitropoulos. On 3d reconstruction of porous media by using spatial correlation functions. *Journal of Engineering Science and Technology Review*, 8, 2015.

[42] Y. Liu, M. Steven Greene, W. Chen, D. Dikin, and W. Liu. Computational microstructure characterization and reconstruction for stochastic multiscale material design. *Computer-Aided Design*, 45:65–76, 2013.

[43] A. Roberts. Statistical reconstruction of three-dimensional porous media from two-dimensional images. *Physical Review E*, 56:3203–3212, 1997.

[44] D. Chen, X. He, Q. Teng, Z. Xu, and Z. Li. Reconstruction of multiphase microstructure based on statistical descriptors. *Physica A: Statistical Mechanics and its Applications*, 415:240–250, 2014.

[45] M. Rintoul and S. Torquato. Reconstruction of the structure of dispersions. *Journal of Colloid and Interface Science*, 186:467–476, 1997.

[46] C. Yeong and S. Torquato. Reconstructing random media. ii. three-dimensional media from two-dimensional cuts. *Physical Review E*, 58:224–233, 1998.

[47] M. Hakamada and M. Mabuchi. Mechanical strength of nanoporous gold fabricated by dealloying. *Scripta Materialia*, 56:1003–1006, 2007.

[48] A. C. To, J. Tao, M. Kirca, and L. Schalk. Ligament and joint sizes govern softening in nanoporous aluminum. *Applied Physics Letters*, 98:051903, 2011.

[49] J. Jiao and N. Huber. Deformation mechanisms in nanoporous metals: Effect of ligament shape and disorder. *Computational Materials Science*, 127:194–203, 2017.

[50] N. Badwe, X. Chen, and K. Sieradzki. Mechanical properties of nanoporous gold in tension. *Acta Materialia*, 129:251–258, 2017.

[51] S. Chen, H. Li, and Y. Jiao. Dynamic reconstruction of heterogeneous materials and microstructure evolution. *Physical Review E*, 92, 2015.

[52] M. Yang, A. Nagarajan, B. Liang, and S. Soghrati. New algorithms for virtual reconstruction of heterogeneous microstructures. *Computer Methods in Applied Mechanics and Engineering*, 338:275–298, 2018.

[53] J. Feng, C. Li, S. Cen, and D. Owen. Statistical reconstruction of two-phase random media. *Computers & Structures*, 137:78–92, 2014.

[54] D. Li. Review of structure representation and reconstruction on mesoscale and microscale. *JOM*, 66:444–454, 2014.

[55] R. Bostanabad, Y. Zhang, X. Li, T. Kearney, L. Brinson, D. Apley, W. Liu, and W. Chen. Computational microstructure characterization and reconstruction: Review of the state-of-the-art techniques. *Progress in Materials Science*, 95:1–41, 2018.

[56] C. Yeong and S. Torquato. Reconstructing random media. *Physical Review E*, 57:495–506, 1998.

[57] H. Kumar, C. Briant, and W. Curtin. Using microstructure reconstruction to model mechanical behavior in complex microstructures. *Mechanics of Materials*, 38:818–832, 2006.

[58] L. Pant, S. Mitra, and M. Secanell. Multigrid hierarchical simulated annealing method for reconstructing heterogeneous media. *Physical Review E*, 92, 2015.

[59] A.P. Roberts and E. J. Garboczi. Elastic properties of model random three-dimensional open-cell solids. *Journal of the Mechanics and Physics of Solids*, 50:33–55, 2002.

[60] S. Domaschke, M. Zündel, E. Mazza, and A. E. Ehret. A 3d computational model of electrospun networks and its application to inform a reduced modelling approach. *International Journal of Solids and Structures*, 158:76–89, 2019.

[61] C. Richert, A. Odermatt, and N. Huber. Computation of thickness and mechanical properties of interconnected structures: Accuracy, deviations, and approaches for correction. *Frontiers in Materials*, 6, 2019.

[62] J. F. Eichinger, M. J. Grill, I. Davoodi Kermani, R. C. Aydin, W. A. Wall, J. D Humphrey, and C. J. Cyron. A computational framework for modeling cell–matrix interactions in soft biological tissues. *Biomechanics and Modeling in Mechanobiology*, 20:1851–1870, 2021.

[63] J. Biener, A. M. Hodge, J. R. Hayes, C. A. Volkert, L. A. Zepeda-Ruiz, A. V. Hamza, and F. F. Abraham. Size effects on the mechanical behavior of nanoporous au. *Nano Letters*, 6:2379–2382, 2006.

[64] X.-Y. Sun, G.-K. Xu, X. Li, X.-Q. Feng, and H. Gao. Mechanical properties and scaling laws of nanoporous gold. *Journal of Applied Physics*, 113:023505, 2013.

[65] C. Richert and N. Huber. Skeletonization, geometrical analysis, and finite element modeling of nanoporous gold based on 3d tomography data. *Metals*, 8:282, 2018.

[66] I. Davoodi Kermani, M. Schmitter, J. F. Eichinger, R. C. Aydin, and C. J. Cyron. Computational study of the geometric properties governing the linear mechanical behavior of fiber networks. *Computational Materials Science*, 199:110711, 2021.

[67] I. Davoodi Kermani, L. Dyckhoff, R. C. Aydin, N. Huber, and C. J. Cyron. Simulated annealing framework for generating representative volume elements of materials with complex ligamentous microstructures. *Computational Materials Science*, 228:112302, 2023.

[68] S. B. Lindström, D. Vader, A. Kulachenko, and D. Weitz. Biopolymer network geometries: Characterization, regeneration, and elastic properties. *Physical Review E*, 82, 2010.

[69] W. Ben-Ameur. Computing the initial temperature of simulated annealing. *Computational Optimization and Applications*, 29:369–385, 2004.

[70] L. J. Gibson and M. F. Ashby. *Cellular Solids: Structure and Properties*. Cambridge University Press, 1997.

[71] D. West. *Introduction to graph theory*. Prentice-Hall of India Private Limited, New Delhi, 2005.

[72] L. Li, D. Alderson, J. Doyle, and W. Willinger. Towards a theory of scale-free graphs: Definition, properties, and implications. *Internet Mathematics*, 2:431–523, 2005.

[73] A. Brouwer and W. Haemers. *Spectra of graphs*. Springer, New York, 2012.

[74] G. Chalancon, K. Kruse, and M. Babu. *Clustering Coefficient*, pages 422–424. Springer New York, New York, 2013.

[75] D. Lyu and S. Li. Multiscale crystal defect dynamics: A coarse-grained lattice defect model based on crystal microstructure. *Journal of the Mechanics and Physics of Solids*, 107, 2017.

[76] D. Lyu and S. Li. A multiscale dislocation pattern dynamics: Towards an atomistic-informed crystal plasticity theory. *Journal of the Mechanics and Physics of Solids*, 122, 2019.

A Full text of publications

A.1 Paper A

Computational study of the geometric properties governing the linear mechanical behavior of fiber networks

Iman Davoodi Kermani, Maximilian Schmitter, Jonas F. Eichinger, Roland C. Aydin, Christian J. Cyron

published in

Computational Materials Science, 10.1016/j.commatsci.2021.110711

Computational Materials Science 199 (2021) 110711

Contents lists available at ScienceDirect

Computational Materials Science

journal homepage: www.elsevier.com/locate/commatsci

Computational study of the geometric properties governing the linear mechanical behavior of fiber networks

Iman Davoodi Kermani [a], Maximilian Schmitter [b], Jonas F. Eichinger [a,b], Roland C. Aydin [c], Christian J. Cyron [b,c,*]

[a] Institute for Computational Mechanics, Technical University of Munich, Boltzmannstrasse 15, 85748 Garching, Germany
[b] Institute for Continuum and Material Mechanics, Hamburg University of Technology, Eissendorfer Str. 42, 21073 Hamburg, Germany
[c] Institute of Material Systems Modeling, Helmholtz-Zentrum Hereon, Max-Planck-Strasse 1, 21502 Geesthacht, Germany

ARTICLE INFO

Keyword:
Descriptors
Fiber network
Representative volume element
Simulated annealing

ABSTRACT

Materials whose microstructure is formed by random fiber networks play an important role both in biology and engineering. So far, it still remains unclear which geometric properties of the fiber network determine the macroscopic mechanical properties of such materials. This paper presents a computational study based on a large number of representative volume elements of random fiber networks. Our study reveals that the linear mechanical properties of fiber networks (i.e., Young's modulus and Poisson's ratio) are largely determined by only four scalar key descriptors. These are the number of fibers per volume, the mean node valency, the mean fiber length, and the mean direction cosine between fibers adjacent to the same node. Number of fibers per volume and node valency were found to be responsible for around 80% of the variance of the mechanical properties, making them the two by far dominant microstructural descriptors. In the part of the configuration space covered by our study, we observed a linear or quadratic relationship between the above four scalar microstructural descriptors and the Young's modulus. For the number of fibers per unit volume we propose a theoretical explanation for this simple relation.

1. Introduction

Fibrous materials are abundant both in nature (e.g., soft tissues such as ligaments and skin or wood), and in engineering (e.g., textile materials, paper). Therefore, the development of numerical models to study their mechanical properties under divers mechanical loading conditions has received significant attention, in materials science, mechanical engineering, biomechanics and biophysics [1–18]. The key to computational modeling of fibrous materials is often the ability to set up a so-called representative volume element (RVE) of their microstructure. The geometric features of these RVEs need to agree with the ones of the microstructure of the real materials with respect to relevant statistical descriptors [19–23]. If so, computational studies with the RVE can help understand the mechanical properties of the materials on the macroscale and also how certain changes of their microstructure could be used to optimize these.

The microstructure of fibrous materials is often defined by a random network structure. Over the last decades, numerous stochastic algorithms were developed and applied to construct RVE of random heterogeneous media [24–28]. For detailed reviews of the current state of research in microstructure characterization, reconstruction approaches and multi-scale modeling of heterogeneous materials the reader is referred to [29–32]. Generally, reconstruction of heterogeneous materials is an optimization problem, which, due to its complexity, typically requires an iterative numerical solution. Among various numerical approaches, simulated annealing (SA) has received much attention. For SA, one defines a desired random microstructure by a set of so-called descriptors (each of which characterizes a specific geometric property of the microstructure). Then one typically starts with some random initial configuration and uses SA to adjust it by random steps until obtains a microstructures whose descriptors match the desired ones. SA was introduced for the reconstruction of dispersions of particles based on correlation functions [33]. Afterwards, the method was extended to the reconstruction of general random heterogeneous media [34], thereby becoming applicable to multidimensional, multiphase and anisotropic structures. Since SA is a method that can be

* Corresponding author at: Institute for Continuum and Material Mechanics, Hamburg University of Technology, Eissendorfer Str. 42, 21073 Hamburg, Germany.
E-mail address: christian.cyron@tuhh.de (C.J. Cyron).

https://doi.org/10.1016/j.commatsci.2021.110711
Received 15 April 2021; Received in revised form 4 July 2021; Accepted 6 July 2021

adapted quite easily to a specific problem, many studies have been performed in the past on the basis of SA [35–38].

Despite the many computational studies that have been performed with fiber networks, it remains to date still unclear which descriptors of their microstructure exactly govern their mechanical properties on the macroscale. To address this question, we propose in this paper an algorithm for the construction of random fiber networks. We use this algorithm to construct a large variety of random RVEs and compute their mechanical properties by finite element simulations to identify the descriptors that mainly govern the mechanical properties of fiber networks on the macroscale.

The present article is organized as follows. In Section 2, we briefly outline a large variety of different descriptors that can be used to characterize the geometry of fiber networks. In Section 3, we describe our algorithm to construct tailor-made RVE whose descriptors match the desired ones. In Section 4, we present the results of a computational study that reveal which of the large variety of considered descriptors are geometrically and mechanically most relevant. Finally, we summarized our results in Section 5.

2. Descriptors

Fiber networks consist of fibers connected to each other at so-called nodes. In order to characterize them or compare them with each other, one can use so-called descriptors. Each descriptor characterizes a different aspect of the geometry of the network. As we study herein random fiber networks, the descriptors are in general related to statistical properties of the networks. The major goal of this paper is to understand which descriptors are primarily governing the mechanical properties of fiber networks. In general there is an infinite number of possible descriptors. As rigorous mathematical proofs about the relevance or irrelevance of a descriptor appear to date impossible in most cases, we have to adopt a heuristic strategy. That is, in the following we present a finite set of the most common descriptors for networks from Euclidean geometry and graph theory. The role of each of these descriptors will then be examined in a computational study. This way, we cannot make mathematically rigorous statements about the set of mechanically relevant descriptors. However, we can at least address this question from a heuristic perspective that can be hoped to be sufficient especially for most purposes in materials research.

2.1. Morphological descriptors

Morphological descriptors are based on the geometry and topology of the network in the Euclidean space. With respect to fiber networks, the following ones are most prominent.

Node density ρ_{node} is the number of nodes (vertices) in the RVE N_{node} divided by the volume of the RVE.

Valency distribution p_v is the probability distribution of valency across the nodes in the RVE. The valency of a node v is the number of fibers (edges) connected to that node.

Fiber length distribution p_l is the probability distribution of the Euclidean length of the fibers l in the RVE.

Direction cosine distribution p_c is the probability distribution for the cosine c of the angles between all pairs of fibers connected to the same node. It describes how much the orientation of fibers joining at the same node is correlated.

Connectedness of the networks is a boolean descriptor which declares whether the fibers in the RVE are all connected to each other in some way, that is, whether between any pair of nodes in the network there exists at least one connection path along the fibers (edges) of the network.

Pore-size distribution function $p_{pore}(r)$ describes in the fiber network the probability for a point in the void phase that the nearest point in the fiber phase is located at a distance of at least r (see also the more general discussion in [39]).

Radial distribution function $p_r(r)$ is a function of distance which describes in a system of point-like particles the probability of finding particles in the distance of r from a reference particle [33]. In this work we apply this descriptor in two different ways to characterize the solid phase (fiber phase). First, we consider the nodes the relevant set of particle and compute the probability of finding nodes in the distance of r from each other denoted as $p_{r-node}(r)$. Second, $p_{r-fiber}(r)$ which is the probability of finding fiber segments in the distance of r from each other. To this end, we discretize all the fiber within the RVE into segments. Then we compute the distance of all pair of segments within the RVE based on their central points.

Geometric moment invariants I are very common and powerful tools for the recognition of objects and patterns in image processing. For an image described by the scalar intensity function $f(x,y,z)$ in three dimensions, the geometric moments are [40]

$$m_{ijk} = \int_{-\infty}^{\infty}\int_{-\infty}^{\infty}\int_{-\infty}^{\infty} x^i y^j z^k f(x,y,z)dxdydz, \tag{1}$$

where the exponents i,j and k are non-negative integers and $r = i+j+k$ is the order of the moment. The low order moments have physical concepts. m_{000} can be interpreted as the mass of an object, $\overline{x} = m_{100}/m_{000}, \overline{y} = m_{010}/m_{000}$ and $\overline{z} = m_{001}/m_{000}$ respectively as the coordinates of the center of mass in x-, y- and z-direction, and the second order moments $m_{200}, m_{020}, m_{002}$ as the moments of inertia around the x-, y- and z- axis respectively. Accordingly, the so-called central geometric moments can be defined as [40]

$$\mu_{ijk} = \int_{-\infty}^{\infty}\int_{-\infty}^{\infty}\int_{-\infty}^{\infty} (x-\overline{x})^i (y-\overline{y})^j (z-\overline{z})^k f(x,y,z)dxdydz. \tag{2}$$

By the combination of different geometric moments, we can define various geometric moment invariants which are unchanged under a group of transformations such as translation, rotation and scaling [41]. A large list of geometric moment invariants can be found in [42]. The invariants of higher order are often extremely small compared to the invariants of lower order and are often neglected in image processing. Thus also we herein use only the first three invariants

$$I_1 = (\mu_{200}+\mu_{020}+\mu_{002})/(\mu_{000})^{(5/3)}, \tag{3}$$

$$I_2 = (\mu_{200}^2+\mu_{020}^2+\mu_{002}^2+2\mu_{110}^2+2\mu_{101}^2+2\mu_{011}^2)/(\mu_{000})^{(10/3)}, \tag{4}$$

$$I_3 = (\mu_{200}^3+\mu_{020}^3+\mu_{002}^3+3\mu_{200}(\mu_{110}^2+\mu_{101}^2)+3\mu_{020}(\mu_{110}^2+\mu_{011}^2) + 3\mu_{002}(\mu_{101}^2+\mu_{011}^2)+6\mu_{110}\mu_{101}\mu_{011})/(\mu_{000})^5. \tag{5}$$

In our fiber networks, we assumed f to be a Dirac-type function with infinite intensity on the (infinitesimally thin) fibers and zero intensity everywhere else. For the practical calculation of the geometric moment invariants, the fibers were divided into a finite number of segments, each associated with a weight according to the segment length, and then an approximation of the moment invariants was calculated based on this discretization.

2.2. Graph descriptors

In mathematics, graphs are formed by a set of vertices (nodes) and edges (links or lines) connecting them. So-called simple graphs are graphs where no vertex is connected by an edge to itself and where the connection between two vertices is always established by exactly one (rather than in general several) edges. Undirected graphs are graphs where the connections between vertices are bidirectional. Apparently, one can interpret networks of thin fibers (on which we solely focus herein) from an abstract point of view as graphs. Doing so, the fibers play the role of the edges and the nodes the one of the vertices, and the

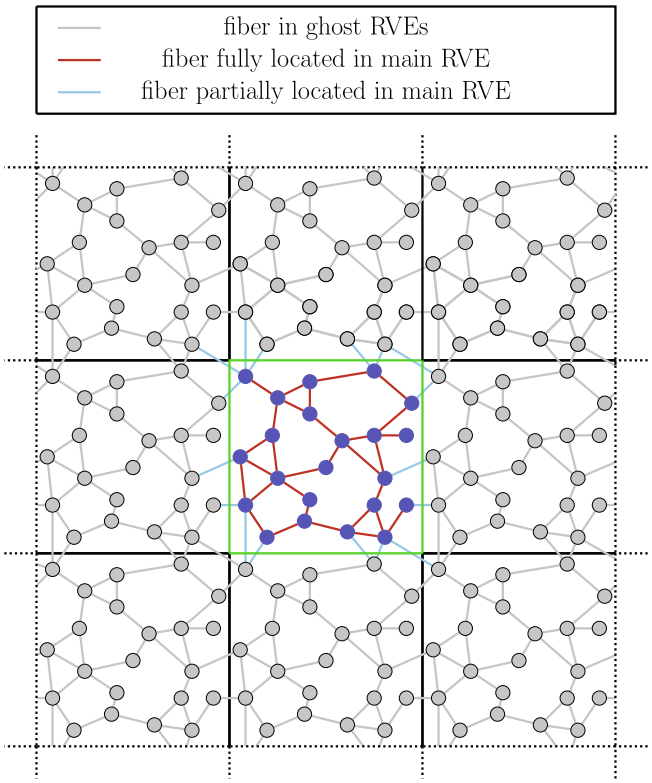

Fig. 1. RVE (center) and surrounding ghost RVEs used to mimic a periodic material structure and to minimize finite size effects.

mathematical quantities that are usually applied to characterize graphs (graph descriptors) can be used to characterize also fiber networks. There are many different descriptors in graph theory [43–46], and it is not possible to study all of them in this paper. Rather we focus on a set of the most common ones briefly summarized in the following.

Clique number is the number of vertices in the largest clique of a graph. A clique is a subset of a graph in which there is an edge between each pair of vertices [45].
Domination number of a graph is the number of vertices in the smallest dominating set of that graph. A dominating set of a graph is a subset of the graph such that every vertex outside this subset is a neighbor of at least one vertex within the subset [43].
Independence number is the number of vertices in the largest independent set of a graph. An independent set of a graph is a subset of vertices within which no pair of vertices is directly connected by an edge [45].
Chromatic number of a graph is the smallest number of colors needed to color the vertices of that graph such that the color of any two adjacent vertices is different [45].
Clustering coefficient in graph theory is a tool to indicate the tendency of the nodes to cluster together. It can be defined either for each node individually (local clustering coefficient) or for the whole graph (global clustering coefficient). The local clustering coefficient of a specific node is the ratio of the actual number of edges between its neighbors and the maximal possibly number of edges between its neighbors. The global clustering coefficient is the ratio of the number of closed triplets over the total number of triplets in the network. A triplet is a set of three vertices, at least one of which is connected to the other two. If also the other two are connected to each other, the triplet is called a closed triplet. The global clustering coefficient is well-known to be a measure of the clustering in the network [46]
S-metric of a graph is the product of the valencies of all vertices [44].
Maximum eigenvalue of adjacency matrix: the adjacency matrix of a graph is a square matrix whose size equals the number of vertices. Its *ij*-elements are the numbers of edges connecting the *i*-th and *j*-th vertex. For the simple undirected graphs corresponding to fiber networks the adjacency matrix is a symmetric matrix of zeros and ones where the diagonal elements are all zero. Thus the adjacency matrix has real eigenvalues. Its maximum eigenvalue is a frequently used descriptor to characterize graphs. [43]
Maximum eigenvalue of Laplacian matrix: the Laplacian matrix equals the difference between the degree matrix and the adjacency matrix. The degree matrix of a graph is a square diagonal matrix whose *ii*-elements equal the valency of the *i*-th vertex. The number of subsets of the graph that are mutually not connected equals to the number of zero eigenvalues of the Laplacian matrix. Hence for a connected graph the Laplacian matrix has exactly one zero eigenvalue. [43]
Algebraic connectivity is the second smallest eigenvalue of the Laplacian matrix and always positive. It is well-known to characterize how well-connected a graph is. [45]
Graph energy equals to the sum of all eigenvalues of the adjacency matrix [45].

3. Construction of representative volume elements

To examine the respective importance of the various descriptors introduced in the previous section, we studied a large number of representative volume elements (RVEs) with fiber networks and examined how the descriptors of these fiber networks correlated with their mechanical properties. To minimize finite size effects in our RVEs, we developed an algorithm mimicking a periodic material structure. This algorithm placed around the main RVE some additional identical ghost RVEs (Fig. 1) that were taken into consideration only when in our main RVE descriptors had to be evaluated at nodes or fibers connected across the boundaries of our main RVE. In general, we focused on the construction of isotropic networks.

To study the correlation between network descriptors and network properties it is necessary to construct networks whose geometry complies with certain predefined values or distributions of the descriptors of interest. To construct such networks we adopted the procedure described in the following subsections.

3.1. Generation of initial network

To construct tailor-made RVEs, we started from fiber networks with a random initial configuration. To speed up the stochastic optimization procedure used subsequently to transform this initial configuration into one exhibiting the desired values and distributions of the descriptors of interest, we ensured that already in the initial configuration some descriptors of the network agreed with the desired ones, namely, its connectedness, valency distribution, maximum fiber length and node density. We chose these descriptors because it is easy to directly construct networks where these descriptors take on desired values and distributions so that it would be a waste of computational time to include these descriptors in the stochastic optimization algorithm described below. Rather this algorithms can then easily be constrained in such a way that it maintains over all iterations the initial values and distributions for these descriptors. To prescribe the above mentioned descriptors already in the otherwise random initial configuration we applied the following procedure.

3.1.1. Node density, connectedness, maximal fiber length

First, we defined a cubic domain of edge length L_{RVE} for our RVE to be constructed. To keep finite size effects acceptably small, we generally imposed without loss of generality $L_{RVE}/3$ as a hard constraint for the maximum fiber length (l_{max}). To keep this constraint already in the initial configuration and ensure a largely homogeneous initial configu-

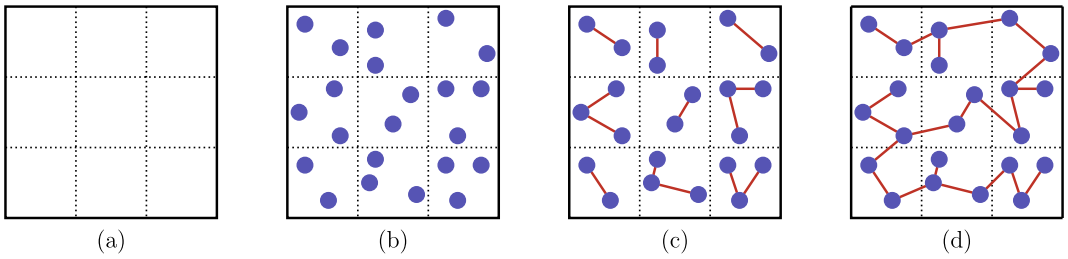

Fig. 2. Four steps to establish an initial random network in (a) a given RVE with (b) a desired node density, (c) maximum fiber length and (d) connectedness.

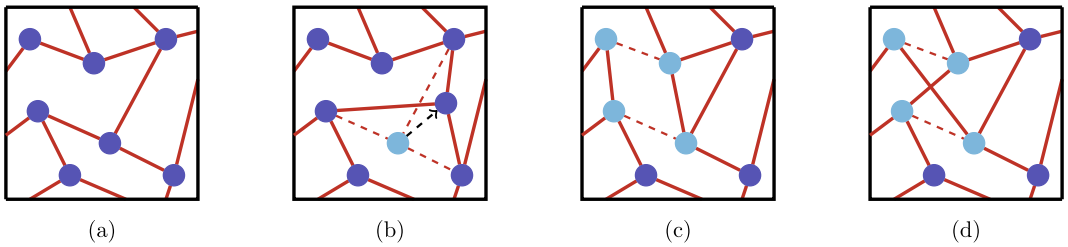

Fig. 3. Herein, in each SA evolution step, the (a) current configuration is altered either by (b) the random displacement of some node or by (c,d) deleting and subsequently adding a pair of fibers in a way that keeps the valency of all nodes unaltered.

ration, we uniformly divided the RVE into a set of $6^3 = 216$ subdomains.

In the next step, we computed the number of nodes $N_{node} = \rho_{node} L^3_{RVE}$ corresponding to the desired node density and distributed them as equally as possible among the subdomains to ensure a largely homogeneous initial configuration (Fig. 2(b)). Note that an exactly equal distribution was not always possible given the predefined node density and number of subdomains, which could be achieved only if in certain cases some subdomains were assigned one node more than others.

In the third step, we connected the nodes within each subdomain by a random polygon chain of initial fibers (Fig. 2(c)), which automatically complied with the given maximum length due to the above chosen edge length of the subdomains.

In the fourth step, we interconnected in each subdomain one node with one node in a neighboring subdomain such that a connected network was achieved (Fig. 2(d)) and the added fibers did not violate the maximum length criterion.

3.1.2. Valency distribution

Let the valency of node i be v_i and $p_v(v_i)$ be the desired probability distribution. The maximum valency allowed is v_{max}, then the number of fibers in the network should be

$$N_{fiber} = N_{node}/2 \sum_{k=1}^{v_{max}} p_v(v_k), \tag{6}$$

Having computed this quantity, fibers were randomly added between pairs of nodes in the network, checking each time whether the maximum length criterion was satisfied and also whether the respective addition of a fiber helped to bring the actual valency distribution closer to the desired one $p_v(v_i)$. Only if so, fibers were actually added. Otherwise another connection between a random pair of nodes was examined. To account for the periodic boundary conditions of our RVE, we allowed also connections from a node inside our RVE to a node in one of the neighboring ghost RVEs (Fig. 1). If such connections were established, the node in the ghost RVE was effectively replaced for all further considerations of the network connectivity by its periodic counterpart within the RVE.

3.2. Simulated annealing

In the previous sections, we pointed out how to construct RVEs of connected fiber networks with a maximal fiber length and a prescribed node density and valency distribution. Here we point out how to transform these RVEs into a final configuration in which also the fiber length distribution and the direction cosine distribution match desired target distributions. To this end, we use the simulated annealing (SA) method [34,4]. SA is a (global) stochastic optimization method. The idea of the approach is to define a cost function

$$E = \sum_{k=1}^{N_d} w_k \cdot E_k. \tag{7}$$

that becomes minimal if all N_d descriptors of interest of the RVE match their target values or distributions. E_k is the cost function (energy function) of the k-th descriptor and w_k its scalar weight. For reasons discussed in more detail below, it turned out to be sufficient for our purposes to consider only two descriptors in (7), namely, the fiber length distribution and the direction cosine distribution. Following [4], we defined the cost function of the k-th descriptor via the Cramer-von Mises test, that is,

$$E_k = \frac{1}{12N_k} + \sum_{i=1}^{N_k} \left[\frac{2i-1}{2N_k} - c_k(x_{ki}) \right]^2, \tag{8}$$

Here we assume that the k-th descriptor is a probability density distribution with N_k realizations x_{ki} across the whole network, ordered such that $x_{k1} < x_{k2} < x_{k3} < \ldots$. For example, if the k-th descriptor is the fiber length distribution, N_k is the number of fibers in the network, and x_{ki} is the length of the i-th fiber. c_k is the cumulative target distribution of the k-th descriptor.

Once a cost function E has been defined that becomes minimal if the network has reached a state where the descriptors match their targets, one uses in SA a procedure of random evolution steps with the aim to decrease E down to its (ideally global) minimum. In our work we used two different types of evolution steps described in the following.

Step type 1 applies a random displacement vector (with a constraint for its maximal absolute value) to a randomly selected vertex (node) in the network (Fig. 3(b)).
Step type 2 deletes a pair of fibers and then adds a new one in such a way that the valency of all the affected nodes remains unaltered. For the configuration in Figs. 3(a), the two alternative ways to

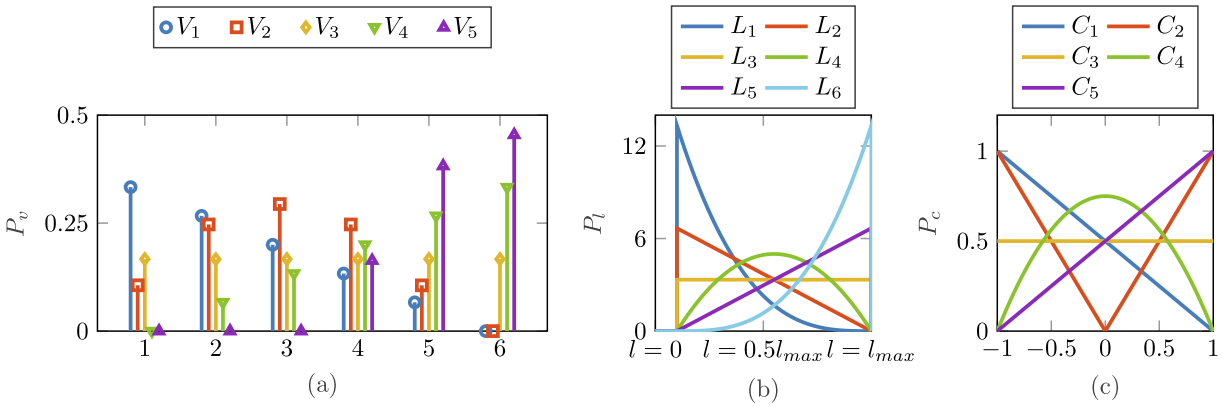

Fig. 4. Trial (a) valency distributions $V_1, \ldots, V_5$ (b) fiber length distributions $L_1, \ldots, L_6$ and (c) direction cosine distributions $C_1, \ldots, C_5$.

Table 1
Possible combinations of V_i, L_j and C_k.

	C_1	C_2	C_3	C_4	C_5
V_1	✓[a]	✓✓[b]	✓✓	✓✓	✓✓
V_2	✓	✓	✓	✓	✓
V_3	—	✓	✓	—	✓
V_4	—	✓	✓	—	✓
V_5	—	✓	✓	—	✓

[a] ✓✓: $L_1, \ldots, L_6$.
[b] ✓: $L_2, \ldots, L_5$.

Table 2
Values for parameters used in SA (see Section 3.2).

Parameter	Value
T_0	1
d_r	0.9
i_{max}	1,000,000
E_{target} for each descriptors	0.01
Maximal displacement step size	$L_{RVE}/20$

accomplish such a step (once a pair of fibers to be deleted has been chosen) are depicted in Fig. 3(c) and (d). For step type 2 we generally checked whether it altered the connectedness of the network and admitted only such steps of type 2 that did not.

It is important to note that neither of the above two types of random steps changes the connectedness nor the valency nor the node density of the network (which we ensured to match their respective targets already in the initial configuration). However, other descriptors such as length and direction cosine between neighboring fibers change. After each random step, we computed ΔE, the change of the cost function E. Using a Metropolis algorithm as already [34], the probability to accept the step was computed in the i-th evolution step as

$$p^i_{accept}(\Delta E) = \begin{cases} 1 & \Delta E \leq 0, \\ exp(-\Delta E/T_i), & \Delta E > 0. \end{cases} \tag{9}$$

Here T_i is a temperature-like parameter. If the energy of a proposed random step decreases or at least not increases the cost function E, it is always accepted in the Metropolis algorithm. However, to avoid getting trapped in local minima, it is essential to endow the algorithm with the ability to perform at least with some likelihood also steps into an energetically unfavorable directions. This ability is ensured by the temperature parameter T_i. The higher T_i the more likely it is that the Metropolis algorithm every so often performs also energetically unfavorable steps. Typically, one starts with high T_i to give the algorithm the chance to explore large parts of the state space and decreases T_i then with an increasing number of random evolution steps [47]. Different approaches are used in the literature for this so-called cooling schedule. We applied the power function

$$T_i = T_0 \cdot d_r^{i-1}, \tag{10}$$

with the initial temperature T_0 and d_r being the temperature decay-rate. SA is stopped if either a predefined maximal number of random evolution steps i_{max} is reached or the cost function is lower than a predefined threshold E_{target}. We used a combination of both conditions (for details see Fig. A.12).

3.3. Definition of RVE set used in our study

As discussed already in [4], fiber length, valency and direction cosine distributions have been reported at several occasions to affect the mechanical properties of fiber networks. It appears mechanically plausible that also the number of fibers plays an important role. For a given valency distribution this number can be expressed equivalently by the node density. The primary objective of this study is identifying the descriptors governing the mechanical behavior of fiber networks. Therefore, we decided to construct for our study a large set of RVEs which sampled specifically variations with respect to the above four descriptors, namely, valency distribution, fiber length distribution, direction cosine distribution and number of fibers in the RVE.

To this end, we discretized the space of possible valency, fiber length, and direction cosine distributions by a set of trial distributions illustrated in Fig. 4. The algebraic formulae for these distributions denoted by V_i, L_j and C_k with $i = 1, 2, \ldots, 5, j = 1, 2, \ldots, 6$ and $k = 1, 2, \ldots, 5$ are specified in Appendix B. The set of trial functions was defined heuristically, though in a manner that allowed us to sample with a relatively small number of trial functions a large part of the possible shapes these functions typically take on in real physical systems. To this end, we included for each descriptor at least a constant, two linear and a quadratic trial function. Moreover, we allowed an independent variation of the number of fibers F_q with $q = 1, 2$ between the two specific values $F_1 = 4000$ and $F_2 = 8000$. Note that we numbered the considered distributions such that the mean value of the respective descriptor increases monotonically with their subscript. For instance, L_1 refers to the distribution with the smallest average length and L_6 to the distribution with largest one.

Our definition of trial functions allowed us to define 300 types of different RVE, each characterized by a specific choice of the descriptors V_i, L_j, C_k, F_q. These different types of RVE are referred to in the following by the abbreviations $V_1L_1C_1F_1, V_2L_1C_1F_1, \ldots, V_5L_6C_5F_2$, respectively. It is worth mentioning that SA did not converge satisfactorily for the combination of V_3, V_4 and V_5 with C_1 and C_4, suggesting that these types of

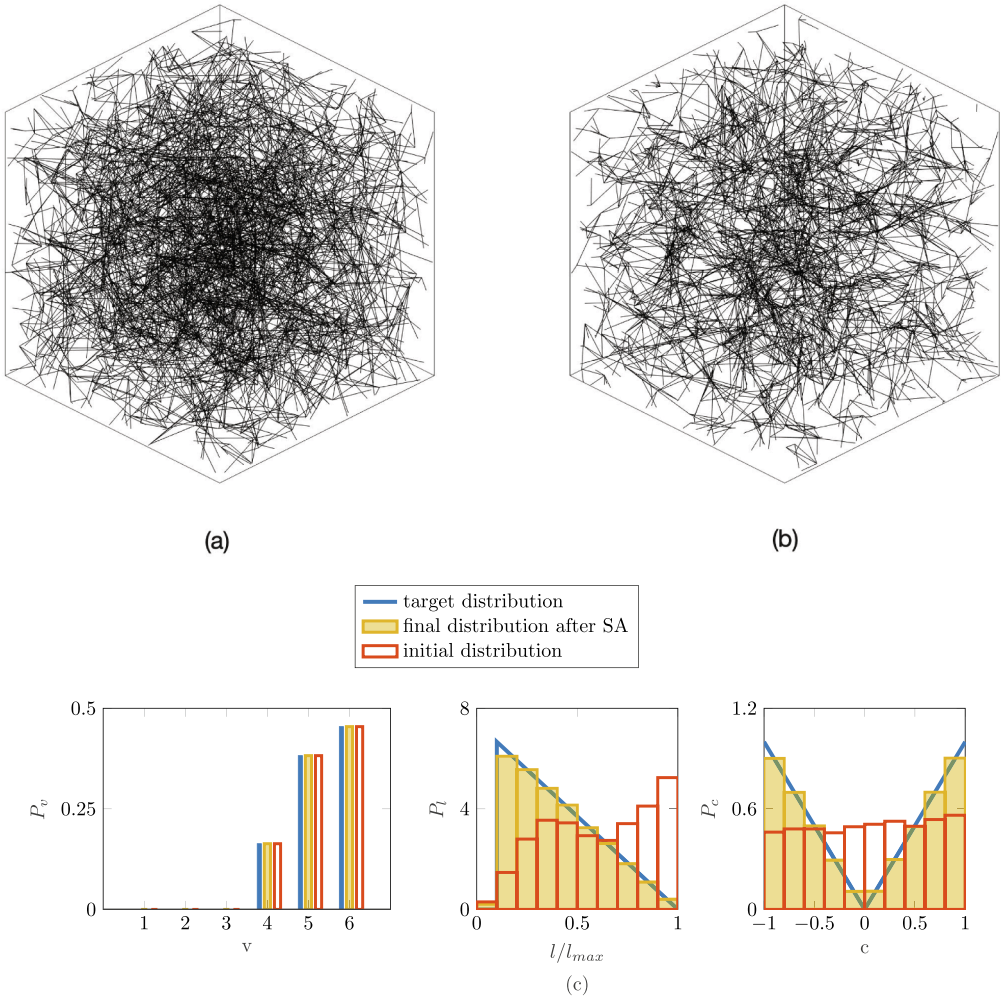

Fig. 5. (a) A random initial configuration is transformed by SA into an (b) RVE of type $V_5L_2C_2F_1$ where (c) valency, fiber length and direction cosine distributions closely match their respective target distributions.

RVE cannot exist due to a violation of intricate, problem-intrinsic geometric constraints. Similarly, RVE with fiber length distributions of L_1 and L_6 could be constructed only for V_1 in combination with all considered direction cosine distributions except C_1. RVE types that could be constructed with F_1 could always be constructed also with F_2. Hence, among the theoretically possible 300 different RVE types only 168 could be constructed, which are summarized in Table 1. For each RVE type, 15 different random realizations were generated by the procedure described in Section 3. Thereby, we used the SA parameters from Table 2 for the construction of all the 2520 RVEs considered in our study. Fig. 5 illustrates the construction of one specific such RVE (of type $V_5L_2C_2F_1$). Starting from a random initial configuration, SA yields an RVE where the descriptors of interest closely match the prescribed target distributions.

4. Results

4.1. Descriptors governing mechanical properties

To understand the influence of the descriptors of the network structure on the network's mechanical properties, we discretized the network RVE generated as described in Section 3.3 by finite beam elements, to which we assigned a circular cross section with a diameter of $L_{RVE}/50$, a Young's modulus of $E_f = 79$ GPa and a Poisson's ratio of $\nu_f = 0.44$. These values are deliberately chosen to resemble those of nanoporous gold as a possible application case. Yet, the exact choice of these parameters is largely irrelevant for the following discussion as long as they enable in principle all relevant deformation modes of the network in a physically realistic range, which we confirmed to be the case. Fibers were discretized using beam finite elements based on the Timoshenko beam theory. At the intersection points of fibers, both translations and rotations were coupled, i.e., rigid joints were assumed. Applying periodic boundary conditions to our RVE according to [48], we computed their (effective, homogenized) Young's modulus E and Poisson's ratio ν by the method suggested in [28].

To investigate the effect of valency distribution, fiber length distribution, direction cosine distribution and the number of fibers on mechanical properties, we divided the 2520 RVEs generated according to Section 3.3 into categories. $V_iL_jC_kF_q$ denotes a category of an RVE where all the four descriptors match their respective target distributions. That is, the RVE category includes the 300 RVE types $V_1L_1C_1F_1, V_2L_1C_1F_1, \ldots, V_5L_6C_5F_2$. Analogously, by leaving out one or several of the descriptors in the list, we denote an RVE category where only the listed descriptors were fixed to certain target distributions and the others were allowed to

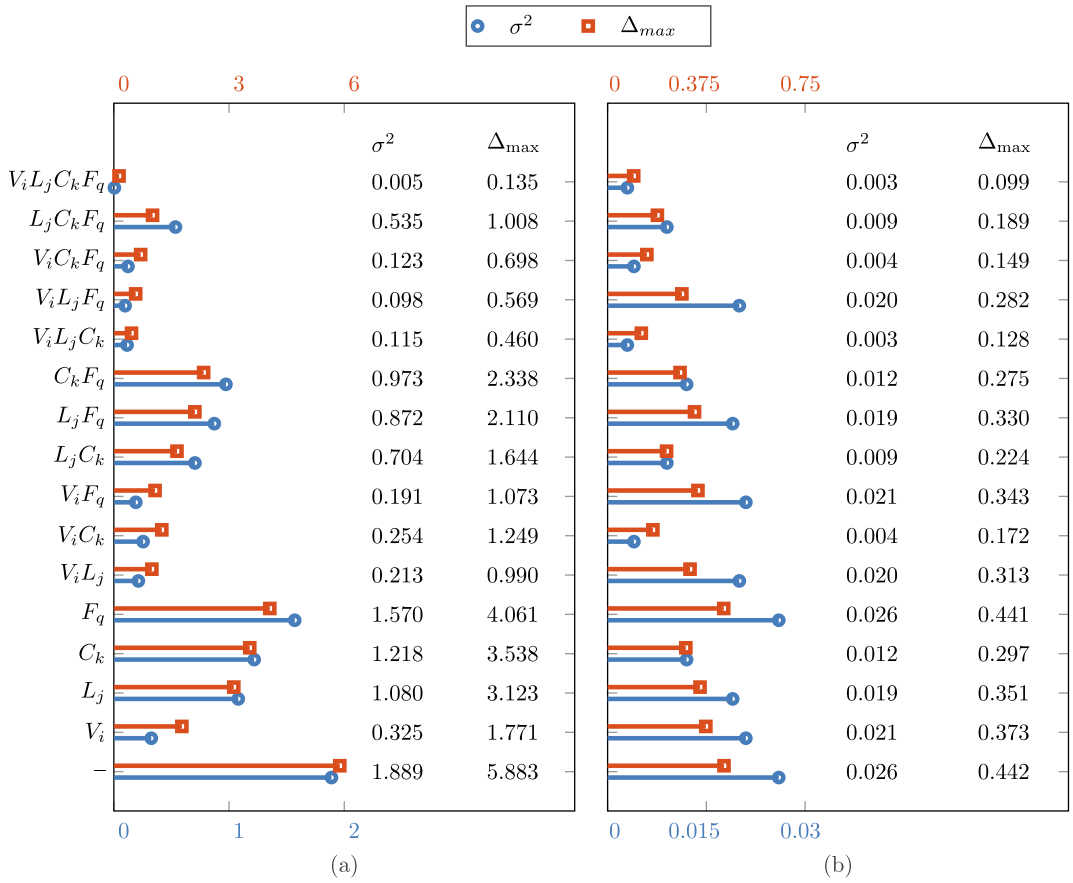

Fig. 6. For the 16 different RVE categories considered in this study, we computed for (a) the Young's modulus and (b) the Poisson's ratio the relative variances and maximal deviations from their mean values, averaged across all RVE types belonging to the respective RVE category. Apparently, fixing the four descriptors valency distribution, fiber length distribution, direction cosine distribution and the number of fibers reduced the statistical variance of the mechanical properties to nearly zero.

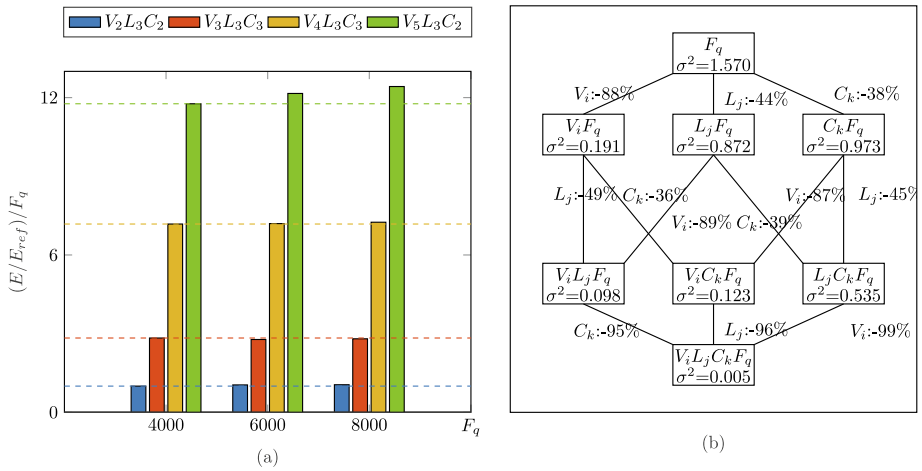

Fig. 7. (a) Young's modulus of a representative selection of RVE types normalized by the number of fibers F_q (and the homogenized mean Young's modulus $E_{ref} = 27.3\ MPa$ of the RVE type $V_2L_3C_2F_1$); (b) fixing more and more descriptors, the relative variance (σ^2) of the Young's modulus in the resulting RVE categories (boxes) decreases by the percentage indicated next to the lines that connect an RVE category with one that results from fixing a further descriptor.

vary freely among all distribution functions included in our study. For example, L_jC_k denotes a category of RVEs where the length distribution matches L_j and the direction cosine distribution C_k, whereas all the other descriptors may be arbitrary (within the set of distributions and values considered herein). As there are altogether 30 different RVE types of the category L_jC_k, denoted by L_1C_1, L_1C_2, L_1C_3, …, L_6C_5, our study includes for each of these RVE types $2520/30 = 84$ realizations (in case all combinations of remaining descriptors be available for the subsets of this category). In the extreme case that all descriptors are allowed to vary freely among the distributions included in this study, we denote the respective RVE category (or type) by '–', including all 2520 RVE generated in our study. As illustrated also in Fig. 6, there are altogether

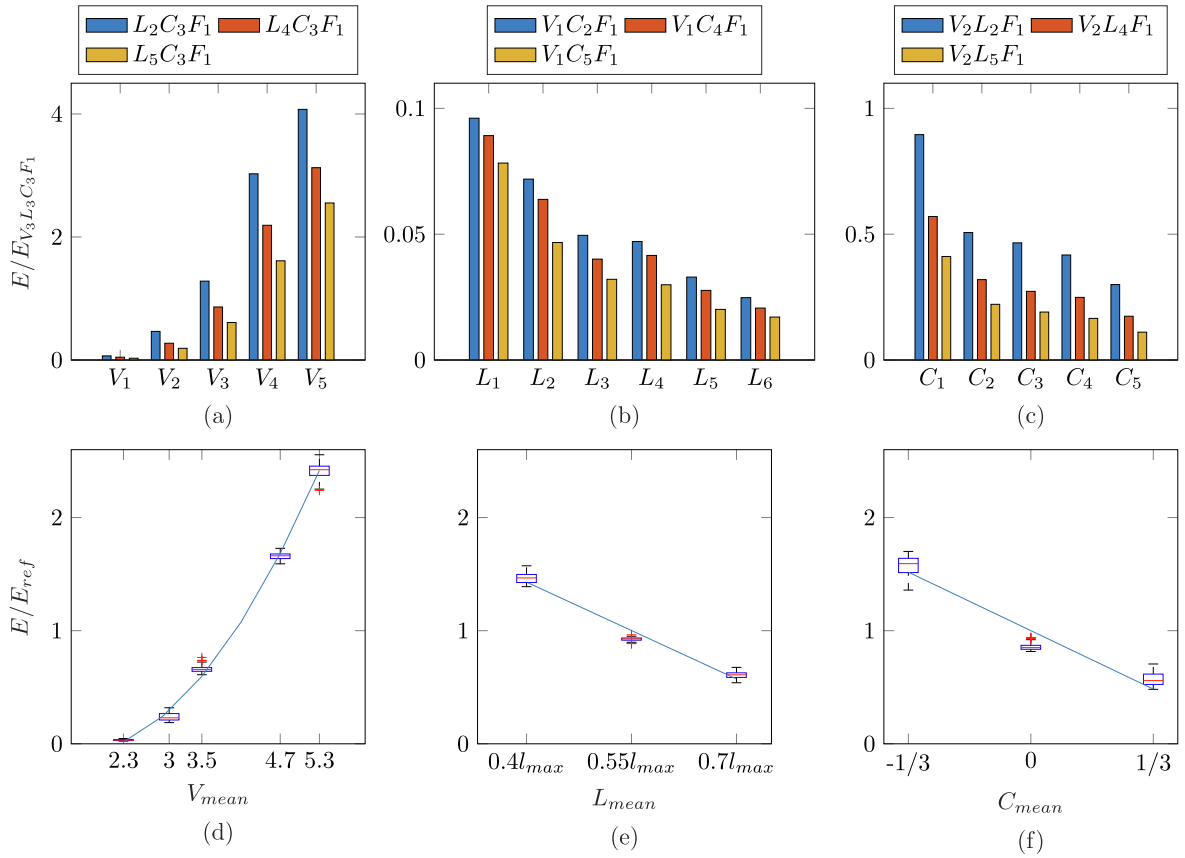

Fig. 8. Young's modulus monotonically increases with the mean valency and monotonically decreases with both mean fiber length and mean direction cosine for a number of representative RVE types. The Young's modulus in (a)–(c) is normalized to the Young's modulus of $E_{V_3L_3C_3F_1} = 77.3\,MPa$ and in (d)–(f) to E_{ref} as defined above.

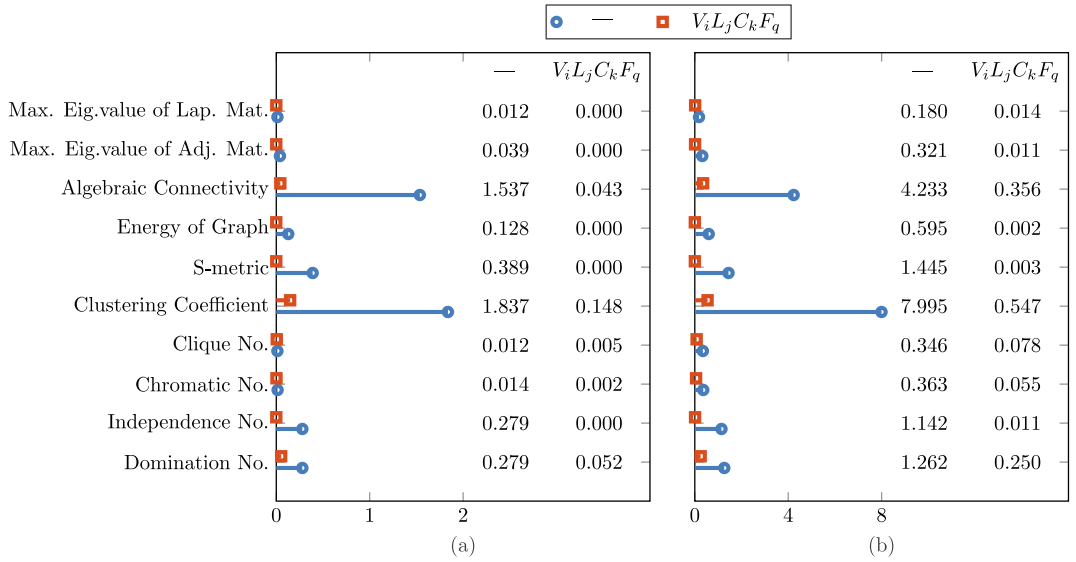

Fig. 9. Mean values of (a) the normalized variance σ^2 and (b) the maximal absolute value of the relative deviation Δ_{max} averaged over all RVE types in the two RVE categories '–' and $V_iL_jC_kF_q$. The mean values of these descriptors of all 2520 RVEs are as follows: Domination No.= 1.11e3, Independence No.= 1.84e3, Chromatic No.= 4.40, Clique No.= 3.06, Clustering Coefficient = 0.01, S-metric = 1.90e5, Energy of Graph = 5.41e3, Algebraic Connectivity = 0.16, Max. Eig. value of Adj. Mat.=4.12, Max. Eig. value of Lap. Mat = 8.65.

16 RVE categories, which are listed on the very left of Fig. 6. For each RVE category, we computed for all RVE types belonging to it the mean values of Young's modulus and Poisson's ratio as well as the variances of these quantities (normalized by their respective mean value) (σ^2). For each RVE category the average variance across all the RVE types belonging to it is plotted in Fig. 6. Moreover, we computed in each RVE category for each RVE type belonging to it for all samples the maximal absolute values of the relative deviations of Young's modulus and

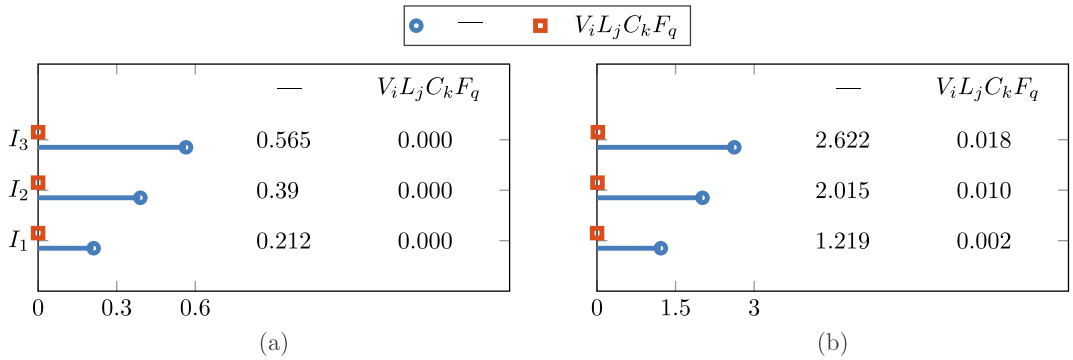

Fig. 10. Comparison of (a) normalized variance σ^2 and (b) the maximal absolute value of the relative deviation Δ_{max} for the first three geometric moment invariants I_1, I_2 and I_3 of the RVEs in the two categories '—' and $V_iL_jC_kF_q$.

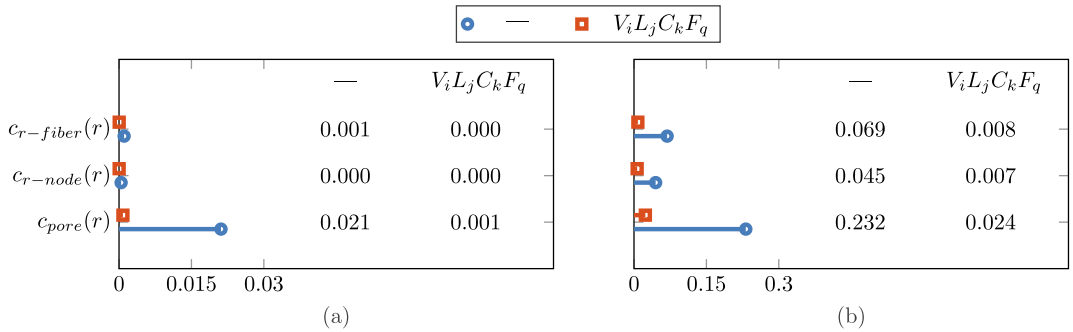

Fig. 11. Comparison of (a) spatially average normalized variance $\overline{\sigma}^2$ and (b) the spatially averaged maximal absolute value of the relative deviation $\overline{\Delta}_{max}$ of $c_{pore}(r)$, $c_{r-node}(r)$ and $c_{r-fiber}(r)$ for RVEs of the categories '—' and $V_iL_jC_kF_q$.

Poisson's ratio from their mean values. This quantity Δ_{max} was averaged for each RVE category and plotted in Fig. 6.

In general, the larger σ^2 and Δ_{max} for a category, the less do the descriptors fixed for this specific RVE category determine the mechanical properties of a network. By contrast, in the theoretical extreme case that σ^2 and Δ_{max} are zero, the descriptors fixed in the related RVE category fully determine the mechanical properties of the fiber network (at least in the theoretical case that for each RVE type an infinite number of realizations is included in the study).

Fig. 6 reveals that for the RVEs in the category '–', the relative variance of Young's modulus across all the subset is as big as 188.9%. By contrast, if all the four descriptors valency distribution, fiber length distribution, direction cosine distribution and the number of fibers are fixed, that is, in the category $V_iL_jC_kF_q$, the relative variance of the Young's modulus is as small as 0.5%. For Poisson's ratio the relative variance in the category $V_iL_jC_kF_q$ takes on the similarly low value of 0.3%. However, for Poisson's ratio the relative variance even in the category of RVE without any geometric constraints is only 2.6%. Together, this leads to the following main conclusions: Poisson's ratio of (initially stress-free) isotropic random fiber network generally exhibits a relatively low statistical variance with a mean value of around 0.25. By contrast Young's modulus strongly depends on the geometry of the fiber network. Nevertheless, the four descriptors valency distribution, fiber length distribution, direction cosine distribution and the number of fibers together suppress around 99.5% the variance of the linear-elastic mechanical properties of fiber networks.

Fig. 7(a) analyzes specifically the effect of F_q by plotting for a representative selection of RVE types on the Young's modulus normalized by the number of fibers. Apparently, this ratio is (except for minor supposedly mainly statistical deviations) constant for each RVE type. In other words, if the other descriptors are fixed, Young's modulus is directly proportional to the number of fibers. This simple law can also be understood analytically. Imagine an RVE with a specific size and F_q fibers. The network in this RVE can be modeled as an elastic spring S. Increasing the number of fibers, for example, by a factor of two can be constructed as process where we add another random fiber network of the same type into the RVE so that the RVE volume is then occupied by two interpenetrating random fiber networks. As these are of the same type, they exhibit the same elastic properties. That is, the RVE harbours then two elastic springs of the kind of S that act in parallel, increasing Young's modulus by a factor of two. By contrast, as both elastic systems of type S exhibit the same deformation behavior, Poisson's ratio is not expected to change if the number of fibers increase by a factor of two. This explains the very low sensitivity of Poisson's ratio to variations of number of fibers observed in our study. Of course, this illustrative explanation is applicable to any scaling factor for F_q, yielding directly the simple linear relation between F_q and Young's modulus observed in Fig. 7(a).

For the RVE category F_q, that is, the one with fixed number of fibers, Fig. 7(b) illustrates how fixing more and more descriptors suppresses in a step-wise manner nearly the whole variance of Young's modulus. Apparently, the mechanically most important single descriptor in this process is the valency distribution, which alone reduces the variance of the mechanical properties by nearly 90% when fixed. In fact, this interpretation qualitatively still holds if we examine in Fig. 7(b) arbitrary transitions from one RVE category to another by fixing one additional descriptor. In every case, fixing the valency distribution reduces

the variance more than fixing any other descriptor. This justifies the conclusion that the valency distribution is generally more important than fiber length distribution and direction cosine distribution.

In order to better understand the influence of the remaining descriptors on the mechanical properties of fiber networks, Young's modulus is plotted in Fig. 8(a)–(c) for a number of representative RVE types.

Fig. 8 illustrates that changes in the valency distribution are associated with changes of Young's modulus by more than one order of magnitude whereas changes in the fiber length and direction cosine distributions typically have a much smaller effect. As the indices of the descriptor distributions increase with their mean values, Fig. 8(a)–(c) demonstrate for a representative selection of RVEs that Young's modulus increases with the mean valency V_{mean} but decreases with mean fibers length L_{mean} and mean direction cosine C_{mean}. To quantify this dependence, Fig. 8(d)–(f) uses a special post-processing of the results of our computational study. Thereby, we first specified a certain *descriptor of interest* (either valency, fiber length or direction cosine distribution) for which we studied its relation to Young's modulus. To do so, we selected from the 16 RVE categories listed in Fig. 6 the ones where the respective descriptor of interest was fixed. For example, if valency distribution is selected as the descriptor of interest, these are the eight categories $V_i, V_iL_j, V_iC_k, V_iF_q, V_iL_jC_k, V_iL_jF_q, V_iC_kF_q, V_iL_jC_kF_q$. For each of these categories, we defined subcategories containing the RVE types where the descriptor of interest was varies across all its possible distributions while all the other descriptors were kept constant at specific values. For example, the category V_iF_q was divided into a subcategory containing the RVE types $V_1F_1, V_2F_1, V_3F_1, V_4F_1, V_5F_1$ (varying the descriptor of interest V_i and keeping F_q constant at F_1), and another subcategory with the RVE types $V_1F_2, V_2F_2, V_3F_2, V_4F_2, V_5F_2$ (varying the descriptor of interest V_i and keeping F_q constant at F_2). For each subcategory we computed for all RVE realizations included in our study Young's modulus normalized by the mean Young's modulus within that category E_{ref} as well as the mean value of the descriptor of interest. We excluded subcategories where not all RVE types were available because they could not be constructed (see Table 1). The results are depicted in Fig. 8(d)–(f), where the descriptor of interest was chosen to be the valency distribution, fiber length distribution and direction cosine distribution, respectively. Interestingly, Fig. 8(d) reveals a quadratic relation between the Young's modulus and the mean value of the valency distribution. This relation is remarkably linear between the Young's modulus and the mean values of the fiber length distribution and the direction cosine distribution (Fig. 8(e) and (f), respectively). The box plots illustrate the statistical deviations from the mentioned relationship in each of the above defined subcategories. The apparently very small size of the boxes reveals that the defined function almost completely characterizes the relation between the considered descriptors and Young's modulus. This observation is remarkable because it means that in discussing the relation between microstructure and mechanical properties of the RVEs, one can focus not only on four key descriptors in the form of probability distributions but in fact largely on mean values. In other words, the linear mechanical properties of the RVEs are largely determined by the number of fibers (per volume) and the scalar mean values of the valency, fiber length and directioncosine distribution. From Fig. 8(d)–(f) it is also apparent that, as discussed already above, mean valency is of much higher importance than mean fiber length and mean direction cosine with respect to the resulting material stiffness. Fig. 8(e) and (f) cover a large part of the range within which fiber length and direction cosine can be varied in a physically and geometrically reasonable way. Yet, they display variations of Young's modulus only by approximately a factor two and three, respectively. By contrast, in Fig. 8 (d) we observe a factor of almost 70. Additionally, it is worth mentioning that the valency range up to slightly above five is well-suited for random fiber networks. However, for ordered ligament systems with hexagonal cells or tetrahedral cells even higher mean valencies may appear (for example six for a uniform cubic mesh and twelve for a uniform tetrahedral mesh), which underlines even more impact on Young's modulus that can in principle be realized in networks of ligaments by varying the mean valency.

As revealed already by Fig. 6, Poisson's ratio is nearly constant across the different RVE types, which is why we omit a detailed discussion of its minor dependencies on the different descriptors. We note, however, that we have shown already above that Poisson's ratio can be expected to be (nearly) independent on the number of fibers F_q. Given that F_q is generally responsible for a large part of the variations of the mechanical properties observed in this study, the insensitivity of Poisson's ratio to it may explain why Poisson's ratio generally exhibits only relatively small variations in the RVE studied herein.

According to [49–51], the ratio of the fiber radius to the fiber length plays an important role for the mechanical properties and deformation of random fiber networks. In networks with higher values of this ratio, stretch is the dominant deformation mode which causes the network to deform affinely. In contrast, if the ratio is small, bending is the predominant deformation mode and the network deforms non-affinely. In order to analyse the dependence of our conclusions in this section on geometrical properties of the fibers such as their slenderness ratio, we repeated the studies discussed in this section with networks with a fiber diameter of $L_{RVE}/500$. The results are presented in Appendix C. They exhibit some minor quantitative differences to the ones obtained with a fiber diameter of $L_{RVE}/50$ but are qualitatively similar, underlining thus the robustness of our conclusions.

4.2. Relation between morphological descriptors and graph descriptors

In Section 4.1 we demonstrated that a set of four geometric descriptors nearly fully determines the mechanical properties of random fiber networks. However, such networks can also be interpreted as mathematical graphs, the nodes forming the vertices of the graph and the fibers its edges. Mathematical graph theory provides a host of descriptors for graphs. It is instructive to study the relation between such graph descriptors and the four geometric descriptors on which Section 4.1 focuses. In this section we examine the graph descriptors introduced in Section 2. As classical graph theory works with finite rather than infinite graphs, most descriptors from graph theory cannot deal with the assumed periodicity of the considered RVEs. Therefore, we evaluated them only within the RVE, ignoring the fibers cutting through the boundaries of the RVE.

In order to investigate the dispersion of graph descriptors, we evaluated the aforementioned statistical quantities σ^2 and Δ_{max} also for a host of graph descriptors and compared the results for the two extreme cases, the RVE category '–' and the RVE category $V_iL_jC_kF_q$. The results are illustrated in Fig. 9. The ones related to $V_iL_jC_kF_q$ are the mean values of the 168 types RVE belonging to the category.

Fig. 9 reveals that fixing the four descriptors valency distribution, fiber length distribution, direction cosine distribution and number of fibers reduces σ^2 and Δ_{max} for all graph descriptors substantially. Except for the clustering coefficient, all graph descriptors seem to be almost fully determined in an implicit manner by fixing the four dominant morphological descriptors, underlining once more their key role in characterizing properties of the fiber network.

4.3. Role of other morphological descriptors

We have established now that fiber length distribution, valency distribution, direction cosine distribution and number of fibers are the four morphological descriptors that nearly fully determine the mechanical properties (and indeed also graph properties) of fiber networks. In this section we analyze, to which extent they determine also the other morphological descriptors introduced in Section 2. The first three geometric moment invariants, I_1, I_2 and I_3 [42] are computed for the RVE types within the two RVE categories'—' and $V_iL_jC_kF_q$. Analogously to the previous sections, the mean values of the normalized variance σ^2 and the maximal absolute value of the relative deviation Δ_{max} averaged over all RVE types in these two categories are plotted in Fig. 10. Apparently, fixing the four above identified morphological main descriptors determines also the three first geometrical moment invariants nearly completely. Higher order moments exhibit very small values compared to the first three ones. They are typically considered as of minor importance compared to the first three ones and thus skipped here.

Furthermore, the pore-size distribution function $p_{pore}(r)$, the radial distribution function of the nodes $p_{r-node}(r)$ and the radial distribution function of the fibers $p_{r-fiber}(r)$ have been studied in this work. To determine the pore-size distribution function, we chose 1000 random points inside the void-phase of the RVE and computed their respective distance to the closest fiber. Then the probability distribution of distances was approximated in a discrete manner by dividing the occurring interval of $0 < r/\mathrm{L_{RVE}} < 0.12$ into 24 bins with equal width. A similar calculation was performed for $p_{r-node}(r)$ and $p_{r-fiber}(r)$ by dividing the occurring interval $0 < r/\mathrm{L_{RVE}} < 2$ into 25 equal-sized bins. For the computation of $p_{r-fiber}(r)$, fibers were divided into segments with a maximum length of $5\%L_{RVE}$. In order to compute statistical quantities comparable to σ^2 and Δ_{max} above, we first converted the probability density functions (PDFs) $p_{pore}(r), p_{r-node}(r)$ and $p_{r-fiber}(r)$ into associated cumulative (CDFs) distribution functions $c_{pore}(r), c_{r-node}(r)$ and $c_{r-fiber}(r)$. For these, we calculated σ^2 and Δ_{max} separately in each bin used for the discretization of the distributions and introduced in general for the characterization of a CDF $c(r)$ the averaged quantities

$$\overline{\sigma}^2(c(r)) = \frac{1}{L_c}\int_{r=0}^{r=L_c} \sigma^2(c(r))dr, \tag{11}$$

$$\overline{\Delta}_{max}(c(r)) = \frac{1}{L_c}\int_{r=0}^{r=L_c} \Delta_{max}(c(r))dr. \tag{12}$$

Here, $L_c = 0.12L_{RVE}$ for $c(r) = c_{pore}(r)$ and $L_c = 2L_{RVE}$ for $c(r) = c_{r-node}(r)$ and $c(r) = c_{r-fiber}(r)$. Fig. 11 compares $\overline{\sigma}^2$ and $\overline{\Delta}_{max}$ for the mentioned distribution functions for the RVEs in the categories '—' and $V_iL_jC_kF_q$. Apparently also $p_{pore}(r), p_{r-node}(r)$ and $p_{r-fiber}(r)$ are at least to a large extent implicitly determined by fixing the four morphological main descriptors identified above.

5. Conclusions

Studies of the mechanical properties of heterogeneous random media have attracted substantial interest over the last two decades. A key question in this area is which descriptors of the microstructure of such media determine to which extend their mechanical properties. Specifically for networks of fibers or ligaments, this has remained unclear so far. Such networks play an important role in biophysics and soft matter physics but also in materials research, in particular with respect to nanoporous metals [52–56]. The microstructure of the latter differs from the fiber networks usually studied in biophysics by the fact that it is formed by a network of ligaments with a considerable thickness and variation in shape. Yet both fiber networks in biophysics and ligament networks as occurring in nanoporous metals appear to share important common properties. For example, in biophysics, it has been suggested that fiber length distribution, valency distribution and direction cosine distribution play important roles in the mechanical behavior of collagen fiber networks [4]. And also for nanoporous metals it has been found that characteristics such as node valency or ligament length have important effects on the macroscopic mechanical properties [57–60]. Yet, so far it remains unclear to which extend these findings in separate areas of materials science are related to each other and which other descriptors are important determinants of the mechanical properties.

To answer these questions, we performed a large computational study including more than 2500 RVEs. Using simulated annealing [33], we constructed these RVEs sampling a large part of the physically reasonable configuration space. As expected, we observed in finite element models a large variance of Young's modulus and Poisson's ratio among these 2520 RVEs. However, we also observed that fixing four morphological key descriptors to specific values or probability distributions reduced this variance by more than 99%. These four key descriptors are the number of fibers per volume (i.e., the fiber density), the node valency distribution, the fiber length distribution, and the direction cosine distribution. We demonstrated that the four key descriptors did not only largely determine the mechanical properties but also a host of other morphological or graph-theory-based descriptors. We thus conclude that the number of fibers per volume, the node valency distribution, the fiber length distribution, and the direction cosine distribution are the key properties of networks of (thin) fibers both with respect to mechanics and geometry.

Remarkably, we observed that the number of fibers per volume is (nearly) linearly related to Young's modulus of fiber networks, which we could also explain by a simple theoretical analysis. Interestingly, we observed that also the effect of valency, fiber length and direction cosine distribution on Young's modulus can be captured to a very large extent by a simple linear or quadratic relationship between the mean values of these distributions and Young's modulus. Thereby stiffness increases with mean valency and decreases with mean fiber length and mean direction cosine. This finding is in excellent agreement with [61], where based on a different approach already previously a remarkably simple ascending relationship between mean valency and stiffness was reported specifically for nanoporous metals.

Given that for valency, fiber length and direction cosine distribution apparently mainly the mean values matter for the stiffness of the network, one can summarized our study as follows: the mechanical properties of fiber networks are largely determined by four scalar descriptors, which are the number of fibers per volume and the mean valency, mean fiber length and mean direction cosine. Among these four scalar descriptors the former two are by far dominant whereas the latter two are modulators of minor importance. Generally, we found that the dependence of Young's modulus on the four key descriptors was much stronger than the dependence of Poisson's ratio.

The identification of four simple scalar descriptors for characterizing the mechanical properties of fiber networks can be expected to be an important step to understand the relation between microstructure and macroscopic mechanical properties of materials consisting of random fiber networks. It should, however, be kept in mind that this study has also certain limitations. First, it focuses on linear mechanical properties (Young's modulus and Poisson's ratio) of isotropic fiber networks only. A generalization to nonlinear anisotropic materials is a natural next step. Since the macroscopic material behavior is strongly influenced by microstructural defects [62–64], large deformation, plasticity and failure of random fiber networks is a promising area of future research. Second, our study largely relies on a computational approach. A

promising next step is underpinning its main findings by a careful theoretical analysis unraveling the rationale behind the role of the different descriptors.

Data availability

The raw/processed data required to reproduce these findings cannot be shared at this time as the data also forms part of an ongoing study.

CRediT authorship contribution statement

Iman Davoodi Kermani: Conceptualization, Formal analysis, Methodology, Software, Validation, Visualization, Writing – original draft. **Maximilian Schmitter:** Conceptualization, Methodology, Software, Writing – review & editing. **Jonas F. Eichinger:** Writing – review & editing. **Roland C. Aydin:** Conceptualization, Methodology. **Christian J. Cyron:** Conceptualization, Formal analysis, Funding acquisition, Methodology, Project administration, Supervision, Writing – review & editing.

Declaration of Competing Interest

The authors declare that they have no known competing financial interests or personal relationships that could have appeared to influence the work reported in this paper.

Acknowledgments

The first author (IDK) acknowledges financial support by German Academic Exchange Service (DAAD), Funding programme/-ID: Graduate School Scholarship Programm, 2016 (57243780). The authors gratefully acknowledge financial support by the International Graduate School of Science and Engineering (IGSSE) of the Technical University of Munich, Germany (Funder ID: 10.13039/501100005713). This work was also funded by the Deutsche Forschungsgemeinschaft (DFG, German Research Foundation) – SFB 986 – 192346071.

Appendix A. Summary of simulated annealing method

See Fig. A.12.

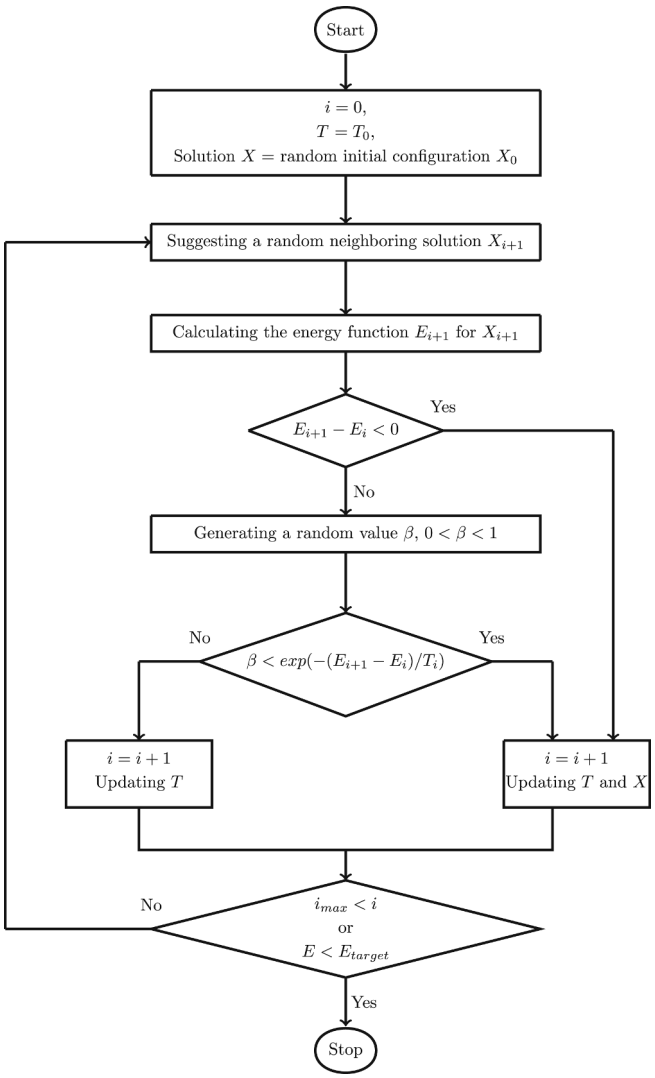

Fig. A.12. Flow chart of the simulated annealing algorithm used herein.

Appendix B. Definition of considered distributions for valency, fiber length and direction cosine

The probability distribution functions (PDFs) for the valency, fiber length and direction cosine used in this article are defined by algebraic equations in the following.

B.1. Valency distributions

$$V_1(v) = \frac{1}{15}(6 - v), \tag{B.1}$$

$$V_2(v) = -\frac{1}{35}v(v - 6) \tag{B.2}$$

$$V_3(v) = \frac{1}{6}, \tag{B.3}$$

$$V_4(v) = \frac{1}{15}(v - 1), \tag{B.4}$$

$$V_5(v) = \begin{cases} 0 & v \leqslant 3, \\ -\frac{1}{22}(v - 3)(v - 9) & 3 < v, \end{cases} \tag{B.5}$$

where v $(v = 1, 2, \ldots, 6)$ represents the node valency.

B.2. Fiber length distributions

$$L_1(l) = \frac{4}{0.3^4}(\frac{1}{3} - l)^3, \tag{B.6}$$

$$L_2(l) = -\frac{200}{9}(l - \frac{1}{3}), \tag{B.7}$$

$$L_3(l) = \frac{10}{3}, \tag{B.8}$$

$$L_4(l) = -\frac{2000}{9}(l - \frac{1}{3})(l - \frac{1}{30}), \tag{B.9}$$

$$L_5(l) = \frac{200}{9}(l - \frac{1}{30}), \tag{B.10}$$

$$L_6(l) = \frac{4}{0.3^4}(l - \frac{1}{30})^3, \tag{B.11}$$

where $l = r/\mathrm{L_{RVE}}$ is a normalized fiber length with $(\frac{1}{30} \leqslant l \leqslant \frac{1}{3})$. The minimum of $l = \frac{1}{30}$ prevents having the fibers of very short length.

B.3. Direction cosine distributions

$$C_1(c) = \frac{1}{2}(1 - c), \tag{B.12}$$

$$C_2(c) = \begin{cases} -c & -1 \leqslant c \leqslant 0, \\ c & 0 < 1, \end{cases} \tag{B.13}$$

$$C_3(c) = \frac{1}{2}, \tag{B.14}$$

$$C_4(c) = \frac{3}{4}(1 - c^2), \tag{B.15}$$

$$C_5(c) = \frac{1}{2}(1 + c), \tag{B.16}$$

where c $(-1 \leqslant c \leq 1)$ is the cosine of the angle between a pair of fibers adjacent to the same network node.

Appendix C. Relation between morphological descriptors and mechanical properties of the networks with fiber diameter of $L_{RVE}/500$

The studies shown in Section 4.1 were performed also for networks with a fiber diameter of $L_{RVE}/500$ (ten times smaller than the one used in Section 4.1). As shown in the following, this changes the results quantitatively, but not qualitatively, underlining the robustness of our conclusions. See Figs. C.13–C.15.

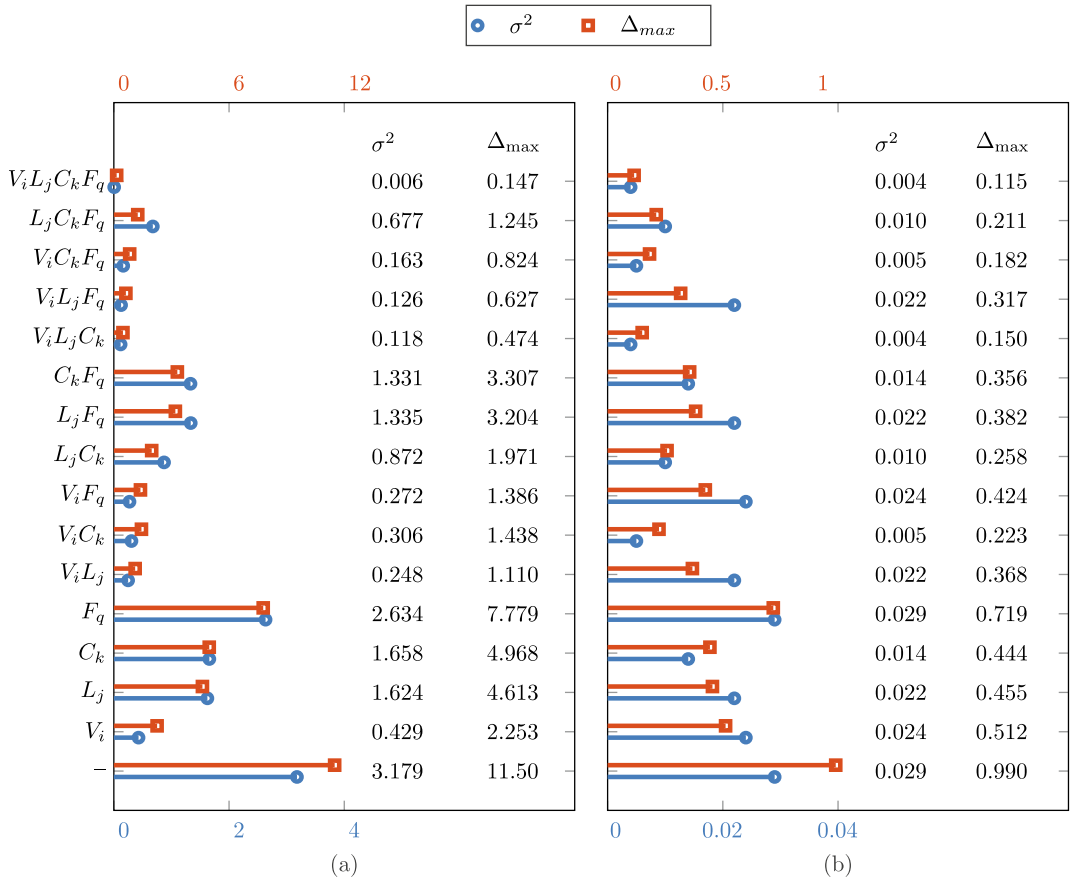

Fig. C.13. For the 16 different RVE categories considered in this study, we computed for (a) Young's modulus and (b) Poisson's ratio the relative variances and maximal deviations from their mean values, averaged across all RVE types belonging to the respective RVE category. Apparently, fixing the four descriptors valency distribution, fiber length distribution, direction cosine distribution and number of fibers reduced the statistical variance of the mechanical properties nearly to zero.

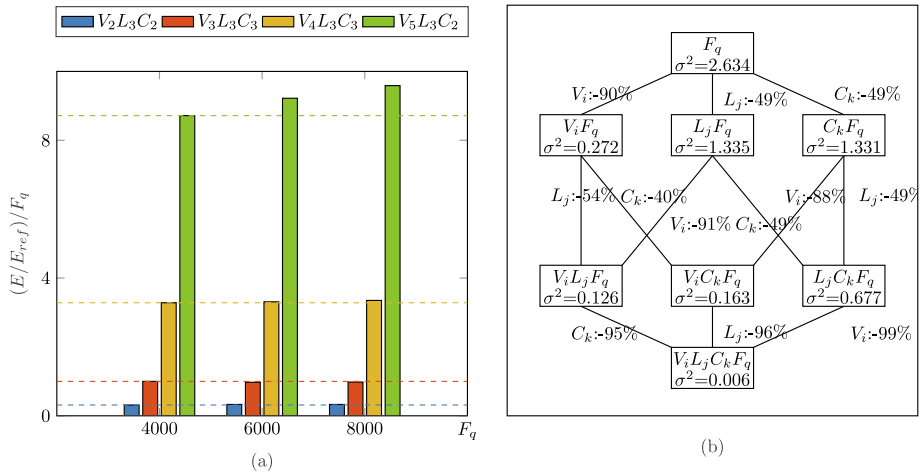

Fig. C.14. (a) Young's modulus for a representative selection of RVE types normalized by the number of fibers F_q (and the homogenized mean Young's modulus $E_{ref} = 9.4e3\ MPa$ of the RVE type $V_3L_3C_3F_1$); (b) fixing more and more descriptors, the relative variance (σ^2) of Young's modulus in the resulting RVE categories (boxes) decreases by a percentage indicated next to the lines connecting an RVE category with one resulting from fixing one more descriptor, respectively.

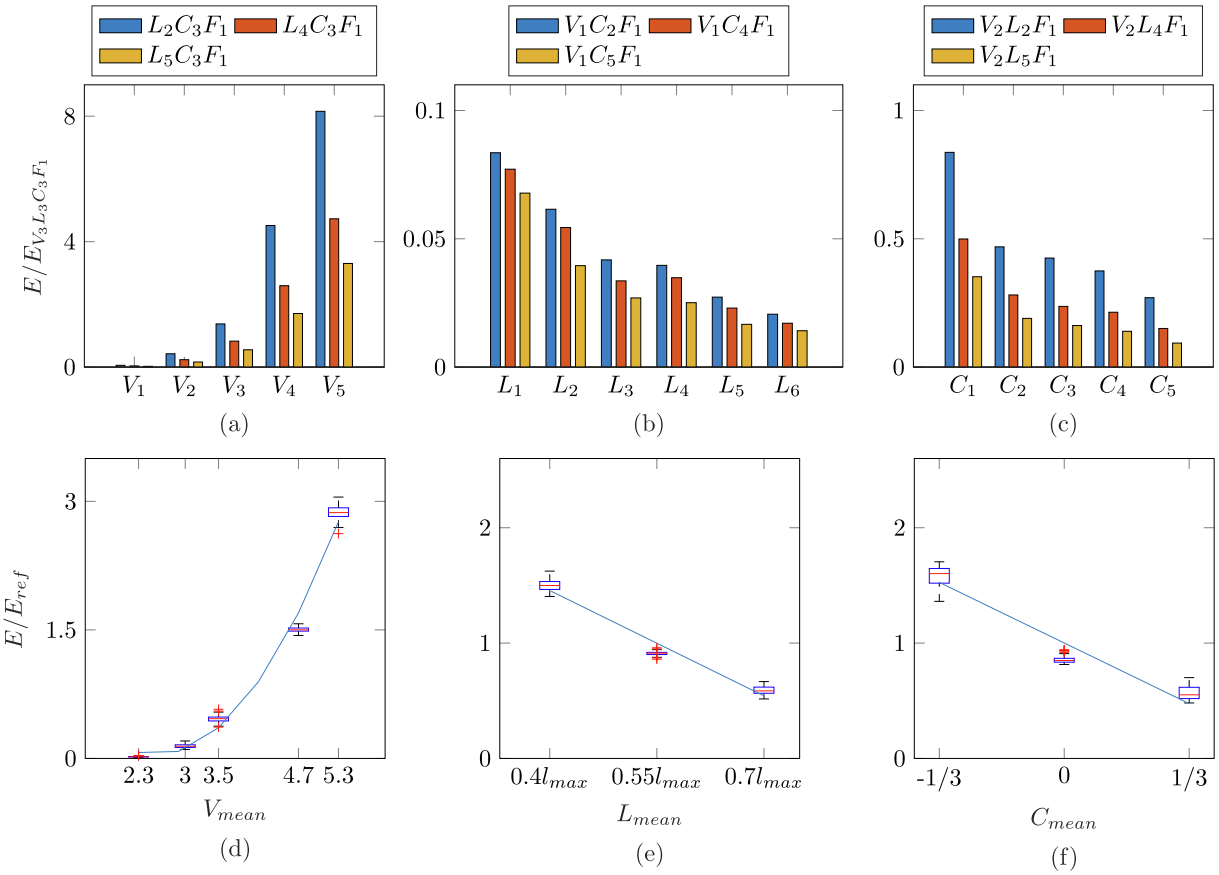

Fig. C.15. Young's modulus monotonically increases with the mean valency and decreases monotonically with mean fibers length and mean direction cosine as illustrated here for a number of representative RVE types. The Young's modulus in (a)-(c) is normalized to the Young's modulus of the RVE type $V_3L_3C_3F_1$ which is $E_{V_3L_3C_3F_1} = 9.4e3\ MPa$ and in (d)-(f) to the E_{ref} according to the definition presented in the text.

References

[1] P.R. Onck, T. Koeman, T. van Dillen, E. van der Giessen, Alternative explanation of stiffening in cross-linked semiflexible networks, Physical Review Letters 95 (2005), https://doi.org/10.1103/physrevlett.95.178102.

[2] A. Kabla, L. Mahadevan, Nonlinear mechanics of soft fibrous networks, Journal of The Royal Society Interface 4 (2006) 99–106, https://doi.org/10.1098/rsif.2006.0151.

[3] E.M. Huisman, T. van Dillen, P.R. Onck, E. van der Giessen, Three-dimensional cross-linked f-actin networks: Relation between network architecture and mechanical behavior, Physical Review Letters 99 (2007), https://doi.org/10.1103/physrevlett.99.208103.

[4] S.B. Lindström, D. Vader, A. Kulachenko, D. Weitz, Biopolymer network geometries: Characterization, regeneration, and elastic properties, Physical Review E 82 (2010), https://doi.org/10.1103/physreve.82.051905.

[5] R. Picu, Mechanics of random fiber networks–a review, Soft Matter 7 (2011) 6768, https://doi.org/10.1039/c1sm05022b.

[6] G. Žagar, P.R. Onck, E. van der Giessen, Elasticity of rigidly cross-linked networks of athermal filaments, Macromolecules 44 (2011), https://doi.org/10.1021/ma201257v.

[7] S. Lavrykov, B.V. Ramarao, S.B. Lindström, K.M. Singh, 3D network simulations of paper structure, Nordic Pulp & Paper Research Journal 27 (2012) 256–263, https://doi.org/10.3183/npprj-2012-27-02-p256-263.

[8] S.B. Lindström, A. Kulachenko, L.M. Jawerth, D.A. Vader, Finite-strain, finite-size mechanics of rigidly cross-linked biopolymer networks, Soft Matter 9 (2013) 7302–7313, https://doi.org/10.1039/c3sm50451d.

[9] C. Cyron, K. Müller, A. Bausch, W. Wall, Micromechanical simulations of biopolymer networks with finite elements, Journal of Computational Physics 244 (2013) 236–251, https://doi.org/10.1016/j.jcp.2012.10.025.

[10] T. Jin, I. Stanciulescu, Numerical simulation of fibrous biomaterials with randomly distributed fiber network structure, Biomechanics and Modeling in Mechanobiology 15 (2015) 817–830, https://doi.org/10.1007/s10237-015-0725-6.

[11] M. Vahabi, A. Sharma, A. Licup, A. van Oosten, P. Galie, P. Janmey, F. MacKintosh, Elasticity of fibrous networks under uniaxial prestress, Soft Matter 12 (2016) 5050–5060, https://doi.org/10.1039/c6sm00606j.

[12] H. Hatami-Marbini, Simulation of the mechanical behavior of random fiber networks with different microstructure, The European Physical Journal E 41 (2018) 817–830, https://doi.org/10.1140/epje/i2018-11673-0.

[13] K. Jansen, A. Licup, A. Sharma, R. Rens, F. MacKintosh, G. Koenderink, The role of network architecture in collagen mechanics, Biophysical Journal 114 (2018) 2665–2678, https://doi.org/10.1016/j.bpj.2018.04.043.

[14] P. Taufalele, J. VanderBurgh, A. Muñoz, M. Zanotelli, C. Reinhart-King, Fiber alignment drives changes in architectural and mechanical features in collagen matrices, PLOS One 14 (2019), e0216537, https://doi.org/10.1371/journal.pone.0216537.

[15] V. Negi, R. Picu, Mechanical behavior of cross-linked random fiber networks with inter-fiber adhesion, Journal of the Mechanics and Physics of Solids 122 (2019) 418–434, https://doi.org/10.1016/j.jmps.2018.09.027.

[16] S. Domaschke, M. Zündel, E. Mazza, A.E. Ehret, A 3D computational model of electrospun networks and its application to inform a reduced modelling approach, International Journal of Solids and Structures 158 (2019) 76–89, https://doi.org/10.1016/j.ijsolstr.2018.08.030.

[17] S. Domaschke, A. Morel, G. Fortunato, A.E. Ehret, Random auxetics from buckling fibre networks, Nature Communications 10 (2019), https://doi.org/10.1038/s41467-019-12757-7.

[18] S. Domaschke, A. Morel, R. Kaufmann, J. Hofmann, R. Rossi, E. Mazza, G. Fortunato, A.E. Ehret, Predicting the macroscopic response of electrospun membranes based on microstructure and single fibre properties, Journal of the Mechanical Behavior of Biomedical Materials 104 (2020), 103634, https://doi.org/10.1016/j.jmbbm.2020.103634.

[19] V. Kouznetsova, M. Geers, W. Brekelmans, Multi-scale constitutive modelling of heterogeneous materials with a gradient-enhanced computational homogenization scheme, International Journal for Numerical Methods in Engineering 54 (2002) 1235–1260, https://doi.org/10.1002/nme.541.

[20] Y. Jiao, F. Stillinger, S. Torquato, Modeling heterogeneous materials via two-point correlation functions: Basic principles, Physical Review E 76 (2007), https://doi.org/10.1103/physreve.76.031110.

[21] Y. Jiao, F. Stillinger, S. Torquato, Modeling heterogeneous materials via two-point correlation functions. ii. algorithmic details and applications, Physical Review E 77 (2008), https://doi.org/10.1103/physreve.77.031135.

[22] S. Chen, H. Li, Y. Jiao, Dynamic reconstruction of heterogeneous materials and microstructure evolution, Physical Review E 92 (2015), https://doi.org/10.1103/physreve.92.023301.

[23] M. Yang, A. Nagarajan, B. Liang, S. Soghrati, New algorithms for virtual reconstruction of heterogeneous microstructures, Computer Methods in Applied Mechanics and Engineering 338 (2018) 275–298, https://doi.org/10.1016/j.cma.2018.04.030.
[24] A. Roberts, Statistical reconstruction of three-dimensional porous media from two-dimensional images, Physical Review E 56 (1997) 3203–3212, https://doi.org/10.1103/physreve.56.3203.
[25] D. Chen, X. He, Q. Teng, Z. Xu, Z. Li, Reconstruction of multiphase microstructure based on statistical descriptors, Physica A: Statistical Mechanics and its Applications 415 (2014) 240–250, https://doi.org/10.1016/j.physa.2014.07.066.
[26] J. Feng, C. Li, S. Cen, D. Owen, Statistical reconstruction of two-phase random media, Computers & Structures 137 (2014) 78–92, https://doi.org/10.1016/j.compstruc.2013.03.019.
[27] G. Papakosta, J. Nolan, N. Vordos, D. Gkika, M. Kainourgiakis, A. Mitropoulos, On 3D reconstruction of porous media by using spatial correlation functions, Journal of Engineering Science and Technology Review 8 (2015), https://doi.org/10.25103/jestr.084.12.
[28] C. Soyarslan, S. Bargmann, M. Pradas, J. Weissmüller, 3D stochastic bicontinuous microstructures: Generation, topology and elasticity, Acta Materialia 149 (2018) 326–340, https://doi.org/10.1016/j.actamat.2018.01.005.
[29] M. Geers, V. Kouznetsova, W. Brekelmans, Multi-scale computational homogenization: Trends and challenges, Journal of Computational and Applied Mathematics 234 (2010) 2175–2182, https://doi.org/10.1016/j.cam.2009.08.077.
[30] D. Li, Review of structure representation and reconstruction on mesoscale and microscale, JOM 66 (2014) 444–454, https://doi.org/10.1007/s11837-013-0848-0.
[31] K. Matouš, M. Geers, V. Kouznetsova, A. Gillman, A review of predictive nonlinear theories for multiscale modeling of heterogeneous materials, Journal of Computational Physics 330 (2017) 192–220, https://doi.org/10.1016/j.jcp.2016.10.070.
[32] R. Bostanabad, Y. Zhang, X. Li, T. Kearney, L. Brinson, D. Apley, W. Liu, W. Chen, Computational microstructure characterization and reconstruction: Review of the state-of-the-art techniques, Progress in Materials Science 95 (2018) 1–41, https://doi.org/10.1016/j.pmatsci.2018.01.005.
[33] M. Rintoul, S. Torquato, Reconstruction of the structure of dispersions, Journal of Colloid and Interface Science 186 (1997) 467–476, https://doi.org/10.1006/jcis.1996.4675.
[34] C. Yeong, S. Torquato, Reconstructing random media, Physical Review E 57 (1998) 495–506, https://doi.org/10.1103/physreve.57.495.
[35] C. Yeong, S. Torquato, Reconstructing random media. ii. three-dimensional media from two-dimensional cuts, Physical Review E 58 (1998) 224–233, https://doi.org/10.1103/physreve.58.224.
[36] H. Kumar, C. Briant, W. Curtin, Using microstructure reconstruction to model mechanical behavior in complex microstructures, Mechanics of Materials 38 (2006) 818–832, https://doi.org/10.1016/j.mechmat.2005.06.030.
[37] Y. Liu, M.S. Greene, W. Chen, D. Dikin, W. Liu, Computational microstructure characterization and reconstruction for stochastic multiscale material design, Computer-Aided Design 45 (2013) 65–76, https://doi.org/10.1016/j.cad.2012.03.007.
[38] L. Pant, S. Mitra, M. Secanell, Multigrid hierarchical simulated annealing method for reconstructing heterogeneous media, Physical Review E 92 (2015), https://doi.org/10.1103/physreve.92.063303.
[39] N. Lang, S. Münster, C. Metzner, P. Krauss, S. Schürmann, J. Lange, K. Aifantis, O. Friedrich, B. Fabry, Estimating the 3D pore size distribution of biopolymer networks from directionally biased data, Biophysical Journal 105 (2013) 1967–1975, https://doi.org/10.1016/j.bpj.2013.09.038.
[40] J. Flusser, B. Zitova, T. Suk, Moments And Moment Invariants In Pattern Recognition, AJOHN WIELEY & SONS, 2009.
[41] M. Hickman, Geometric moments and their invariants, Journal of Mathematical Imaging and Vision 44 (2011) 223–235, https://doi.org/10.1007/s10851-011-0323-x.
[42] http://zoi.utia.cas.cz/files/rot3dinvs8web.pdf.
[43] D. West. Introduction to Graph Theory, Prentice-Hall of India Private Limited, New Delhi, 2005.
[44] L. Li, D. Alderson, J. Doyle, W. Willinger, Towards a theory of scale-free graphs: Definition, properties, and implications, Internet Mathematics 2 (2005) 431–523, https://doi.org/10.1080/15427951.2005.10129111.
[45] A. Brouwer, W. Haemers. Spectra of Graphs, Springer, New York, 2012.
[46] G. Chalancon, K. Kruse, M. Babu, Clustering Coefficient, Springer, New York, New York, 2013, pp. 422–424. https://doi.org/10.1007/978-1-4419-9863-7_1239.
[47] W. Ben-Ameur, Computing the initial temperature of simulated annealing, Computational Optimization and Applications 29 (2004) 369–385, https://doi.org/10.1023/b:coap.0000044187.23143.bd.
[48] K. Schneider, Computational micromechanics of matrix-inclusion composites, Dr.-ing. thesis, Technischen Universität Hamburg (TUHH), 2019.
[49] K. Berkache, S. Deogekar, I. Goda, R.C. Picu, J.-F. Ganghoffer, Construction of second gradient continuum models for random fibrous networks and analysis of size effects, Composite Structures 181 (2017), https://doi.org/10.1016/j.compstruct.2017.08.078.
[50] H. Reda, K. Berkache, J.-F. Ganghoffer, H. Lakiss, Dynamical properties of random fibrous networks based on generalized continuum mechanics, Waves in Random and Complex Media 30 (2018), https://doi.org/10.1080/17455030.2018.1478468.
[51] K. Berkache, S. Deogekar, I. Goda, R.C. Picu, J.-F. Ganghoffer, Identification of equivalent couple-stress continuum models for planar random fibrous media, Continuum Mechanics and Thermodynamics 31 (2019), https://doi.org/10.1007/s00161-018-0710-2.
[52] H. Rösner, S. Parida, D. Kramer, C. Volkert, J. Weissmüller, Reconstructing a nanoporous metal in three dimensions: An electron tomography study of dealloyed gold leaf, Advanced Engineering Materials 9 (2007) 535–541, https://doi.org/10.1002/adem.200700063.
[53] J. Weissmüller, R. Newman, H. Jin, A. Hodge, J. Kysar, Nanoporous metals by alloy corrosion: Formation and mechanical properties, MRS Bulletin 34 (2009) 577–586, https://doi.org/10.1557/mrs2009.157.
[54] Z. Qi, J. Weissmüller, Hierarchical nested-network nanostructure by dealloying, ACS Nano 7 (2013) 5948–5954, https://doi.org/10.1021/nn4021345.
[55] Z. Qi, U. Vainio, A. Kornowski, M. Ritter, H. Weller, H. Jin, J. Weissmüller, Porous gold with a nested-network architecture and ultrafine structure, Advanced Functional Materials 25 (2015) 2530–2536, https://doi.org/10.1002/adfm.201404544.
[56] J. Jiao, N. Huber, Deformation mechanisms in nanoporous metals: Effect of ligament shape and disorder, Computational Materials Science 127 (2017) 194–203, https://doi.org/10.1016/j.commatsci.2016.10.035.
[57] C. Richert, N. Huber, Skeletonization, geometrical analysis, and finite element modeling of nanoporous gold based on 3D tomography data, Metals 8 (2018) 282, https://doi.org/10.3390/met8040282.
[58] C. Richert, A. Odermatt, N. Huber, Computation of thickness and mechanical properties of interconnected structures: Accuracy, deviations, and approaches for correction, Frontiers in Materials 6 (2019), https://doi.org/10.3389/fmats.2019.00327.
[59] C. Richert, N. Huber, A review of experimentally informed micromechanical modeling of nanoporous metals: From structural descriptors to predictive structure–property relationships, Materials 13 (2020) 3307, https://doi.org/10.3390/ma13153307.
[60] A. Odermatt, C. Richert, N. Huber, Prediction of elastic-plastic deformation of nanoporous metals by FEM beam modeling: A bottom-up approach from ligaments to real microstructures, Materials Science and Engineering: A 791 (2020), 139700, https://doi.org/10.1016/j.msea.2020.139700.
[61] N. Huber, Connections between topology and macroscopic mechanical properties of three-dimensional open-pore materials, Frontiers in Materials 5 (2018), https://doi.org/10.3389/fmats.2018.00069.
[62] S. Li, B. Ren, H. Minaki, Multiscale crystal defect dynamics: a dual-lattice process zone model, Philosophical Magazine 94 (2014), https://doi.org/10.1080/14786435.2014.887859.
[63] D. Lyu, S. Li, Multiscale crystal defect dynamics: A coarse-grained lattice defect model based on crystal microstructure, Journal of the Mechanics and Physics of Solids 107 (2017), https://doi.org/10.1016/j.jmps.2017.07.006.
[64] D. Lyu, S. Li, A multiscale dislocation pattern dynamics: Towards an atomistic-informed crystal plasticity theory, Journal of the Mechanics and Physics of Solids 122 (2019), https://doi.org/10.1016/j.jmps.2018.09.025.

A.2 Paper B

Simulated annealing framework for generating representative volume elements of materials with complex ligamentous microstructures

Iman Davoodi Kermani, Lena Dyckhoff, Roland C. Aydin, Norbert Huber, Christian J. Cyron

published in

Computational Materials Science, 10.1016/j.commatsci.2023.112302

Computational Materials Science 228 (2023) 112302

Contents lists available at ScienceDirect

Computational Materials Science

journal homepage: www.elsevier.com/locate/commatsci

Full length article

Simulated annealing framework for generating representative volume elements of materials with complex ligamentous microstructures

Iman Davoodi Kermani [a,b,*], Lena Dyckhoff [c], Roland C. Aydin [b], Norbert Huber [c,d], Christian J. Cyron [b,e]

[a] Institute for Computational Mechanics, School of Engineering and Design, Technical University of Munich, Boltzmannstrasse 15, D-85748 Garching, Germany
[b] Institute of Material Systems Modeling, Helmholtz-Zentrum Hereon, Max–Planck Strasse 1, 21502 Geesthacht, Germany
[c] Institute of Materials Mechanics, Helmholtz-Zentrum Hereon, Max–Planck Strasse 1, 21502 Geesthacht, Germany
[d] Institute of Materials Physics and Technology, Hamburg University of Technology, Eissendorfer Strasse 42 (M), 21073 Hamburg, Germany
[e] Institute for Continuum and Material Mechanics, Hamburg University of Technology, Eissendorfer Strasse 42 (M), 21073 Hamburg, Germany

ARTICLE INFO

Keywords:
Descriptors
Microstructure
Network
Representative volume element
Simulated annealing

ABSTRACT

At the microscale, various materials from biological tissues to nanoporous metals are formed by networks of ligaments. Here we propose a highly efficient simulated annealing (SA) framework for generating synthetic representative volume elements (RVE) of such materials. It can produce RVE where the microstructural characteristics both on the network level (e.g., node valency and ligament length) and on the level of individual ligaments (e.g., curvature) can be predefined by the user via probability distributions. As an application example of our framework, we generate a large variety of RVEs, analyze their mechanical properties by the finite element method, and establish through this approach links between microstructural descriptors and macromechanical properties of materials with ligamentous microstructures.

1. Introduction

Numerous natural and industrial materials exhibit a microstructure that is essentially a network of ligaments. These ligaments can be different kinds of bio-fibers [1–4] or metallic ligaments as arising in nanoporous metals (NPMs) [5–8]. Therefore the generation, characterization, and analysis of fiber structures increasingly came into focus in recent years [9–22]. Theoretical predictions of the macroscopic properties of materials based on their microstructure are typically possible only for materials with a relatively simple microstructure or in the sense of general scaling relations. For complex microstructures, the quantitative prediction of macroscopic mechanical properties is typically possible only by computational modeling. Such computational models analyze so-called *representative volume elements* (RVE). These are (typically cubic) domains just large enough to represent the essential macroscopic properties of a material of interest and at the same time, small enough to keep computations affordable [23–29].

RVEs of ligamentous materials are composed by a number of ligaments (e.g., fibers) connected to each other at specific points called junctions or nodes. In some cases, the ligaments may be arranged following a specific (deterministic) structure and they may exhibit a uniform shape (e.g., straight cylindrical fibers). However, in general, both shape and arrangement of the ligaments are random [30–32]. So far, computational studies of ligamentous RVE are largely limited to ligament arrangements that are either fully structured [33–36] or exhibit only slight random perturbations of very specific properties [37–42]. Comprehensive studies beyond this scope remain still wanting because they require efficient algorithms for the generation of RVEs with general ligamentous random microstructures. To overcome this limitation at least in parts, we recently proposed an algorithm that was able to generate (nearly) arbitrary RVE with ligamentous microstructure with the only major limitation that the individual ligaments were cylindrical [28].

In this paper, we propose an extension of [28]. This extension enables the generation of RVE with a microstructure where not only the network structure formed by the ligaments is arbitrary but also the shape of the individual ligaments. To achieve this, we present a two-stage approach. During the first stage, a random network of ligaments is generated by so-called *simulated annealing* (SA) [10,43–46]. During the second stage of our framework, the individual ligaments are assigned shapes following user-defined random distributions. Specifically, we use the ligament thickness and curvature as primary descriptors of their shape. Our two-stage approach for generating ligamentous RVE can

* Corresponding author at: Institute for Computational Mechanics, School of Engineering and Design, Technical University of Munich, Boltzmannstrasse 15, D-85748 Garching, Germany.
E-mail address: iman.davoodi@tum.de (I. Davoodi Kermani).

https://doi.org/10.1016/j.commatsci.2023.112302
Received 8 February 2023; Received in revised form 26 May 2023; Accepted 28 May 2023

be understood as a divide-and-conquer approach gradually adding up geometrical complexities of the final microstructure. This divide-and-conquer approach is computationally highly efficient. It provides for the first time a framework to produce random ligament networks which conform to specific predefined microstructural descriptors both on the network and the ligament level. The RVEs generated with our method are homogeneous, isotropic, fully periodic and connected network of ligaments. This means in particular, the ligament phase is continuous within a single RVE and, if we repeat that RVE in one of the three directions aligned with its edges, the resulting larger material volume has still a continuous ligament phase.

To demonstrate the advantages of our new approach, we employed it to generate a large variety of different RVEs with systematic variations of their key microstructural descriptors. Subsequently, we employed the finite element method (FEM) to study the macroscopic mechanical behavior of the generated RVEs [47,48]. This provided important insights into the relation between the macroscopic properties and microstructure.

This article is organized as follows: In Section 2, we present the mathematical definition of the microstructural descriptors used in this study. The novel two-stage approach for generating tailor-made ligamentous RVEs is introduced step by step in Section 3. The numerical examples are presented in Section 4. Finally, the article closes with the conclusions in Section 5.

2. Descriptors of ligamentous microstructures

Microstructures can in general be characterized by a number of so-called descriptors. These descriptors are measure of certain geometric properties of the microstructure. In a porous material, such descriptors can, for example, be the solid and void volume fractions or the average pore size or also the statistical distribution of pore sizes. A ligamentous microstructure contains a number of ligaments connected at specific points called nodes or junctions. In other words, nodes and ligaments are the key constituents of a ligamentous RVE. Hence, to characterize a ligamentous RVE, one needs descriptors characterizing the geometry of ligaments and junctions in some sense. Generally, one can distinguish between descriptors at the network level and descriptors at the component (ligament or node) level as discussed in more detail in Sections 2.1 and 2.2. Herein, the superscript i denotes descriptors related to the ith junction or the ith ligament.

2.1. Network level descriptors

The network level descriptors are the descriptors which define the network's morphology independent of its components' shape. This means, they define the position of the junctions in space and their connectivity, that is, which junction is connected to which other junction by a ligament. In the first stage of the method developed herein, we focus on network level descriptors only. As demonstrated by [28], among the numerous theoretically possible network descriptors, only the following four are important for the mechanical behavior of the network (and thus considered in this article).

Junction valency distribution V is the probability distribution of the junction valencies in the network. The valency of the ith junction v^i is the number of ligaments connected to this junction.

Adjacent junctions' distance distribution L is the probability distribution of the euclidean distance between all pairs of adjacent junctions. In a ligamentous network, two junctions are called adjacent if and only if they are connected to each other directly by a single ligament. In a network with straight ligaments, the distance between adjacent junctions equals the length of corresponding ligament. By contrast, if a ligament is curved, its length is larger than the euclidean distance between the two junctions it connects. In general the distance between the two junctions connected by the ith ligament is denoted as l^i.

Direction cosine distribution C : assume junction i has the valency v^i. Then we can define pairs of ligaments mutually connected at this junction. For example, if $v^i = 3$, three such pairs can be defined, formed by the first and second ligament, the first and third ligament, and the second and third ligament, respectively. For each ligament we can define a straight line between the two junctions it connects. Then, for each pair of ligaments, one can compute the cosine of the angle between these two lines. This can be done for all junctions in the network. The set of all cosines computed this way yields a specific distribution. This distribution is called the direction cosine distribution C of the network.

Compactness of the network is determined by N_j, the mean number of junctions per unit volume of the RVE, and N_l, the mean number of ligaments per unit volume of the RVE. For an RVE with edge length of l_{RVE} and n_j junctions, the following relation exists

$$N_l = \frac{1}{2 \times (l_{RVE})^3} \sum_{i=1}^{n_j} v^i. \tag{1}$$

That is, N_j and N_l are not independent and we need only one of both to specify the compactness of the network.

2.2. Component level descriptors

The component level descriptors are the descriptors which define the geometry of individual network components (i.e. junctions and ligaments) and are used in the second stage of our suggested approach. A large variety of component level descriptors could in principle be defined. As the main focus of this article is a proof of concept how RVE can be generated in a two-stage procedure distinguishing between network and component level descriptors, we limit the scope of this article to three particularly prominent component level descriptors. We note, however, that the addition of further component level descriptors into our framework would be straightforward. The definitions of the following three component level descriptors are also illustrated in Fig. 1 for a specific ligament.

Junction's radius distribution r_j is the probability distribution governing the radius of all the junctions in the RVE. That is, the junctions are modeled as spheres where the radius of ith junction is indicated by r_j^i, which can be considered a random variable drawn from the distribution r_j.

Ligament's cross-section radius r_l is considered to be variable along the ligament. For the ith ligament we define a local coordinate system whose first axis, the x^i-axis, connects the start and end point of the ligament by a straight line. Then the variation of the cross-section radius along the ith ligament can be described by $r_l^i(x^i)$ (Fig. 1). This function can be expressed as a sum of polynomials

$$r_l^i(x^i) = \sum_{k=0}^{k_{max}} d_k^i (x^i)^k, \qquad 0 \le x^i \le l^i, \tag{2}$$

where l^i is the euclidean distance between the start point and end point of the ith ligament. In case the function $r_l^i(x^i)$ is known – for example from experimental imaging data – the coefficients d_k^i directly result from a Taylor series

$$d_k^i = \frac{r_l^{i(k)}(0)}{k!}, \tag{3}$$

where $r_l^{i(k)}(0)$ is the kth derivative of $r_l^i(x^i)$ at $x^i = 0$. To generate synthetic RVE, the function $r_l^i(x^i)$ can be defined by selecting coefficients d_k^i according to certain criteria. This selection can be deterministic or stochastic according to certain predefined random distributions.

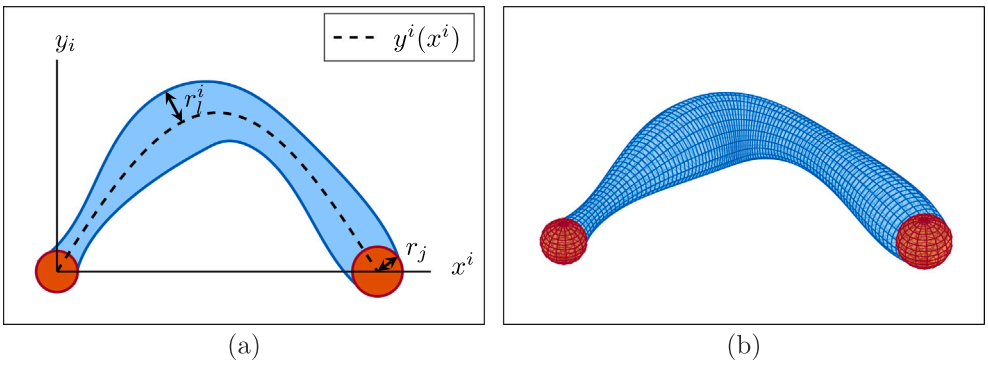

Fig. 1. (a) 2D and (b) 3D view of ith ligament (blue) and its adjacent junctions (red).

Ligament's curvature κ : assume a local $x^i - y^i - z^i$-coordinate system attached to the ith ligament where the x^i-axis is defined as pointed out above. In general ligaments may exhibit a curved shape. Herein, we consider for simplicity only ligaments with a non-zero curvature in the $x^i - y^i$-plane. In this case, the shape of the ligament can be modeled by a function $y^i(x^i)$ (Fig. 1), which can in general be expressed by a Fourier series:

$$y^i\left(x^i\right) = \frac{a_0^i}{2} + \sum_{n=1}^{f_{max}} \left[a_n^i \, cos\left(\frac{\pi n x^i}{l^i}\right) + b_n^i \, sin\left(\frac{\pi n x^i}{l^i}\right)\right], \tag{4}$$

where

$$a_n^i = \frac{2}{l^i}\int_0^{l^i} y^i\left(x^i\right) cos\left(\frac{\pi n x^i}{l^i}\right) dx^i, \tag{5a}$$

$$b_n^i = \frac{2}{l^i}\int_0^{l^i} y^i\left(x^i\right) sin\left(\frac{\pi n x^i}{l^i}\right) dx^i. \tag{5b}$$

If $y^i\left(x^i\right)$ is given, the coefficients a_n^i and b_n^i can be calculated from Eqs. (5a) and (5b). Conversely, defining the coefficients a_n^i and b_n^i during the RVE generation allows the generation of arbitrary ligament shapes (if a sufficient number n of Fourier modes is included and under the limitation of non-zero curvature in the $x^i - y^i$-plane only). Given $y^i\left(x^i\right)$, the ligament's curvature can be computed as

$$\kappa^i\left(x^i\right) = \frac{\left|\frac{d^2 y^i}{\left(dx^i\right)^2}\right|}{\left[1 + \left(\frac{dy^i}{dx^i}\right)^2\right]^{\frac{3}{2}}}. \tag{6}$$

3. RVE generating methodology

Due to the stochastic microstructure of typical ligamentous materials, it is not possible to define a unique unit cell for them. Rather an RVE with a stochastic structure is required that is large enough to represent the essential properties of the material with sufficiently low random variations. Here, we propose a two-stage approach to generate ligamentous RVE whose microstructure can be tailored by pre-defining certain characteristic descriptors. In Section 3.1 we briefly introduced simulated annealing (SA), the general concept on which our approach relies. Subsequently, in Section 3.2 we point out in detail how SA can be used in the first stage of our approach to generate a ligamentous RVE considering the descriptors of network level. In Section 3.3 we explain how in the second stage we can assign the descriptors of component level to the overall network structure generated in the first stage.

3.1. Simulated annealing method

Simulated annealing (SA) is a numerical optimization method for creating complex random structures according to certain predefined criteria. The method's name refers to annealing in metallurgy which entails systematic heating and gradual cooling to achieve desired changes of a material's microstructure via stochastic, thermally driven rearrangement. SA starts with a certain random structure and optimizes that structure step by step until the optimal agreement with the predefined criteria is achieved. The intermediate steps are stochastic, which endows SA with a relatively high ability to find global optima rather than getting trapped in local optima. That is, the intermediate steps of SA are not strictly seeking to further optimize the structure but also allow transient worsening with a certain likelihood that is governed by a temperature-like variable. Initially, this temperature-like variable is chosen high and then gradually decreased. In this way, SA initially can explore large parts of the parameter space whereas in the later stage it increasingly seeks straightforward optimization, finally yielding a converged solution.

To measure optimality of a given configuration, SA requires a *cost function*, which is often also referred to as *energy function* (noting that annealing in metallurgy seeks to minimize free energy). In short, the application of SA requires the definition of the following:

(1) *Initial configuration* and constraints of the optimization problem;
(2) *Perturbation mechanism* defining how the solution at the $(i+1)$-th iteration is obtained from the solution at the ith iteration. The perturbation mechanism has to be compatible with the problem constraints;
(3) *Energy function* measuring the optimality of a given configuration by a scalar value;
(4) *Cooling schedule* determining how the probability of accepting iterations decreasing the optimality of the configuration changes;
(5) *Cut-off criterion* terminating SA (e.g., when a maximal number of iterations is reached or when the cost function is acceptably small).

The following subsection explains how SA is applied herein to generate ligamentous RVE.

3.2. RVE generation at network level

In Section 2, we categorized the RVE descriptors into the two groups of network level descriptors and component level descriptors. Our suggested RVE generating algorithm also uses a similar classification and generates the RVE at two stages. In the first stage, it generates the overall network structure (defined by the position, valency, and connectivity of the junctions) without taking into consideration the

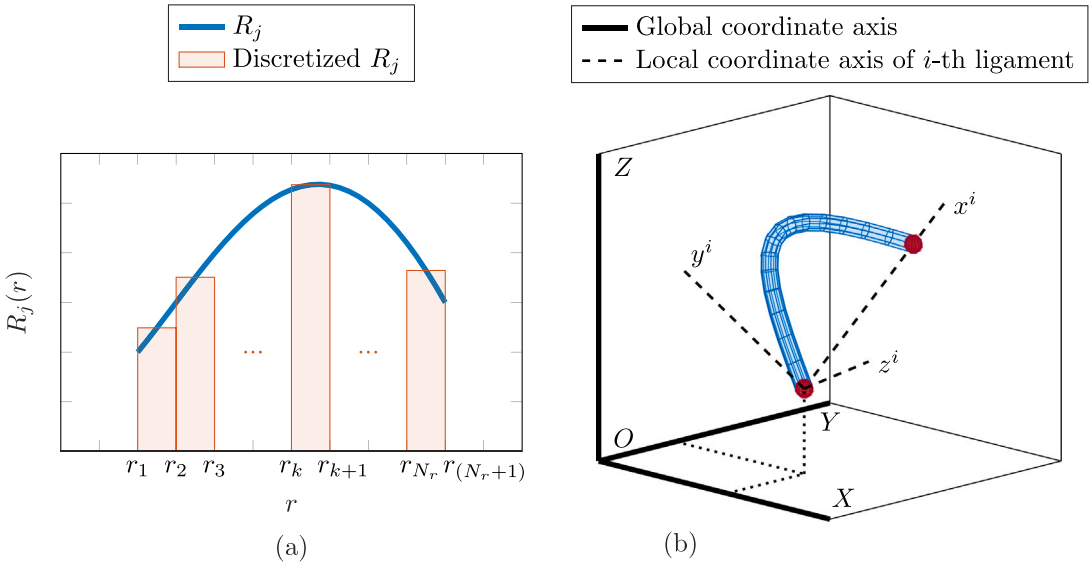

Fig. 2. (a) Discretization of a continuous probability distribution using N_r bins to each of which we assign a likelihood representative of the likelihood of the continuous distribution in the domain of that bin; (b) Local coordinate system (x^i, y^i, z^i) of ith ligament and global coordinate systems (X, Y, Z).

shape of junctions or ligaments. To generate the network structure, we use the method previously introduced in [28]. That is, we generate a (fully connected) random initial network consisting of a number of junctions that exactly matches a predefined target value. Moreover, each junction is randomly assigned a valency according to a predefined target valency distribution. During the subsequent SA, the number of junctions as well as the junction valency distribution are kept constant to ensure that both descriptors match their targets in each SA step. Hence, during the SA the network structure need only be rearranged such that it matches as well as possible target distributions predefined for the adjacent junctions' distance and the direction cosine, the other two key descriptors at network level. To this end, a cost function (energy function) is defined that penalizes deviations of the current values of these descriptors from their respective predefined targets. For more details, the reader is referred to [28].

3.3. RVE generation at component level

After we have generated an overall network structure in the first stage, we assign in the second stage of our framework to each ligament and junction a specific shape using the above introduced component level descriptors.

3.3.1. Radius of junctions

The junctions are modeled as spheres with a radius of r_j^i. This radius is considered a random variable drawn from some predefined continuous distribution R_j allowing junction radii in the range $r_{min} \leq r_j^i < r_{max}$. For our numerical implementation, we first discretize the distribution R_j. To this end, we uniformly divide the interval $[r_{min}, r_{max}]$ into N_r bins. Each bin is represented by the radius value in its center. This discrete radius value is assigned a likelihood proportional to the value of R_j at this center (normalized such that the sum of the likelihoods of all bins equals one). This discretization is illustrated in Fig. 2-(a). Given a total number of N_j junctions (predefined as a network level descriptor), each bin is randomly assigned a number of junctions in the network that is proportional to its discrete likelihood. The respective junctions are assigned the radius value at the center of their respective bin. This way, we have created a set of junctions with a radius distribution following a predefined distribution R_j.

3.3.2. Radius of ligaments

After assigning shapes to the junctions, we can shape the ligaments by applying the Eq. (2). Each ligament is shaped independently, which allows efficient parallel computing in case of large RVE. As boundary conditions we impose that the radius of a ligament at its two ends must be equal to the radius of the respective junctions at these ends. If we choose $r_l^i(x^i)$ in Eq. (2) as a linear function this automatically determined the two available polynomial coefficients d_0^i and d_1^i. By contrast, if one decides to generate RVE with ligaments where the radius of the ligaments varies along the ligaments according to a higher order polynomial function, further coefficients have to be chosen. These can either be chosen deterministically or by a method similar to the one described in Section 3.3.1 for the junction radius based on some predefined distributions.

3.3.3. Curvature of ligaments

Our RVE are endowed with a fixed global coordinate system (X, Y, Z) whose axes are aligned with the edges of our RVE and whose origin is located in one of the corners of the RVE. From this global coordinate system, we create for each ith ligament a local one in three steps: first, we compute an intermediate coordinate system (X^i, Y^i, Z^i) resulting from the (X, Y, Z) system by rotation with a random angle θ^i around the X-axis. In the second step, we compute the Euler angle between the X^i-axis and the line that connects the two junctions confining the ith ligament. In the third step, we rotate the whole intermediate system (X^i, Y^i, Z^i) by that Euler angle and translate its origin into the center of one of the two junctions confining the ith ligament. This rotation yields us a local coordinate system (x^i, y^i, z^i) whose x^i-axis connects the two junctions of the ith ligament. Drawing the random angle θ^i from a uniform distribution in the range $[0, 2\pi]$ ensures that the directions of the y^i-axes are uniformly distributed in the plane perpendicular to the x^i-axis. The local coordinate system (x^i, y^i, z^i) is illustrated in Fig. 2-(b). Within this system, the curvature of the ligament is defined according to (4).

4. Numerical examples

4.1. Generations of sample RVE

The whole above described two-stage workflow for generating RVE is summarized in Fig. 3. We used this workflow to generate a large number of RVEs sampling the configurational space by systematic variations of the descriptors both at the network and component level within the physically reasonable bounds.

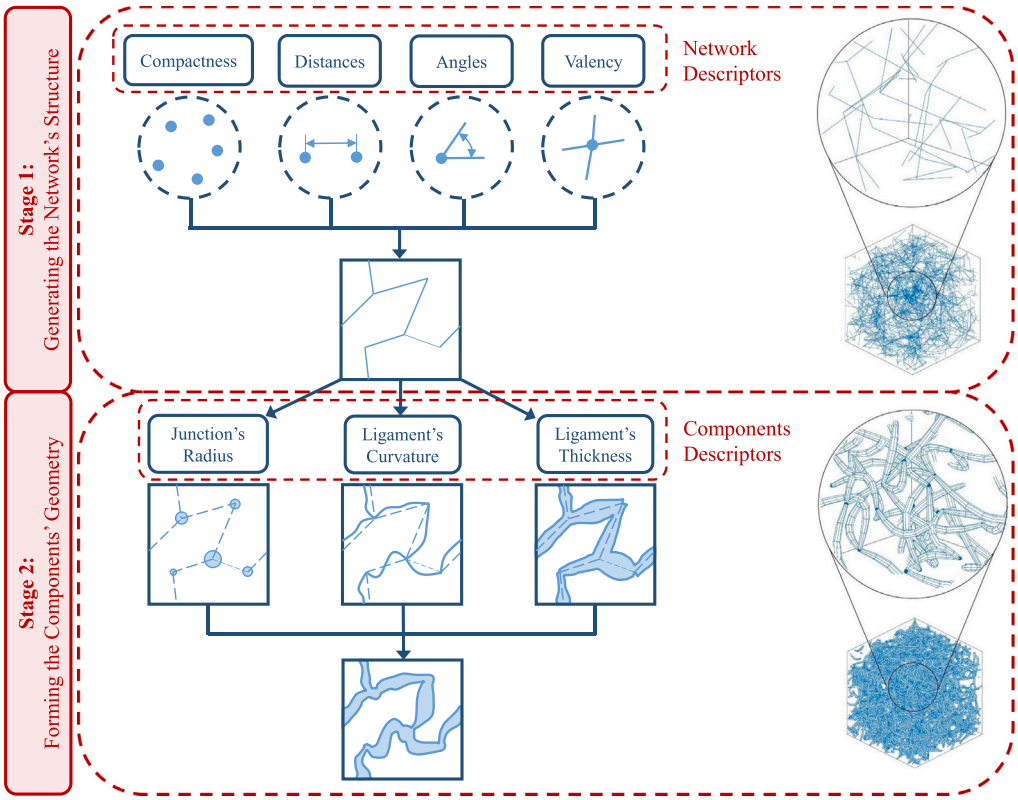

Fig. 3. Workflow of the suggested two-stage ligamentous network generating approach. At the first stage, it generates the network structure based on predefined network descriptors. At the second stage, it adds the junction's and ligament's geometry to the product of stage one. A sample realization of a generated RVE at the first stage and second stage of this approach is also presented.

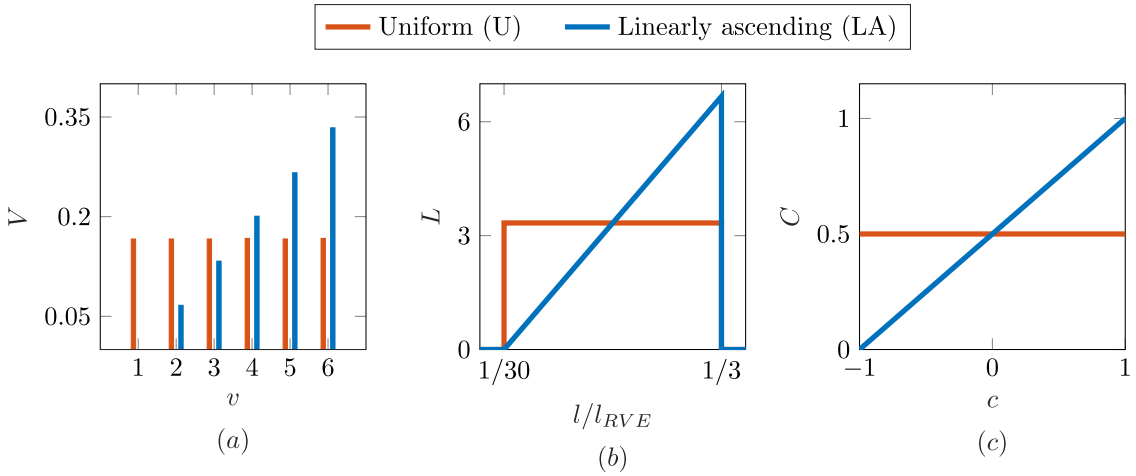

Fig. 4. Target distributions of (a) junction valency V, (b) adjacent junctions' distance L and (c) direction cosine C.

4.1.1. Descriptors at network level

For the three network descriptors junction valency (V), adjacent junctions' distance (L), and direction cosine (C), one uniform probability distribution (U) and one linearly ascending probability distribution (LA) were sampled as target distributions for the RVE generation (Fig. 4) for a total number of ligaments of 2000 ($N_l = 2000$). These variations result in $2^3 = 8$ different network morphologies referred to in the following as $NM_1, \ldots, NM_8$. Their specifications are listed in Table 1.

4.1.2. Descriptors at component level

At component level, target descriptors for the RVE generation were defined in the following way.

(1) Junctions' radii: First, we studied the case that all junctions had the same radius. In this case, we studied the radii $r_j/l_{RVE} = 0.005, 0.01, 0.015, 0.02$. Second, we studied the case of junction radii uniformly distributed in the interval $[0.005, 0.02]/l_{RVE}$.

Table 1
Selection of junction valency distribution V, adjacent junctions' distance distribution L and direction cosine distribution C for different network morphologies (NMs) (U: uniform probability distribution; LA: linearly ascending probability distribution).

Label	V	L	C
NM_1	U	U	U
NM_2	U	U	LA
NM_3	U	LA	U
NM_4	U	LA	LA
NM_5	LA	U	U
NM_6	LA	U	LA
NM_7	LA	LA	U
NM_8	LA	LA	LA

Table 2
For ligaments confined by two junctions of equal radius r_j the following parameters for Eq. (7) were tested. The 5th column lists the ligament radii at the ligament center and the 6th one V_{rel}, the ratio of the ligament volume compared to the case of a ligament with equal radius at the two ends but cylindrical shape.

Label	d_2^i	d_1^i	d_0^i	$r_l^i(l^i/2)/r_j$	V_{rel}
Convex II	$-4r_j/(l^i)^2$	$4r_j/l^i$	r_j	2	43/15
Convex I	$-2r_j/(l^i)^2$	$2r_j/l^i$	r_j	3/2	9/5
Cylindrical	0	0	r_j	1	1
Concave I	$4r_j/3(l^i)^2$	$-4r_j/3l^i$	r_j	2/3	83/135
Concave II	$2r_j/(l^i)^2$	$-2r_j/l^i$	r_j	1/2	7/15

Table 3
For ligaments confined by two junctions of in general different radius, the following parameters for Eq. (7) were tested where Δr_l^i is the absolute value of the difference between the radii of the two junctions confining the ligament.

Label	d_2^i	d_1^i	d_0^i
Convex	$-\Delta r_l^i/(l^i)^2$	$2\Delta r_l^i/l^i$	$r_l^i(0)$
Conical	0	$\Delta r_l^i/l^i$	$r_l^i(0)$
Concave	$\Delta r_l^i/(l^i)^2$	0	$r_l^i(0)$

(2) Ligaments' cross-sections radius: setting $k_{max} = 2$, we included in the Taylor series in Eq. (2) terms up to the second order, that is,

$$r_l^i(x^i) = d_2^i (x^i)^2 + d_1^i x^i + d_0^i. \tag{7}$$

For each ligament, we assigned a desired value to the coefficient d_2^i then the two other coefficients d_1^i and d_0^i were determined by the constraint that the ligament radius at both ends had to be equal to the radius of the respective junction. Note that $d_2^i < 0$ yields a convex ligament shape, $d_2^i > 0$ a concave shape, and $d_2^i = 0$ ligaments with a linear transition between the two adjacent junctions.
For the RVE where all junctions had an equal radius, we studied five different values for d_2^i as defined in Table 2. In the case of networks with variable junction radii, the three different sets of coefficients defined in Table 3 were used.

(3) Ligaments' curvature: for simplicity, we focused on fibers with sinusoidal curvature only. That is, in Eq. (4) we set $f_{max} = 1$ and $a_n^i = 0$ yielding the simplified version

$$y^i(x^i) = b_1^i \, sin(\pi x^i/l^i). \tag{8}$$

with b_1^i the only free parameter for each ligament. In our study, we examined RVE with the specific values $b_1^i = 0.03, 0.06, \ldots, 0.15$.

A schematic two-dimensional illustration of the different ligament shapes generated in the above way and tested in our study is presented in Fig. 5.

4.2. Finite element analysis

To determine the mechanical properties of the RVE generated as described in Section 4.1, we used a previously established and validated analysis pipeline based on the finite element (FE) software Abaqus, which translates the RVE geometries into finite element models using beam elements of type B31 [38,41]. So far, this pipeline had been applied only to unit cells with cubic boundaries, such as diamond or fcc (face-centered cubic) cells that allowed to generate larger microstructures with multiple copies of the unit cell and subsequent randomization. By contrast, for this work, a Python interface was written that reads the nodes and topology information along with the microstructure descriptors from the output of the simulated annealing code described in Section 3. Instead of applying a distortion of the connection between two junctions for generating curved ligaments as proposed in [38,39], a meshing subroutine generated FE nodes along the curved path defined by Eq. (8).

Commonly, models with variable ligament radius and curved ligament axis are meshed with 20 beam elements per ligament [38,39,41,48]. Because of the larger number of ligaments modeled in the RVE, here each ligament is discretized with 10 finite beam elements, as an acceptable trade-off between computational cost and accuracy. The mesh study provided in Appendix A demonstrates that this leads to a negligible increase in macroscopic stiffness of 1.5%. For each element, the radius at its center was calculated according to Eq. (7) and assigned as element radius. For simplicity, the nodal correction proposed in [48], which requires 20 elements per ligament, was not applied in this work. This as well as neglecting contact interactions lead to a systematic underestimation of the stiffness of the RVE. This underestimation affected all RVE in a similar manner and, therefore did not pose a major obstacle in determining the relation between specific microstructural descriptors and the RVE stiffness.

The microstructure generated by the simulated annealing algorithm is not a solid cube. Instead of the common approach of creating periodic boundary conditions using ordered node sets for faces, edges, and corners, we hence applied periodic boundary conditions to individual FE nodes and their periodic counterparts in one, two, or three coordinate directions. Depending on the number of nodes to be coupled per node set, a suitable periodic boundary condition was written that ensured that degrees of freedom were not eliminated more than once through the coupling equations. Macroscopic displacement boundary conditions were applied through dummy nodes, which allowed loading of the RVE by arbitrary normal and shear strains. Some examples of loaded RVEs are shown in Fig. 6 for an increasing number of ligaments N_l. The examples demonstrate that the stress was distributed well within the RVE and across the boundaries. Because the simulated annealing code created also dangling ligaments with a valency of $v^i = 1$ at one end, some ligaments were unstressed (blue) over their whole length. Other ligaments that visually appeared to be dangling or disconnected, preferably located at the boundaries, showed non-zero stress due to the applied periodic boundary conditions. The resulting stress state of the RVE was computed from the reaction forces in the dummy-nodes assuming small deformations. For computing the constants of the elasticity tensor, three independent normal and shear deformations were analyzed with strains of 0.1%. Young's moduli E_i are determined from predefined normal strains ϵ_i and resulting stress σ_i of the uniaxially deformed RVE by $E_i = \sigma_i/\epsilon_i$. Poisson's ratios ν_{ij} are determined from predefined normal strains ϵ_i and resulting lateral strains ϵ_j by $\nu_{ij} = -\epsilon_j/\epsilon_i$ with $i \neq j$. The shear moduli are determined from simple shear deformations $\gamma_{ij} = \epsilon_{ij} + \epsilon_{ji} = 0.1\%$ and the resulting shear stress τ_{ij} by $G_{ij} = \tau_{ij}/\gamma_{ij}$.

Averaged values of the elastic constants were computed from all loading directions by assuming cubic symmetry. Too small number of ligaments N_l can lead to two problems: first, the mechanical properties of the examined microstructure may be subject to large stochastic variations (i.e., the examined volume element is not yet statistically

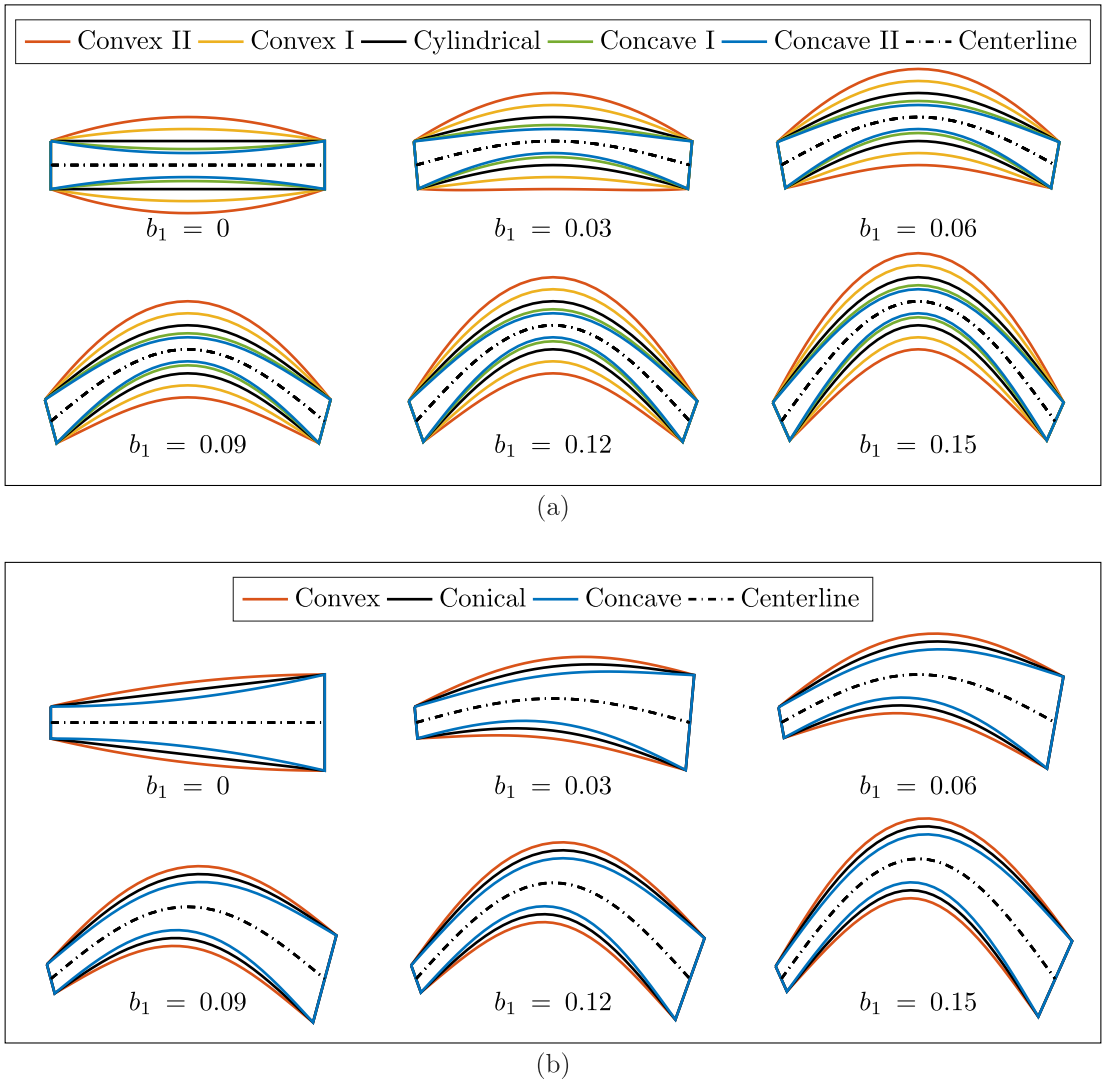

Fig. 5. In our study we examined 48 different types of ligament shapes for networks with (a) uniform and (b) nonuniform radii of the junctions. Note that for clarity of the illustration, the horizontal and vertical scales are not equal so that angle in this illustration do not agree with the ones of the actual ligaments.

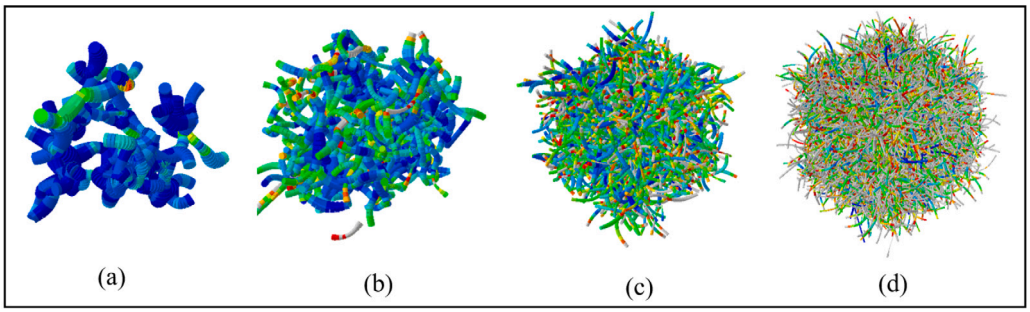

Fig. 6. Examples of FE beam models created from the output of our two-stage simulated annealing approach with an increasing number of ligaments (a) $N_l = 135$, (b) $N_l = 540$, (c) $N_l = 2160$, (d) $N_l = 8640$.

representative); second, an apparent anisotropy may be observed (as a statistical artifact). To ensure that $N_l = 540$ was sufficiently high to represent truly isotropic representative volume elements, we first performed a parameter study whose results are shown in Fig. 7. In this study, we generated RVEs with different numbers of ligaments N_l. Each RVE had the same solid fraction of $\varphi = 0.28$. For each value of N_l we generated 10 different RVEs (with the same statistical distributions for the key microstructural descriptors). For each RVE we calculated the elastic constants from our finite element simulations. For numbers of ligaments $N_l \geq 540$, the scatter of the calculated elastic constants E, G, and ν was negligibly small. Moreover, G agreed very well with the value $G_{iso} = E/[2(1+\nu)]$ expected for isotropic materials. We thus concluded that a number of ligaments of $N_l \geq 540$ was sufficient for our purposes. That is, $N_l \geq 540$ ensures that the volume elements are mechanically representative. Our volume elements are also representative in a geometric sense because in our RVE with $N_l \geq$

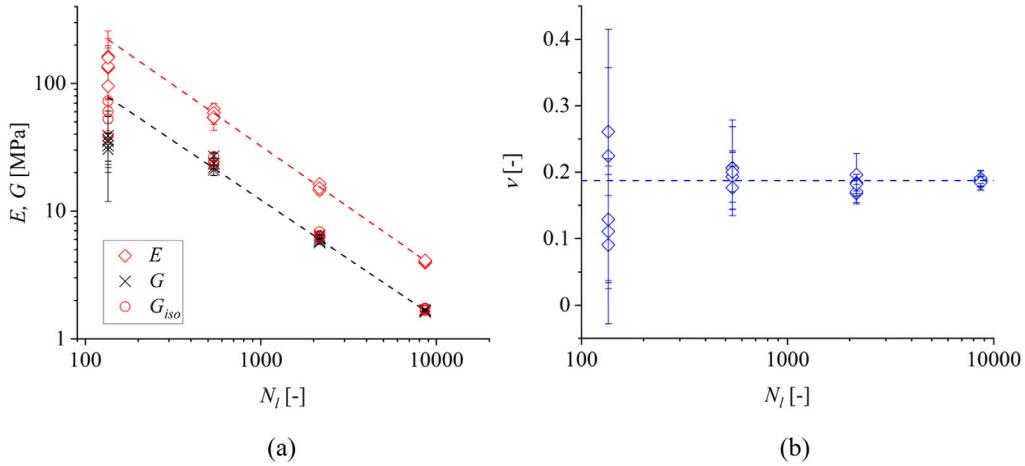

Fig. 7. Scatter in the determined elastic properties for varying number of ligaments N_l: (a) Young's modulus E, shear modulus G, and $G_{iso} = E/[2(1+\nu)]$; (b) Poisson's ratio ν.

540 the mesh size of the network is much smaller than edge length of the RVE.

We note that in the current model for simplicity the interference and contact mechanics of ligaments was not taken into consideration. According to [49], this simplification has only a minor effect for solid volume fractions up to 20%. For higher volume fractions, the results reported herein still allow us to understand general trends in the relation between microstructural descriptors and macroscopic properties, though their quantitative accuracy will be increasingly compromised as the volume fraction increased.

4.3. Interpretation of results of the finite element analysis

In porous structures, it is very common to model the macroscopic Young's modulus E as a function of the solid volume fraction φ which is the relative volume of the solid phase (i.e. ligament phase) to the volume of the RVE [38,39,41,50,51]. This goes back to the famous Gibson-Ashby model [52]

$$\frac{E}{E_b} = C_E \varphi^m, \tag{9}$$

where E and E_b are the macroscopic elasticity of network and bulk solid phase respectively, and C_E is the leading constant. According to [53], the exponent m in Eq. (9) is 1 for networks with a tension/compression-dominated behavior and it is 2 if the main deformation mode of the ligaments is bending.

Under the assumption that the ligaments in the random network deform dominantly by bending [38], it is expected at the first glance that Young's modulus follows the Gibson-Ashby scaling law (9), i.e. the macroscopic modulus should be constant for unchanged solid fraction. However, as can be seen from Fig. 7, in our networks Young's modulus and shear modulus decreased with increasing number of ligaments, even when the solid volume fraction φ was kept constant. This is because C_E in (9) is only constant as long as the network architecture is constant. This, however, was not the case in parameter study illustrated in Fig. 7. Generally, this observation indicates that further descriptors beyond the solid volume fraction φ need to be taken into account to interpret the results of a mechanical analysis of our RVE. To overcome this problem, [41] proposed a multiplicative decomposition of the form

$$\frac{E}{E_b} = \hat{E}_0(\varphi) \cdot \hat{E}_C(v_i), \tag{10}$$

where the functions $\hat{E}_0$ and $\hat{E}_C$ define the dependencies of the solid fraction φ and of the connectivity, respectively. This concept can be further generalized to a relation of the type

$$\frac{E}{E_b} = f_1(P_1) \cdot f_2(P_2) \cdot ..., \tag{11}$$

with some functions f_i each depending on some specific microstructural descriptor P_i. Herein, we used such generalized Gibson-Ashby scaling relations to interpret the results of the finite element analyses performed.

4.4. Mechanical properties of sample RVE

4.4.1. Networks with junctions of equal size

First, we studied networks where all the junctions had the same radius. Combining all the aforementioned values of descriptors at network and component level, this lead to 960 different types of RVE: (8 network morphologies) × (5 ligament shapes) × (6 degrees of curvature) × (4 junction sizes). For each of these RVE types, we generated 5 different realizations. Hence, 4800 sample RVE were generated, among which 4220 RVE were acceptable from a physical point of view (RVE with $\varphi > 1$ were discarded as physically meaningless). The averaged values of the mechanical properties for these different realizations were used for further discussion.

The relation between the macroscopic Young's modulus E and Poisson's ratio ν on the one hand and the junction radius on the other hand is plotted in Fig. 8 (normalized by the Young's modulus of the bulk solid phase $E_b = 80$ GPa and its Poisson's ratio $\nu_b = 0.42$, respectively). In this figure, only the results of straight ligaments with a constant cross-section radius are plotted. Note that in this case all the ligaments within the network had the same cross-section radius, which is the respective junction radius r_j. The plots for different ligament shapes and curvatures are presented in Appendix B. To identify deviations from the original Gibson-Ashby scaling law in Eq. (9), the macroscopic Young's modulus is normalized by $E_b\varphi^2$. The results presented in Fig. 8-(a) underline that, as already discussed above, Young's modulus is not exclusively governed by the solid volume fraction (as in the Gibson-Ashby theory) but strongly depends also on the network morphology. However, for a specific network morphology, Eq. (9) appears to form a reasonable approximation, given that for many morphologies the normalized Young's modulus is a largely constant function of the ligament radius. According to Fig. 8-(b), also Poisson's ratio only weekly depends on the junction radius.

Fig. 9 shows the scaled Young's modulus and Poisson's ratio of RVE with the network morphology NM_1 and $r_j/l_{RVE} = 0.005$ for all considered values of b_1 and d_2^i. It illustrates how the RVE properties change with the ligament curvature and shape. As expected, the scaled Young's modulus decreases with increasing curvature of the ligament axis although an increasing curvature is associated with an increasing volume fraction. This means that the stiffness loss due to curved ligaments dominates the change in the macroscopic properties. For RVE with constant ligament curvature, Young's modulus increases

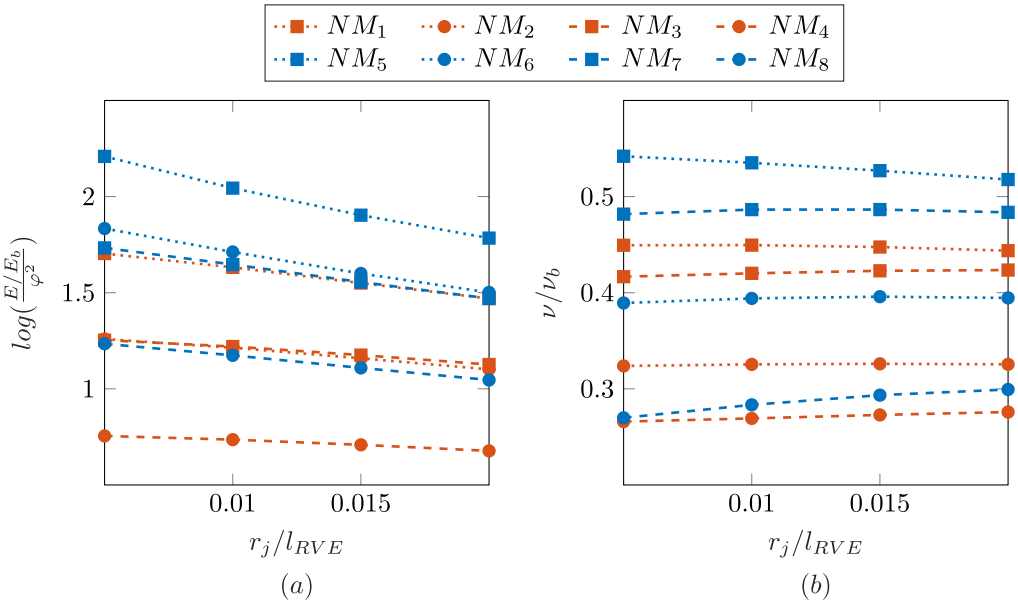

Fig. 8. (a) Scaled Young's modulus and (b) Poisson's ratio versus radius of junctions in the RVEs with different network morphologies and straight cylindrical ligaments. Results for the uniform valency distribution are in red, for the linearly ascending distribution in blue. Uniform and linearly ascending distributions of L are distinguished by dotted and dashed lines, respectively. Circle and square markers denote a uniform and linearly ascending distribution of C, respectively.

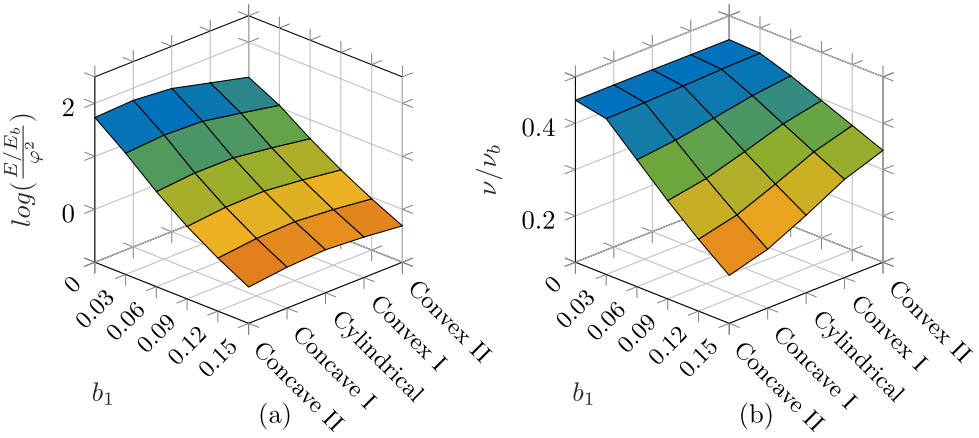

Fig. 9. (a) Scaled Young's modulus and (b) Poisson's ratio of RVE with network morphology NM_1 (uniform valency, adjacent junctions' distance, and direction cosine distributions) and $r_j/l_{RVE} = 0.005$ with various ligament convexities and curvatures.

when the ligament shape change from concave to convex (particularly clearly visible from Figs. B.13 and B.14 where the results are shown with a different scaling of the vertical axis). Both observations are in agreement with findings in [39,48] obtained for the special case of diamond structures ($v^i = 4$). Poisson's ratio, shown in Fig. 9-(b), exhibits a qualitatively similar behavior.

4.4.2. Networks with uniform junction size distribution

Considering for junction sizes uniformly distributed in the interval $[0.005, 0.02]/l_{RVE}$ five networks for each possible combination of the descriptors V, L, C, d_2^i, b_1 (within the above specific bounds and distributions) resulted in 720 RVE. In analogy to Section 4.4.1, the averaged values of the mechanical properties of the 5 realizations of each network type are presented in Fig. 10. Again, the variation of the mechanical properties due to variations of descriptors at the component and at the network level were found to be largely independent. Therefore, in Fig. 10, we categorized all the sample RVEs into three groups (convex, conical and concave) and normalized Young's modulus and Poisson's ratio by the reference values E_{ref} and ν_{ref} of an RVE with the same network morphology NM_i, straight ligaments ($b_1 = 0$) and conical shape ($d_2^i = 0$).

Fig. 10 reveals that both Young's modulus and Poisson's ratio decrease with increasing (the absolute value of) the curvature of the ligament. Young's modulus clearly increases with ligament convexity. This is in agreement with previous studies for the special case of diamond structures ($v^i = 4$) with cylindrical ligaments [38,39], where a different approach for the randomization of the ligament axis was used. Poisson's ratio is almost independent of the ligaments' convexity. This can be interpreted such that the lateral expansion of the network is mainly controlled by the network architecture rather than the shape of the individual ligaments.

4.4.3. Scaling law for the Young's modulus

The interpretation of experimental results and the prediction of mechanical properties of open pore foams and nanoporous metals is often based on the Gibson-Ashy scaling laws, where the focus is on the volume fraction φ [52]. The literature provides various modifications of Gibson-Ashy scaling laws, taking additional effects into account, see e.g. [54]. Therein, a comparably simple network structure is assumed,

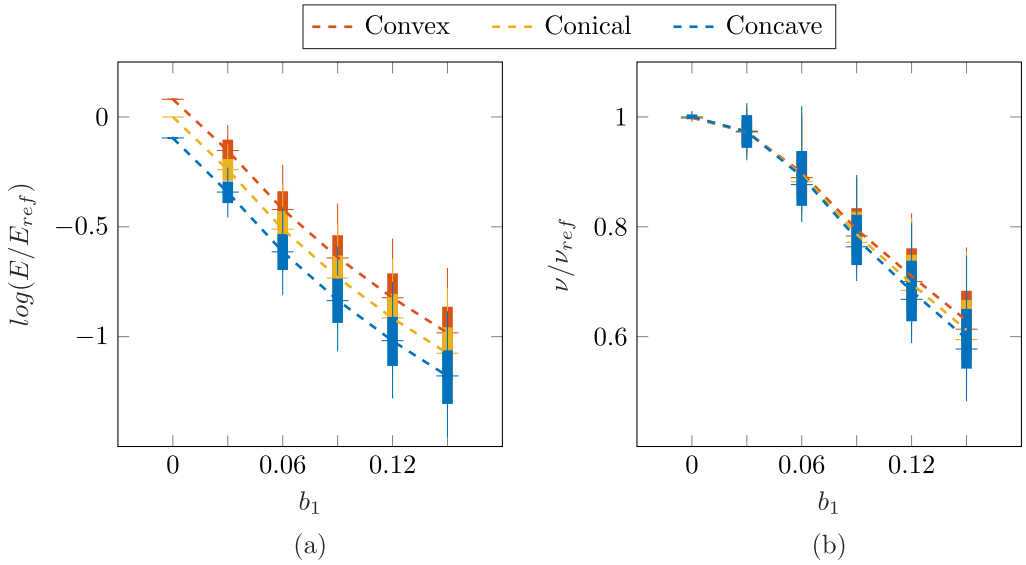

Fig. 10. Macroscopic normalized (a) Young's modulus and (b) Poisson's ratio of the RVE with different descriptors at network and component levels where the junction radii within the network were distributed uniformly in the interval $[0.005, 0.02]/l_{RVE}$.

in which the individual ligaments undergo bending deformation. In our case, the network structure is not fixed but a result of the choice of descriptors. This is demonstrated in Fig. 7, where the solid fraction is kept constant and, nevertheless, the macroscopic moduli drop dramatically with increasing number of ligaments and junctions. In the general case considered in this work, the network structure is not fixed and each descriptor may change the Young's modulus beyond its effect on the solid fraction. The investigation of this in detail is difficult, because it is usually not possible to generate various configurations of a fiber network in which a group of descriptors (either on the network level or on the component level) are kept constant while one or a few others are varied. Our novel two-stage simulated annealing algorithm for generating RVE with tailor-made descriptors can overcome exactly this key problem. It allows us to vary a single descriptor – while keeping all the others constant – and study how variations of this descriptor affect Young's modulus. To underline how this focus changes the situation compared to the situation classically studied with Gibson-Ashby relations (where the network morphology is kept constant while the solid volume fraction is varied) we present our results as graphs revealing the relation between Young's modulus and the solid volume fraction. The latter, however, is now defined as a parameter whose changes are driven by changes of one of the RVE descriptors. For example, φ_b denotes the solid volume fraction in cases where the ligament curvature parameter in Eq. (8) is varied and all the other descriptors of the RVE are kept constant. Analogously, φ_d, φ_r, and φ_L denote the solid volume fraction if the ligament convexity parameter in (7) or the junction radius or distance between neighboring junctions are changed while keeping all the other descriptors constant, respectively.

If we plot Young's modulus against φ_b, φ_d, and φ_r, we do not necessarily expect any longer a quadratic dependence on the solid volume fraction because now we consider changes of the solid volume fraction associated with simultaneous changes of one other characteristic of the microstructure. This is indeed what Fig. 11 shows for the network morphology NM_1. In Fig. 11-(a), the macroscopic Young's modulus was normalized by the Young's modulus E_{ref} of RVE with straight cylindrical ligaments and a junction radius equal to $5 \cdot 10^{-3} l_{RVE}$. In Fig. 11-(b), the macroscopic Young's modulus of the network with straight conical ligaments was chosen as E_{ref}. The normalized Young's modulus increases with φ_r and φ_d but decreases with φ_b. This is in line with the above discussion of Figs. 8 and 9. That is, increasing the descriptors r_j and d_2^i increases the ligament cross-sections at junctions and along the ligament axis, respectively, and thus increases the solid volume fraction as well as the macroscopic stiffness. By contrast, the descriptor b_1 increases the curvature of the ligament axis. This also leads to a volume increase but at the same time to a softening of the network structure. Among the curves plotted in Fig. 11, $E(\varphi_r)$ and $E(\varphi_d)$ agree well with the quadratic slope ($m = 2$) expected from the classical Gibson-Ashby law. This is the case because variations of the junction radius or also the ligament convexity alter the amount of solid volume but not the overall architecture of the network so that we arrive at a situation largely comparable to the one studied by Gibson and Ashby. Deviations from their theory for larger values of the solid volume fraction can be explained by the transition from an Euler–Bernoulli type to a Timoshekno type bending behavior of the ligaments as already discussed in [38].

The situation is very different for $E(\varphi_b)$. Variations of the ligament curvature fundamentally change the type of microstructure. Therefore, the Gibson-Ashby theory is no longer applicable. Rather we observe a negative slope which is due to the softening of the ligament stiffness with increasing curvature of the ligament axis. Using the solid volume fraction as a common basis allows comparing our results with previous results reported by [39]. There, the effect of random perturbations of a regular diamond microstructure on the macroscopic mechanical properties was studied. In particular, the effect of the out-of-axis distortion A with $0 \leq A \leq 0.5$ was examined. The results of [39] are included in Fig. 11-(a) for $r/l = 0.087$. Apparently, they reveal a negative slope close to the one we found for $E(\varphi_b)$ in the asymptotic limit. Of note, however, our data start out from an undistorted axis, which may explain the significantly higher slope for small solid volume fractions.

For the RVE with uniformly distributed junction radii, Young's modulus versus volume fraction is plotted in Fig. 11-(b). Because the junction radii were statistically distributed, φ_r could not directly be controlled for this plot. We note, however, that $E(\varphi_d)$ is again in excellent agreement with the Gibson-Ashby scaling law and that $E(\varphi_b)$ is again in excellent agreement with previously reported results of [39] and qualitatively very similar to the relation found in Fig. 11-(a).

The results reported in Fig. 11 suggest that stiffness of nanoporous materials may be captured by a generalized Gibson-Ashby law of the type

$$E = C_E f_r(\varphi_r) f_b(\varphi_b) f_d(\varphi_d) f_L(\varphi_L). \tag{12}$$

However, noting in particular $E(\varphi_b)$ in Fig. 11, one may assume that the functions f_r, f_b, f_d, and f_L are not necessarily simple power laws. Determining them would require many more samples and a

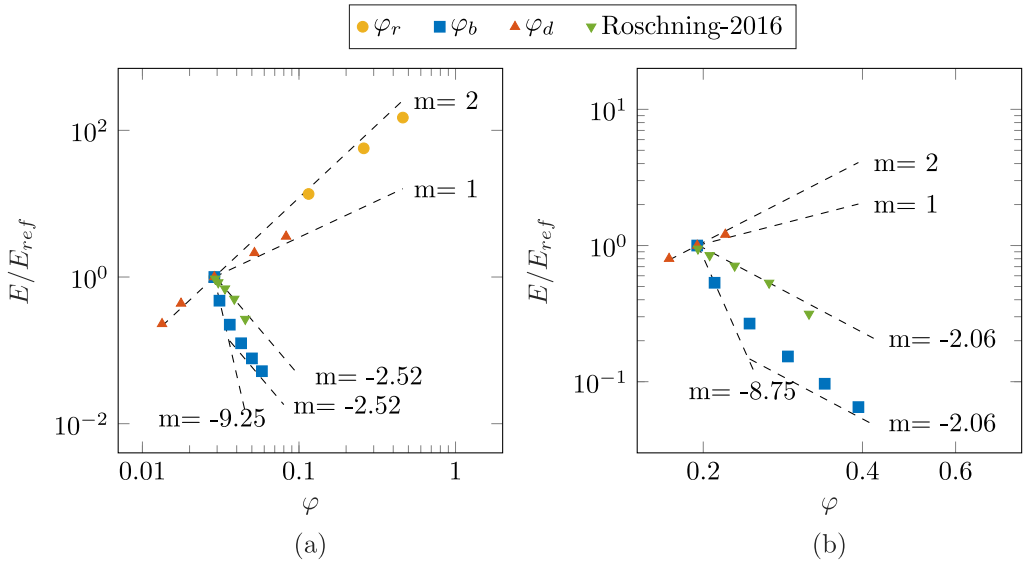

Fig. 11. Normalized macroscopic Young's modulus of RVE with the network morphology of NM_1 versus solid volume fraction φ in case the junctions have (a) an equal radius or (b) a uniformly distributed radius. The dashed lines indicate slopes m in the log–log plot.

careful study of possible interactions between the variations of different descriptors. This is beyond the main objective of this paper which is simply introducing a new two-stage algorithm for the generation of RVE with ligament microstructure. The specific example and discussion in Section 4.4.3 underline, however, the great potential, which this algorithm offers for future computational studies of the micromechanics of nanoporous materials.

5. Conclusion

In this paper, we proposed a two-stage simulated annealing algorithm to generate networks of ligaments, where both the geometric properties of the network structure and of the ligaments can be tightly controlled by prescribed descriptors. The first stage relies on the approach previously developed in [28] for generating the network architecture (determined by the number of ligaments, the junction valency distribution, the adjacent junctions' distance distribution, and the direction cosine distribution). In the second stage, the geometry of the ligaments is formed based on ligament level descriptors such as the radius of the junctions, and the convexity and curvature of the ligaments. Our algorithm ensures that the generated networks are fully connected, homogeneous, and isometric. Our approach is computationally efficient at both stages and the second stage is even trivial to parallelize. We introduced it on the basis of a certain set of widely used descriptors of the network architecture and ligament geometry. However, this set could easily be extended by further descriptors without altering the major structure of the algorithm.

To demonstrate the potential of our new algorithm, we generated 5000 RVEs covering a large range of different microstructures. Computing their mechanical properties by finite element analyses, we performed a systematic study of the relation between microstructure and mechanical properties in ligamentous RVEs. We found that the Gibson-Ashby scaling law cannot easily be applied to cases where a variation of the solid volume fraction is associated with a change of the ligament network architecture itself. Rather, our results suggest that in such cases a sort of generalized Gibson-Ashby law following the concept of (12) may be required. The development and discussion of such a law in a very general sense may be a promising avenue of future research. The results of our analysis are consistent with previous studies [38,39] but significantly go beyond them because our new algorithm can tightly control variations of each single microstructural descriptor in the RVE generation process so that the role of each descriptor can be examined in a unprecedentedly systematic way. This underlines the potential of our new algorithm that can be hoped to become a valuable tool in future computational studies of nanoporous materials, which are a class of materials that has attracted fast rising attention over the last decade.

CRediT authorship contribution statement

Iman Davoodi Kermani: Conceptualization, Methodology, Software, Validation, Analysis, Visualization, Writing – original draft. **Lena Dyckhoff:** Software. **Roland C. Aydin:** Writing – review & editing. **Norbert Huber:** Software, Validation, Analysis, Writing – review & editing. **Christian J. Cyron:** Conceptualization, Analysis, Writing – review & editing, Supervision, Funding acquisition.

Declaration of competing interest

The authors declare that they have no known competing financial interests or personal relationships that could have appeared to influence the work reported in this paper.

Data availability

The raw/processed data required to reproduce these findings cannot be shared at this time as the data also forms part of an ongoing study.

Acknowledgments

The first author (IDK) acknowledges financial support by German Academic Exchange Service (DAAD), Funding programme/-ID: Graduate School Scholarship Programm, 2016, Germany (57243780) and additional support by the International Graduate School of Science and Engineering (IGSSE) of the Technical University of Munich, Germany. NH and CJC acknowledge financial support by the Deutsche Forschungsgemeinschaft (DFG, German Research Foundation) – Project Number 192346071 – SFB 986 "Tailor-Made Multi-Scale Materials Systems: M^3", project B4 and B9.

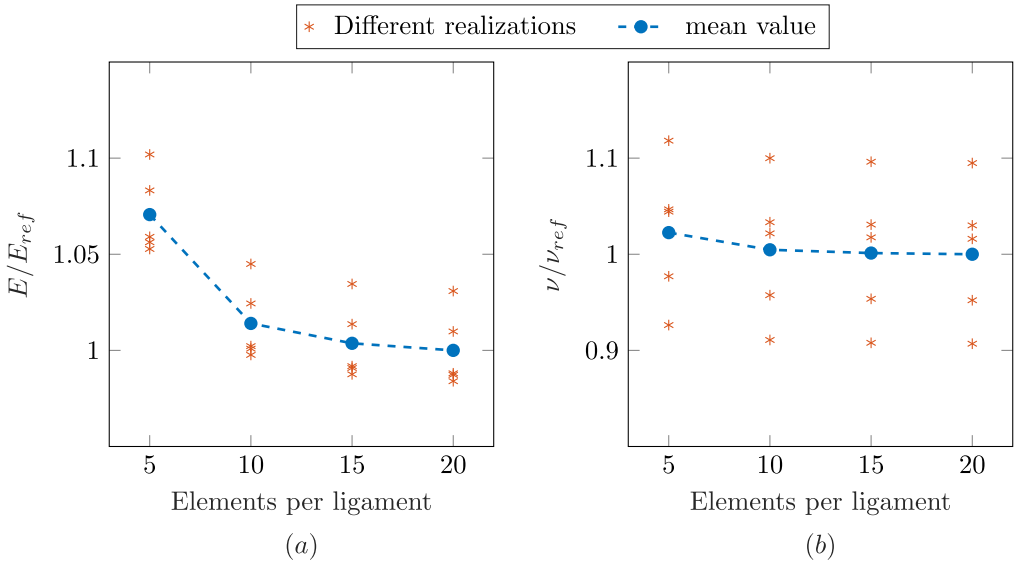

Fig. A.12. (a) Young's modulus and (b) Poisson's ratio of the RVEs of NM_8 with uniform junction size distribution and curved conical ligaments where $b_1 = 0.15$. The average values corresponding to 20 elements per ligament are chosen as reference values.

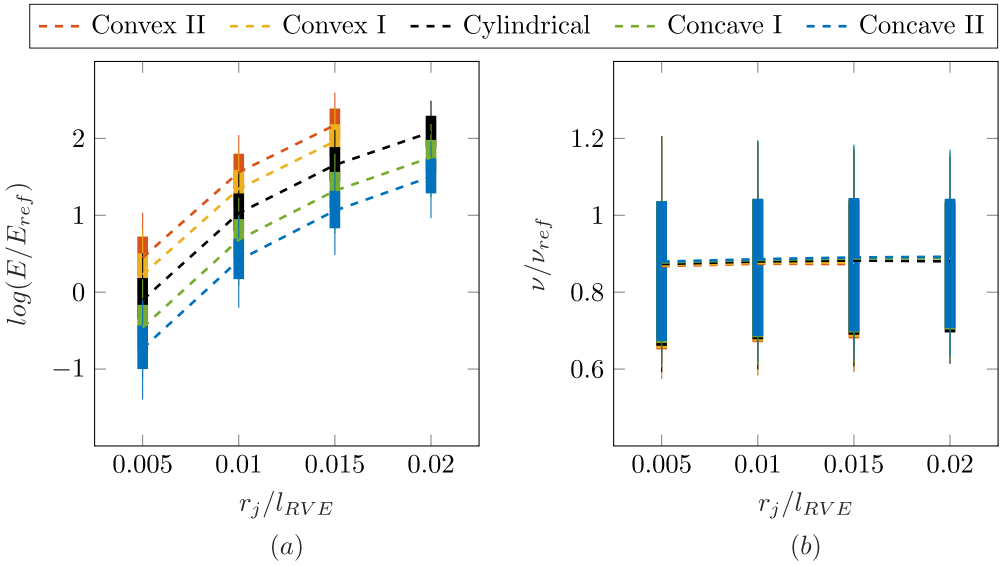

Fig. B.13. Macroscopic (a) Young's modulus and (b) Poisson's ratio of RVEs with different ligament convexities (constant junction radius across RVE and straight ligaments). E_{ref} and ν_{ref} are respectively Young's modulus and Poisson's ratio of the RVE with the network morphology NM_1, straight cylindrical ligaments and a junction radius equal to $5l_{RVE}/1000$.

Appendix A. Mesh study of finite element analysis

To study the dependency of macroscopic mechanical properties on the number of elements per ligament, we performed a mesh study for the networks of NM_1 with uniform junction size distribution and curved conical ligaments where $b_1 = 0.15$ (see Section 4.4.2). To this end, for each of 5 RVE samples, we repeated the finite element calculations for 5, 10, 15 and 20 elements per ligament and the corresponding Young's modulus and Poisson's ratio are presented in Fig. A.12. This figure confirms that the accuracy of results does not change significantly by increasing the number of elements to more than 10 per ligament. By increasing the number of elements per ligament from 10 to 20, the Young's modulus decreases by only about 1.5%, which is negligible compared to other simplifications in modeling. Therefore, 10 elements per ligament as used in this work for the calculation of the mechanical properties ensures sufficient accuracy.

Appendix B. Mechanical properties of various network morphologies with curved ligaments of variable thickness

Fig. 8 presents data for networks with straight ligaments and constant thickness. In this appendix we present further data for networks with more general ligament geometries (but constant junction radius) and all the 8 network morphologies listed in Table 2. The macroscopic mechanical properties for the networks with different ligament convexities and different ligament curvatures are plotted in Figs. B.13 and B.14, respectively. To draw the box plots presented in these figures, the data

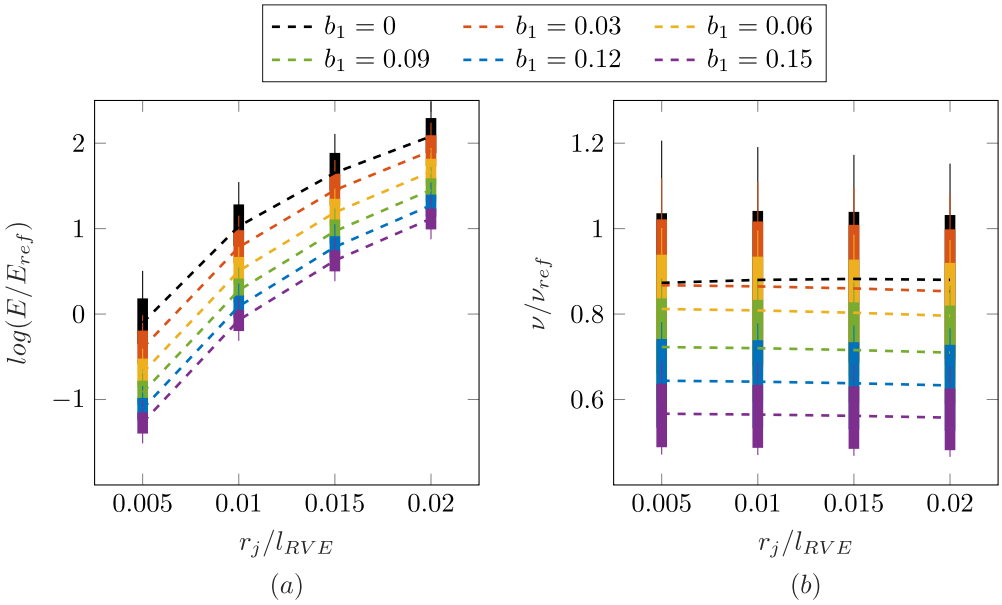

Fig. B.14. Macroscopic (a) Young's modulus and (b) Poisson's ratio of RVEs with different ligament curvatures (constant junction radius across RVE and cylindrical ligaments). E_{ref} and ν_{ref} are respectively Young's modulus and Poisson's ratio of the RVE with the network morphology NM_1, straight cylindrical ligaments and a junction radius equal to $5l_{RVE}/1000$.

for all network morphologies (NMs) are categorized into four categories based on their junctions' radius.

References

[1] A. Kabla, L. Mahadevan, Nonlinear mechanics of soft fibrous networks, J. R. Soc. Interface 4 (2006) 99–106, http://dx.doi.org/10.1098/rsif.2006.0151.

[2] E.M. Huisman, T. van Dillen, P.R. Onck, E. van der Giessen, Three-dimensional cross-linked F-actin networks: Relation between network architecture and mechanical behavior, Phys. Rev. Lett. 99 (2007) http://dx.doi.org/10.1103/physrevlett.99.208103.

[3] W. Krasny, H. Magoariec, C. Morin, S. Avril, Kinematics of collagen fibers in carotid arteries under tension-inflation loading, J. Mech. Behav. Biomed. Mater. 77 (2018) 718–726, http://dx.doi.org/10.1016/j.jmbbm.2017.08.014.

[4] J.F. Eichinger, M.J. Grill, I. Davoodi Kermani, R.C. Aydin, W.A. Wall, J.D. Humphrey, C.J. Cyron, A computational framework for modeling cell–matrix interactions in soft biological tissues, Biomech. Model. Mechanobiol. 20 (2021) 1851–1870, http://dx.doi.org/10.1007/s10237-021-01480-2.

[5] H. Rösner, S. Parida, D. Kramer, C. Volkert, J. Weissmüller, Reconstructing a nanoporous metal in three dimensions: An electron tomography study of dealloyed gold leaf, Adv. Eng. Mater. 9 (2007) 535–541, http://dx.doi.org/10.1002/adem.200700063.

[6] Z. Zhang, Y. Wang, Z. Qi, W. Zhang, J. Qin, J. Frenzel, Generalized fabrication of nanoporous metals (Au, Pd, Pt, Ag, and Cu) through chemical dealloying, J. Phys. Chem. C 113 (2009) 12629–12636, http://dx.doi.org/10.1021/jp811445a.

[7] J. Weissmüller, R.C. Newman, H. Jin, A.M. Hodge, J.W. Kysar, Nanoporous metals by alloy corrosion: Formation and mechanical properties, MRS Bull. 34 (2009) 577–586, http://dx.doi.org/10.1557/mrs2009.157.

[8] E. Larsson, D. Gürsoy, F.D. Carlo, E. Lilleodden, M. Storm, F. Wilde, K. Hu, M. Müller, I. Greving, Nanoporous gold: a hierarchical and multiscale 3D test pattern for characterizing X-ray nano-tomography systems, J. Synchrotron Radiat. 26 (2019) 194–204, http://dx.doi.org/10.1107/s1600577518015242.

[9] M. Hakamada, M. Mabuchi, Mechanical strength of nanoporous gold fabricated by dealloying, Scr. Mater. 56 (2007) 1003–1006, http://dx.doi.org/10.1016/j.scriptamat.2007.01.046.

[10] S.B. Lindström, D.A. Vader, A. Kulachenko, D.A. Weitz, Biopolymer network geometries: Characterization, regeneration, and elastic properties, Phys. Rev. E 82 (2010) http://dx.doi.org/10.1103/physreve.82.051905.

[11] A.C. To, J. Tao, M. Kirca, L. Schalk, Ligament and joint sizes govern softening in nanoporous aluminum, Appl. Phys. Lett. 98 (2011) 051903, http://dx.doi.org/10.1063/1.3549858.

[12] R. Xia, R. Wu, Y. Liu, X. Sun, The role of computer simulation in nanoporous metals—A review, Materials 8 (2015) 5060–5083, http://dx.doi.org/10.3390/ma8085060.

[13] M. Vahabi, A. Sharma, A. Licup, A. van Oosten, P. Galie, P. Janmey, F. MacKintosh, Elasticity of fibrous networks under uniaxial prestress, Soft Matter 12 (2016) 5050–5060, http://dx.doi.org/10.1039/c6sm00606j.

[14] H. Hatami-Marbini, Simulation of the mechanical behavior of random fiber networks with different microstructure, Eur. Phys. J. E 41 (2018) 817–830, http://dx.doi.org/10.1140/epje/i2018-11673-0.

[15] K. Jansen, A. Licup, A. Sharma, R. Rens, F. MacKintosh, G. Koenderink, The role of network architecture in collagen mechanics, Biophys. J. 114 (2018) 2665–2678, http://dx.doi.org/10.1016/j.bpj.2018.04.043.

[16] Y. Ji, Y. Xing, F. Zhou, X. Li, Y. Chen, L. Shao, The mechanical characteristics of monolithic nanoporous copper and its composites, Adv. Eng. Mater. 20 (2018) 1800574, http://dx.doi.org/10.1002/adem.201800574.

[17] P.M. Godinho, M. Jajcinovic, L. Wagner, V. Vass, W.J. Fischer, T.K. Bader, U. Hirn, W. Bauer, J. Eberhardsteiner, C. Hellmich, A continuum micromechanics approach to the elasticity and strength of planar fiber networks: Theory and application to paper sheets, Eur. J. Mech. A Solids 75 (2019) 516–531, http://dx.doi.org/10.1016/j.euromechsol.2018.10.005.

[18] C. Richert, N. Huber, A review of experimentally informed micromechanical modeling of nanoporous metals: From structural descriptors to predictive structure–property relationships, Materials 13 (2020) 3307, http://dx.doi.org/10.3390/ma13153307.

[19] C. Morin, C. Hellmich, Z. Nejim, S. Avril, Fiber rearrangement and matrix compression in soft tissues: Multiscale hypoelasticity and application to tendon, Front. Bioeng. Biotechnol. 9 (2021) http://dx.doi.org/10.3389/fbioe.2021.725047.

[20] A. Morel, A.G. Guex, F. Itel, S. Domaschke, A.E. Ehret, S.J. Ferguson, G. Fortunato, R.M. Rossi, Tailoring the multiscale architecture of electrospun membranes to promote 3D cellular infiltration, Mater. Sci. Eng. C 130 (2021) 112427, http://dx.doi.org/10.1016/j.msec.2021.112427.

[21] A. Stracuzzi, B.R. Britt, E. Mazza, A.E. Ehret, Risky interpretations across the length scales: Continuum vs. discrete models for soft tissue mechanobiology, Biomech. Model. Mechanobiol. 21 (2022) 433–454, http://dx.doi.org/10.1007/s10237-021-01543-4.

[22] B.R. Britt, A.E. Ehret, Constitutive modelling of fibre networks with stretch distributions. part I: Theory and illustration, J. Mech. Phys. Solids 167 (2022) 104960, http://dx.doi.org/10.1016/j.jmps.2022.104960.

[23] T. Kanit, S. Forest, I. Galliet, V. Mounoury, D. Jeulin, Determination of the size of the representative volume element for random composites: statistical and numerical approach, Int. J. Solids Struct. 40 (2003) 3647–3679, http://dx.doi.org/10.1016/s0020-7683(03)00143-4.

[24] L.T. Harper, C. Qian, T.A. Turner, S. Li, N.A. Warrior, Representative volume elements for discontinuous carbon fibre composites – Part 1: Boundary conditions, Compos. Sci. Technol. 72 (2012) 225–234, http://dx.doi.org/10.1016/j.compscitech.2011.11.006.

[25] L.T. Harper, C. Qian, T.A. Turner, S. Li, N.A. Warrior, Representative volume elements for discontinuous carbon fibre composites – Part 2: Determining the critical size, Compos. Sci. Technol. 72 (2012) 204–210, http://dx.doi.org/10.1016/j.compscitech.2011.11.003.

[26] K. Hu, M. Ziehmer, K. Wang, E.T. Lilleodden, Nanoporous gold: 3D structural analyses of representative volumes and their implications on scaling relations of mechanical behaviour, Phil. Mag. 96 (2016) 3322–3335, http://dx.doi.org/10.1080/14786435.2016.1222087.

[27] C. Soyarslan, S. Bargmann, M. Pradas, J. Weissmüller, 3D stochastic bicontinuous microstructures: Generation, topology and elasticity, Acta Mater. 149 (2018) 326–340, http://dx.doi.org/10.1016/j.actamat.2018.01.005.
[28] I. Davoodi Kermani, M. Schmitter, J.F. Eichinger, R.C. Aydin, C.J. Cyron, Computational study of the geometric properties governing the linear mechanical behavior of fiber networks, Comput. Mater. Sci. 199 (2021) 110711, http://dx.doi.org/10.1016/j.commatsci.2021.110711.
[29] A. El Moumen, T. Kanit, A. Imad, Numerical evaluation of the representative volume element for random composites, Eur. J. Mech. A Solids 86 (2021) 104181, http://dx.doi.org/10.1016/j.euromechsol.2020.104181.
[30] R. Picu, Mechanics of random fiber networks—a review, Soft Matter 7 (2011) 6768, http://dx.doi.org/10.1039/c1sm05022b.
[31] L. Bouaoune, Y. Brunet, A. El Moumen, T. Kanit, H. Mazouz, Random versus periodic microstructures for elasticity of fibers reinforced composites, Composites B 103 (2016) 68–73, http://dx.doi.org/10.1016/j.compositesb.2016.08.026.
[32] V. Negi, R. Picu, Mechanical behavior of cross-linked random fiber networks with inter-fiber adhesion, J. Mech. Phys. Solids 122 (2019) 418–434, http://dx.doi.org/10.1016/j.jmps.2018.09.027.
[33] R. Xia, X. Feng, G. Wang, Effective elastic properties of nanoporous materials with hierarchical structure, Acta Mater. 59 (2011) 6801–6808, http://dx.doi.org/10.1016/j.actamat.2011.07.039.
[34] G. Pia, F. Delogu, Mechanical properties of nanoporous Au: From empirical evidence to phenomenological modeling, Metals 5 (2015) 1665–1694, http://dx.doi.org/10.3390/met5031665.
[35] G. Pia, F. Delogu, Nanoporous Au: Statistical analysis of morphological features and evaluation of their influence on the elastic deformation behavior by phenomenological modeling, Acta Mater. 85 (2015) 250–260, http://dx.doi.org/10.1016/j.actamat.2014.11.040.
[36] M. Nasr Esfahani, M. Jabbari, Molecular dynamics simulations of deformation mechanisms in the mechanical response of nanoporous gold, Materials 13 (2020) 2071, http://dx.doi.org/10.3390/ma13092071.
[37] A. Roberts, E.J. Garboczi, Elastic properties of model random three-dimensional open-cell solids, J. Mech. Phys. Solids 50 (2002) 33–55, http://dx.doi.org/10.1016/s0022-5096(01)00056-4.
[38] N. Huber, R.N. Viswanath, N. Mameka, J. Markmann, J. Weißmüller, Scaling laws of nanoporous metals under uniaxial compression, Acta Mater. 67 (2014) 252–265, http://dx.doi.org/10.1016/j.actamat.2013.12.003.
[39] B. Roschning, N. Huber, Scaling laws of nanoporous gold under uniaxial compression: Effects of structural disorder on the solid fraction, elastic Poisson's ratio, Young's modulus and yield strength, J. Mech. Phys. Solids 92 (2016) 55–71, http://dx.doi.org/10.1016/j.jmps.2016.02.018.
[40] J. Jiao, N. Huber, Deformation mechanisms in nanoporous metals: Effect of ligament shape and disorder, Comput. Mater. Sci. 127 (2017) 194–203, http://dx.doi.org/10.1016/j.commatsci.2016.10.035.
[41] N. Huber, Connections between topology and macroscopic mechanical properties of three-dimensional open-pore materials, Front. Mater. 5 (2018) http://dx.doi.org/10.3389/fmats.2018.00069.
[42] C. Richert, A. Odermatt, N. Huber, Computation of thickness and mechanical properties of interconnected structures: Accuracy, deviations, and approaches for correction, Front. Mater. 6 (2019) http://dx.doi.org/10.3389/fmats.2019.00327.
[43] M. Rintoul, S. Torquato, Reconstruction of the structure of dispersions, J. Colloid Interface Sci. 186 (1997) 467–476, http://dx.doi.org/10.1006/jcis.1996.4675.
[44] C. Yeong, S. Torquato, Reconstructing random media, Phys. Rev. E 57 (1998) 495–506, http://dx.doi.org/10.1103/physreve.57.495.
[45] L. Pant, S. Mitra, M. Secanell, Multigrid hierarchical simulated annealing method for reconstructing heterogeneous media, Phys. Rev. E 92 (2015) http://dx.doi.org/10.1103/physreve.92.063303.
[46] L. Lakhal, Y. Brunet, T. Kanit, Evaluation of second-order correlations adjusted with simulated annealing on physical properties of unidirectional nonoverlapping fiber-reinforced materials (UD Composites), Internat. J. Modern Phys. C 30 (2019) 1950017, http://dx.doi.org/10.1142/s0129183119500177.
[47] C. Richert, N. Huber, Skeletonization, geometrical analysis, and finite element modeling of nanoporous gold based on 3D tomography data, Metals 8 (2018) 282, http://dx.doi.org/10.3390/met8040282.
[48] A. Odermatt, C. Richert, N. Huber, Prediction of elastic-plastic deformation of nanoporous metals by FEM beam modeling: A bottom-up approach from ligaments to real microstructures, Mater. Sci. Eng. A 791 (2020) 139700, http://dx.doi.org/10.1016/j.msea.2020.139700.
[49] N. Huber, C. Richert, Comment to "skeletonization-based beam finite element models for stochastic bicontinuous materials: Application to simulations of nanoporous gold" by C. Soyarslan et al. [J. mater. res. 33(20), 3371 (2018)], J. Mater. Res. 35 (2020) 2831–2834, http://dx.doi.org/10.1557/jmr.2020.257.
[50] X.-Y. Sun, G.-K. Xu, X. Li, X.-Q. Feng, H. Gao, Mechanical properties and scaling laws of nanoporous gold, J. Appl. Phys. 113 (2013) 023505, http://dx.doi.org/10.1063/1.4774246.
[51] N. Badwe, X. Chen, K. Sieradzki, Mechanical properties of nanoporous gold in tension, Acta Mater. 129 (2017) 251–258, http://dx.doi.org/10.1016/j.actamat.2017.02.040.
[52] L.J. Gibson, M.F. Ashby, Cellular Solids: Structure and Properties, Cambridge University Press, 1997, http://dx.doi.org/10.1017/cbo9781139878326.
[53] M.F. Ashby, Y.J.M. Bréchet, Designing hybrid materials, Acta Mater. 51 (2003) 5801–5821, http://dx.doi.org/10.1016/s1359-6454(03)00441-5.
[54] Y.-H. Xiang, L.-Z. Liu, J.-C. Shao, H.-J. Jin, A universal scaling relationship between the strength and Young's modulus of dealloyed porous FE0.80Cr0.20, Acta Mater. 186 (2020) 105–115, http://dx.doi.org/10.1016/j.actamat.2019.12.046.